

NATIONAL AERONAUTICS AND SPACE ADMINISTRATION

*Technical Report 32-1218*

*Mariner Venus 67 Flight Acceptance  
Pyrotechnic Test*

*P. M. Barnett*

FACILITY FORM 602	N 68 - 21760	
	(ACCESSION NUMBER)	(THRU)
	94	1
	(PAGES)	(CODE)
	CF-94158	31
	(NASA CR OR TMX OR AD NUMBER)	(CATEGORY)

JET PROPULSION LABORATORY  
CALIFORNIA INSTITUTE OF TECHNOLOGY  
PASADENA, CALIFORNIA

December 15, 1967



CFSTI PRICE(S) \$

Hard copy (HC) —

Microfiche (MF) —

ff 653 July 65

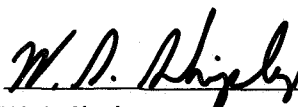
NATIONAL AERONAUTICS AND SPACE ADMINISTRATION

*Technical Report 32-1218*

*Mariner Venus 67 Flight Acceptance  
Pyrotechnic Test*

*P. M. Barnett*

Approved by:

A handwritten signature in dark ink, appearing to read "W. S. Shipley", is written over a horizontal line.

W. S. Shipley, Manager  
Environmental Requirements Section

JET PROPULSION LABORATORY  
CALIFORNIA INSTITUTE OF TECHNOLOGY  
PASADENA, CALIFORNIA

December 15, 1967



**TECHNICAL REPORT 32-1218**

Copyright © 1968

Jet Propulsion Laboratory  
California Institute of Technology

Prepared Under Contract No. NAS 7-100  
National Aeronautics & Space Administration

## Contents

<b>I. Introduction</b>	1
A. General	1
B. M67-1	1
C. M67-2	2
<b>II. Test Objectives</b>	2
A. Objectives for the M67-1 Test	2
B. Objectives for the M67-2 Test	3
<b>III. Conclusions</b>	3
A. Effect of Pyro Firings	3
B. Verification of Operations	3
C. Response of Structure	3
<b>IV. General Test Description</b>	3
A. Test Vehicle	3
B. Test Configuration	3
C. Test Sequence	4
D. Instrumentation	4
E. Data Handling	5
1. Data acquisition	5
2. Data reduction and analysis	5
<b>V. Test Results</b>	6
A. M67-1 Results	6
B. M67-2 Results	7
C. Comparison of M67-1 and M67-2 Responses	9
<b>Appendix. Transient Response of Umbilical Door Slam Recorded Prior to                   M67-1 Pyro Test</b>	67

## Tables

1. Accelerometer locations for M67-1 and M67-2 pyro tests	2
2. M67-1 summary of pyro event and peak-g levels	7

## Contents (contd)

### Tables (contd)

3. M67-1 summary of accelerometer locations and predominant pyro events . . .	8
4. M67-2 pyro test peak-g level tabulation . . . . .	9

### Figures

1. Accelerometer locations F4 and F4A; adapter flight location . . . . .	10
2. Accelerometer location F1; adapter foot G . . . . .	11
3. Accelerometer location F3; adapter foot C . . . . .	12
4. Accelerometer locations B1A, B2A, and B3A; top of bus leg B . . . . .	13
5. Accelerometer locations B4, B5, and B6; top of bus leg F . . . . .	14
6. Accelerometer locations BB1, BB2, and BB3; bottom of bus leg B . . . . .	15
7. Accelerometer locations SS4A, SS5A, and SS6A; secondary structure . . . . .	16
8. Accelerometer locations AS1 and AS2; antenna superstructure . . . . .	17
9. Accelerometer location F1C4, solar panel 1, and 3T3 on panel 3 . . . . .	18
10. Accelerometer locations MC4 and MCV4; midcourse motor . . . . .	19
11. Accelerometer location MCV1; midcourse nitrogen valve . . . . .	20
12. Accelerometer location MCV4; midcourse motor fuel valve . . . . .	21
13. M67-1 accelerometer locations . . . . .	23
14. M67-1 spacecraft pyro test configuration showing shroud, spacecraft, and adapter . . . . .	25
15. Spacecraft adapter . . . . .	25
16. Shroud V-band explosive bolt release assembly . . . . .	26
17. Spacecraft V-band release assembly . . . . .	26
18. One-degree-of-freedom oscillator model for shock spectra representation . . . . .	26
19. M67-1 primary shock spectra composite and transient-time history at accelerometer B3 . . . . .	27
20. M67-1 primary shock spectra composite and transient-time history at accelerometer F4 . . . . .	28
21. M67-1 primary shock spectra composite and transient-time history at accelerometer F1 . . . . .	29
22. M67-1 primary shock spectra composite and transient-time history at accelerometer F3 . . . . .	31
23. M67-1 primary shock spectra composite and transient-time history at accelerometer F4A . . . . .	32

## Contents (contd)

### Figures (contd)

24. M67-1 primary shock spectra composite and transient-time history at accelerometer B1A . . . . .	33
25. M67-1 primary shock spectra composite and transient-time history at accelerometer B2A . . . . .	34
26. M67-1 primary shock spectra composite and transient-time history at accelerometer B3A . . . . .	35
27. M67-1 primary shock spectra composite and transient-time history at accelerometer B4 . . . . .	36
28. M67-1 primary shock spectra composite and transient-time history at accelerometer B5 . . . . .	37
29. M67-1 primary shock spectra composite and transient-time history at accelerometer B6 . . . . .	38
30. M67-1 primary shock spectra composite and transient-time history at accelerometer BB1 . . . . .	39
31. M67-1 primary shock spectra composite and transient-time history at accelerometer BB2 . . . . .	40
32. M67-1 primary shock spectra composite and transient-time history at accelerometer BB3 . . . . .	41
33. M67-1 primary shock spectra composite and transient-time history at accelerometer SS4A . . . . .	43
34. M67-1 primary shock spectra composite and transient-time history at accelerometer SS5A . . . . .	44
35. M67-1 primary shock spectra composite and transient-time history at accelerometer SS6A . . . . .	45
36. M67-1 primary shock spectra composite and transient-time history at accelerometer AS1 . . . . .	47
37. M67-1 primary shock spectra composite and transient-time history at accelerometer AS2 . . . . .	49
38. M67-1 primary shock spectra composite and transient-time history at accelerometer FIC4. . . . .	51
39. M67-1 primary shock spectra composite and transient-time history at accelerometer 3T3 . . . . .	52
40. M67-1 primary shock spectra composite and transient-time history at accelerometer MCV1 . . . . .	53
41. M67-1 primary shock spectra composite and transient-time history at accelerometer MCV4 . . . . .	54
42. M67-1 primary shock spectra composite and transient-time history at accelerometer MC4. . . . .	55

## Contents (contd)

### Figures (contd)

43. M67-1 maximum enveloping primary shock spectra from accelerometers B1A, B2A, and B3A for all pyro events . . . . .	56
44. M67-1 maximum enveloping primary shock spectra from accelerometers B4, B5, and B6 for all pyro events . . . . .	56
45. M67-1 maximum enveloping primary shock spectra from accelerometers SS4A, SS5A, and SS6A for all pyro events . . . . .	56
46. M67-1 maximum enveloping primary shock spectra from accelerometers BB1, BB2, and BB3 for all pyro events . . . . .	56
47. M67-2 primary shock spectra composite and transient-time history at accelerometer B3 . . . . .	57
48. M67-2 primary shock spectra composite and transient-time history at accelerometer F4 . . . . .	58
49. M67-2 primary shock spectra composite and transient-time history at accelerometer F1 . . . . .	59
50. M67-2 primary shock spectra composite and transient-time history at accelerometer F3 . . . . .	60
51. M67-2 primary shock spectra composite and transient-time history at accelerometer F4A . . . . .	61
52. M67-1 and M67-2 comparison of primary shock spectra for spacecraft V-band release at accelerometer B3 . . . . .	62
53. M67-1 and M67-2 comparison of primary shock spectra for spacecraft V-band release at accelerometer F4 . . . . .	62
54. M67-1 and M67-2 comparison of primary shock spectra for spacecraft V-band release at accelerometer F1 . . . . .	62
55. M67-1 and M67-2 comparison of primary shock spectra for spacecraft V-band release at accelerometer F3 . . . . .	62
56. M67-1 and M67-2 comparison of primary shock spectra for spacecraft V-band release at accelerometer F4A . . . . .	63
57. M67-1 and M67-2 comparison of primary shock spectra for solar panel deploy pyro at accelerometer B3 . . . . .	63
58. M67-1 and M67-2 comparison of primary shock spectra for solar panel deploy pyro at accelerometer F1 . . . . .	63
59. M67-1 and M67-2 comparison of primary shock spectra for solar panel deploy pyro at accelerometer F3 . . . . .	63
60. M67-1 and M67-2 comparison of primary shock spectra for solar panel deploy pyro at accelerometer F4A . . . . .	64
61. M67-1 and M67-2 comparison of primary shock spectra for APAC pyro event at accelerometer F1 . . . . .	64

## Contents (contd)

### Figures (contd)

62. M67-1 and M67-2 comparison of primary shock spectra for APAC pyro event at accelerometer F3 . . . . .	64
63. M67-2 spacecraft V-band release device during pyro firing . . . . .	65

#### Umbilical Door Slam Event Transient Responses

A-1. Transient response and shock spectra at accelerometer B3 . . . . .	68
A-2. Transient response and shock spectra at accelerometer F4 . . . . .	68
A-3. Transient response and shock spectra at accelerometer F1 . . . . .	69
A-4. Transient response and shock spectra at accelerometer F3 . . . . .	69
A-5. Transient response and shock spectra at accelerometer F4A . . . . .	70
A-6. Transient response and shock spectra at accelerometer B1A . . . . .	70
A-7. Transient response and shock spectra at accelerometer B2A . . . . .	71
A-8. Transient response and shock spectra at accelerometer B3A . . . . .	71
A-9. Transient response and shock spectra at accelerometer BB1 . . . . .	72
A-10. Transient response and shock spectra at accelerometer BB2 . . . . .	72
A-11. Transient response and shock spectra at accelerometer BB3 . . . . .	73
A-12. Transient response and shock spectra at accelerometer AS2 . . . . .	73
A-13. Transient response and shock spectra at accelerometer 1C4 . . . . .	74
A-14. Transient response and shock spectra at accelerometer 3T3 . . . . .	74
A-15. Transient response and shock spectra at accelerometer MCV1 . . . . .	75
A-16. Transient response and shock spectra at accelerometer MCV4 . . . . .	75
A-17. Transient response and shock spectra at accelerometer MC4 . . . . .	76

## **Abstract**

The *Mariner* Venus 67 spacecraft transient responses to the firing of pyrotechnic devices located on or near the spacecraft are presented in the form of transient-time histories and shock spectra. Acceleration transient response measurements at selected spacecraft locations were recorded for these pyrotechnic events. Relative severity, based on maximum shock spectra, of the various pyrotechnic events is discussed for different areas of the spacecraft. Data handling and analysis techniques are described. Comparisons are made between the responses of the M67-1 (flight support spacecraft) and M67-2 (*Mariner* V) spacecraft.

# Mariner Venus 67 Flight Acceptance Pyrotechnic Test

## I. Introduction

### A. General

Both the *Mariner Venus 67* M67-1 (flight support spacecraft) and M67-2 (*Mariner V*) spacecraft were subjected to pyrotechnic (pyro) shock tests as a part of the system level flight acceptance (FA) test program. This document presents a summary of all of the transient acceleration response data recorded and analyzed during these tests.

This document includes (for both the M67-1 and M67-2 system level tests) the following items:

- (1) Test objectives.
- (2) Description of test configurations.
- (3) Test sequences.
- (4) Instrumentation, data handling and analysis methods, and techniques.
- (5) Test results including acceleration vs time-transient responses and shock spectra (primary and residual) derived from the transient responses.

### B. M67-1

Testing of the M67-1 spacecraft included the firing of all of the pyro devices located on or near the spacecraft. These devices consisted of the following:

- (1) Shroud V-band pyrotechnic (initiates shroud separation from *Agena* booster).
- (2) Spacecraft V-band pyrotechnic (initiates spacecraft separation from *Agena*).
- (3) Solar panel deploy pyros.
- (4) Post injection propulsion system (PIPS) pyros (mid-course motor)—two separate pyrotechnic events.
- (5) High-gain antenna pointing angle change (APAC) pyrotechnic.

The shock instrumentation consisted of 24 accelerometers located in the Lockheed Missile and Space Company (LMSC) adapter and on the bus structure, as shown in Table 1 and Figs. 1-13.



**Table 1. Accelerometer locations for M67-1 and M67-2 pyro tests**

General location	Component code	Sensitive spacecraft axis	Maximum useful <sup>a</sup> frequency, Hz	Figure
Upper bus leg B (flight location)	B3 <sup>b</sup>	Z	8000	—
Adapter bay II (flight location)	F4 <sup>b</sup>	Z	8000	1
Adapter foot G	F1 <sup>b</sup>	Radial	20,000	2
Adapter foot C	F3 <sup>b</sup>	Tangential	20,000	3
Adapter near F4	F4A <sup>b</sup>	Z	20,000	1
Bus top leg B	B1A	X	20,000	4
Bus top leg B	B2A	Y	20,000	4
Bus top leg B	B3A	Z	20,000	4
Bus top leg F	B4	X	9000	5
Bus top leg F	B5	Y	9000	5
Bus top leg F	B6	Z	9000	5
Bus bottom leg B	BB1	X	20,000	6
Bus bottom leg B	BB2	Y	20,000	6
Bus bottom leg B	BB3	Z	20,000	6
Secondary structure (near bay IV)	SS4A	Z	7500	7
Secondary structure (near bay IV)	SS5A	XY bays IV—VIII	7500	7
Secondary structure (near bay IV)	SS6A	XY bays II—VI	7500	7
Antenna superstructure	AS1	⊥ antenna axis	15,000	8
Antenna superstructure	AS2	II antenna axis	15,000	8
Solar panel 1 (lower center)	IC4	X	15,000	9
Solar panel 3 (Rt. tip)	3T3	Y	15,000	9
PIPS nitrogen valve	MCV1	XY bays II—VI	20,000	11
PIPS fuel valve	MCV4	XY bays II—VI	20,000	10 and 12
PIPS frame	MC4	XY bays II—VI	20,000	10 and 12

<sup>a</sup>Maximum frequency where response is flat to within  $\pm 10\%$ .  
<sup>b</sup>Accelerometer locations recorded during M67-1 and M67-2 tests.

### C. M67-2

The M67-2 test consisted of firing those pyro devices that would produce the maximum primary shock spectra response throughout the spacecraft (adapter excluded). These events were selected after analysis of the shock spectra response recorded during the M67-1 test. The pyro events specified and performed were as follows:

- (1) Spacecraft V-band release.
- (2) Solar panel deploy.
- (3) The APAC.

The instrumentation for M67-2 was limited to the two flight accelerometers (B3 and F4) and three additional accelerometers located in the adapter (see Table 1 and Fig. 13). Those accelerometer locations, marked in Table 1 and Fig. 13 with the superscript <sup>b</sup>, were recorded during the M67-1 and M67-2 tests.

## II. Test Objectives

### A. The objectives for the M67-1 test were:

- (1) To initiate all pyro devices on or near the spacecraft in the natural flight sequence to verify the

operation of the pyrotechnic control assembly (PCA), central control and sequencer (CC&S), and pyrotechnics.

- (2) To verify that spacecraft operation was not adversely affected by the detonation of the pyro.
- (3) To measure, record, and analyze the shock transients at selected locations on the adapter, structure, and secondary structure, high-gain antenna, solar panels, and midcourse valves for all the pyros located on or near the spacecraft and for the umbilical door slam event, which occurs when the umbilical cable is removed.

#### B. The objectives for the M67-2 pyro test were:

- (1) To initiate those pyros on or near the spacecraft that would produce maximum shock spectra responses throughout the spacecraft (adapter excluded) and verify the operation of the pyrotechnic control assembly, CC&S, and pyrotechnics.
- (2) To verify that the spacecraft operation was not adversely affected by the detonation of the pyrotechnics.
- (3) To measure, record, and analyze the response at the two flight transducer locations and the adapter.

### III. Conclusions

#### A. Effect of Pyro Firings

Spacecraft operation was unaffected by the detonation of the pyros for both M67-1 and M67-2; there were no failures during testing.

#### B. Verification of Operations

Operation of the pyro control assembly, CC&S and all pyrotechnics have been verified for both the M67-1 and M67-2.

#### C. Response of Structure

The desired transient responses for the M67-1 and M67-2 have been recorded and the data are of high quality. The most severe pyro event, based on shock spectra analysis, for the bus structure is the spacecraft V-band release. In general, the solar panel pyros, APAC pyros, and the midcourse pyros cause spectra maxima in the local area of the respective pyro devices only. The shroud V-band-release pyro event produces maximum

spectra in the LMSC adapter. To generate maximum enveloping shock spectra throughout the spacecraft (excluding the LMSC adapter), it is not necessary to initiate all the spacecraft pyrotechnics. Only the spacecraft V-band pyro, solar panel deploy pyro, and the APAC pyro events are required. These data and the conclusions drawn are presented more fully in the following sections.

### IV. General Test Description

#### A. Test Vehicle

The test vehicles for these test programs were the M67-1 and M67-2 spacecraft. Each spacecraft was equipped with flight hardware and assemblies with the following exceptions:

Exceptions to M67-1 flight hardware	Hardware used
Attitude control system	STM <sup>a</sup>
Canopus	STM <sup>a</sup>
Power subsystem bay I	STM <sup>a</sup>
Solar panels } 3 and 4 } others	Flight spares STM <sup>a</sup>
Exceptions to M67-2 flight hardware	Hardware used
PIPS	STM <sup>a</sup>
Attitude control system	STM <sup>a</sup>
Solar panels } 3 and 4 } others	Flight spares STM <sup>a</sup>
<sup>a</sup> Structural test model	

#### B. Test Configuration

The M67-1 FA pyro test was conducted with the spacecraft in its flight configuration secured atop the LMSC adapter and an *Agna* forward equipment rack. The rack, in turn, was bolted to a 2-in.-thick steel plate. Prior to the shroud V-band pyro release, the test configuration was as shown in Fig. 14. The shroud shown in Fig. 14 was secured to the LMSC adapter with a tensioned shroud

V-band. The spacecraft was secured to this adapter with another V-band. This spacecraft V-band secured the eight feet of the spacecraft to eight mating surfaces on the adapter. The tension in each of the eight individual segments of the spacecraft V-band was continuously adjustable and measurable (by means of a strain gage bridge in each of the eight segments) in order to provide a uniform load at each of the eight mounting feet. Figure 15 shows the LMSC adapter and interface between the spacecraft and shroud.

There were two explosive bolt release assemblies on the shroud V-band, spaced 180 deg apart around the V-band. Similarly, there were two release devices on the spacecraft V-band, located in two segments of the V-band (spaced 180 deg apart at bays II and VI). The shroud V-band explosive bolt release is shown in Fig. 16 and the spacecraft V-band release assembly is shown in Fig. 17. The test configuration for the M67-2 was identical to the M67-1, except for the shroud, which was omitted for M67-2 because there was no shroud V-band pyro event specified. In addition, the M67-2 spacecraft adapter was not mounted on the *Agena* forward equipment but was secured to a handling fixture.

### C. Test Sequence

The M67-1 test consisted of firing all the pyro devices on or near the spacecraft in the sequence they would be fired during an actual mission. In addition, the spring-loaded umbilical door in the LMSC shroud was opened fully and allowed to slam shut while recording all accelerometers on the spacecraft. High-speed (approximately 5000 frames/s) motion pictures were taken of the release devices during both the shroud and spacecraft V-band pyro events to record the first motion of the V-bands. The test sequence was as follows:

- (1) Umbilical door slam (two runs).
- (2) Shroud V-band pyro release.
- (3) Spacecraft V-band pyro release.
- (4) Solar panel pyro deploy.
- (5) Post injection propulsion system pyro 1 (PIPS 1).
- (6) Post injection propulsion system pyro 2 (PIPS 2).
- (7) High-gain antenna pointing angle change (APAC).

Prior to the pyro events, dry runs were performed by firing fuses instead of pyros and running the high-speed movie cameras and associated lighting equipment. During the dry runs, the response accelerometers on the spacecraft were carefully monitored and recorded to determine if there were any unwanted electrical transients present, which might result from ground loops resulting from the turn-on of the ancillary equipment.

The M67-2 test sequence consisted of firing those pyros that would produce the maximum shock spectra throughout the spacecraft (exclusive of the adapter). These events were selected after analysis of the shock spectra recorded during the M67-1 pyro test. These events included the following:

- (1) Spacecraft V-band release pyros.
- (2) Solar panel release pyros.
- (3) The APAC.

As a result of the success with eliminating electrical transients in the recording system during the M67-1 test, there were no preliminary fuse firings prior to the M67-2 test.

High-speed movies again were taken of the spacecraft V-band release.

### D. Instrumentation

To record and analyze the transient response, the M67-1 spacecraft was instrumented with 24 high-frequency accelerometers. The accelerometers were located on the LMSC adapter, top and bottom of the spacecraft structure, secondary structure, antenna superstructure, solar panels, and midcourse motor valves and frame. Table 1 shows a tabulation of all accelerometers used during the M67-1 test, detailing general locations, sensitive axes, and maximum useful frequency. Wherever possible (within the constraints imposed by instrumenting a flight-worthy spacecraft), the bus accelerometers were bolted to aluminum adapter blocks which, in turn, were bolted to the bus structure. The solar panel and antenna superstructure accelerometers were cemented in place. Where bolting was not possible, the accelerometers were secured with Eastmen 910 cement. Figures 1-12 show the accelerometer locations recorded during the M67-1 and M67-2 tests. Figure 13 is an over-all schematic of the spacecraft instrumentation for the M67-1 and M67-2 tests.

The V-bands (both shroud and spacecraft) were instrumented with strain gages in each segment to record tension during the tensioning operations. There were four gages on the shroud V-band and eight gages (one in each of the eight sections) on the spacecraft V-band.

These gages were used to measure and adjust V-band tension only, and were not recorded during the V-band releases.

Great care was exercised during the spacecraft instrumentation to isolate all accelerometers and recording electronics to avoid recording unwanted electrical transients and ground loops.

The M67-2 instrumentation was abbreviated and included only five accelerometers. This instrumentation was limited due to the JPL test practice of using absolutely minimal instrumentation on prime flight spacecraft. The accelerometers used for this M67-2 test are marked with the superscript <sup>b</sup> in Table 1. Similarly, the photographs marked with <sup>b</sup> show both M67-1 and M67-2 accelerometer locations. Figures 2 and 3 (accelerometers F1 and F3) were taken prior to the M67-2 vibration test and, as such, show a lower natural frequency vibration transducer and not the transducer used in the tests. However, for these tests, the F1 and F3 transducers used had a natural frequency of 80,000 Hz. The photographs are presented to show the exact location and orientation of the instrumentation.

It was desired to use accelerometers with as high a natural frequency as possible for these tests. Table 1 shows the maximum useful frequency (response flat to within  $\pm 10\%$ ) for each of the accelerometers used. This frequency is approximately 0.3 of the accelerometer natural frequency. Some of these accelerometers had natural frequencies of 80,000 Hz (see Table 1), in which case the upper frequency was limited by the 20,000-Hz limit of the recording system.

## E. Data Handling

**1. Data acquisition.** All accelerometers were recorded on FM magnetic type recorders with frequency response flat to 20,000 Hz. The static load strain gage data were recorded, during the V-band tensioning operation, on chart paper and digital readout. Prior to the test, the V-bands were pulled in a tensile-testing machine and the strain gages calibrated in pounds.

## 2. Data reduction and analysis

**a. On-site data reduction.** After each pyrotechnic event, the recorded data were played back into a calibrated oscilloscope in order to obtain a quick-look analysis of the data. This was done to determine:

- (1) If the sensitivities of the recording system were properly set.
- (2) The approximate values for peak-g levels at the various locations around the spacecraft for that pyro event.
- (3) If there were any spurious electrical transients present in the response traces which could be eliminated prior to the next pyro event.

**b. Digital data reduction and analysis.** All recorded transient data were reduced digitally to plots of raw data (time history) and shock spectra (both primary and residual). The shock spectra information was obtained by using JPL Program No. 5628<sup>1</sup> and the following digital-analysis parameters:

- (1) Sample rate: 160,000 samples/s.
- (2) Aliasing filter: none.
- (3) Analysis interval: 30 ms.

The shock spectra data presented herein represent the peak response of one-degree-of-freedom oscillator to the shock transient in question. The peak response of the oscillator is presented as a function of the natural frequency of the oscillator over the frequency range of interest. There are two spectra curves associated with each transient: the primary and residual spectra. The primary spectrum represents the peak response of the one-degree-of-freedom oscillator during the time the transient exists. The residual spectrum represents the peak response of the oscillators after the pulse has passed. The analysis can be performed for any chosen value of oscillator damping. In this report, the damping ratio was chosen as 0.025 (or  $Q = 20$ ). Figure 18 shows a simplified oscillator (one-degree-of-freedom) model of the shock spectra analysis process.

The spectra data presented herein are only the primary spectra. Residual spectra data are available.

<sup>1</sup>Snyder, D. C., and Wiksten, D. B., *Shock Spectrum Analysis Program*, Technical Memorandum 33-326, Jet Propulsion Laboratory, Pasadena, Calif., March 1, 1967.

## V. Test Results

### A. M67-1 Results

Figures 19–42 are the composite shock spectra data recorded at each accelerometer location for all the pyro events performed during the M67-1 test. Included in each of these figures are curves of the significant transient response-time histories at these accelerometer locations. Some of the composites show more time histories than shock spectra. The spectra for these transients are too low to be plotted on the scale used and still show the larger, more significant spectra. It can be seen that these data are very complex and are characterized by relatively high peak-g levels, many frequency components, a jagged, irregular decay of the peak-g levels with time, and almost zero net velocity change.

Table 2 is a tabulation of all accelerometers mounted on the M67-1 spacecraft and peak-g levels recorded for all pyro events and the umbilical door slam event.

Table 3 is a tabulation of all M67-1 accelerometer locations and those pyro events which produce the maximum spectra responses at these specified locations.

Typically, it can be stated that for the M67-1 test and at those locations indicated, the following response trends apply (see Figs. 19–42):

- (1) The bottom of the bus (accelerometers BB1, BB2, and BB3) responds greatest to the spacecraft V-band pyro event (Figs. 30, 31, 32, and 46).
- (2) The LMSC adapter (accelerometers F1, F3, F4, and F4A) response is greatest as a result of the shroud V-band pyro event (Figs. 20, 21, 22, and 23).
- (3) In the areas at the top of the bus (accelerometers B1A, B2A, B3A, B4, B5, and B6) the maximum responses result from the pyro events associated with spacecraft V-band pyro, PIPS pyros and the APAC pyro. The maxima occur at varying frequencies and depend on location around the bus (Figs. 24, 25, 26, 27, 28, 29, 43, and 44). The PIPS pyro events resulted in maximum shock spectra response at leg B and only in the frequency range from 2000 to 20,000 Hz. Below 2000 Hz, the spacecraft V-band release produced the maximum

spectra at this location. In addition, in the 2000–20,000-Hz range, there is little difference between the maximum response produced by the PIPS events and the slightly lower response produced by the spacecraft V-band event.

- (4) The solar panels exhibit maximum shock spectra responses for the solar panel deploy pyro event.

The spacecraft response to the umbilical door-slam events were also recorded and digitally reduced to transient time history and shock spectra. These data are presented in the Appendix.

Figures 43–46 are plots of the maximum shock spectra envelope recorded during the M67-1 test for four triaxial accelerometer locations independent of pyro event and direction. These data represent the maximum spectra recorded in three orthogonal axes at the locations indicated for all the pyro events performed. It can be seen that the bottom of the bus at leg B (see Fig. 46) is the greatest response area recorded during this test. A local resonance is evident from 1200 to 2000 Hz in the Z axis, which contributes to the peak in the maximum spectra envelope and can also be observed in Fig. 32 (composite spectra of all transient responses at accelerometer BB3). By comparing the maximum spectra envelope at the top and bottom of the bus at leg B (Figs. 43 and 46) it can be seen that the response spectra at the bottom of the bus are typically between two and three times greater than the response recorded at the top of the bus. The predominant pyro event for both locations is the spacecraft V-band release event. In addition, note the maximum envelope response at the top of the bus at leg F (B4, B5, and B6 in Fig. 44). The maximum enveloping shock spectra presentation closely approximates the response at leg B top of bus in the low-frequency range (up to 2000 Hz) but the response keeps increasing (as opposed to the leveling-off of the leg B response) in the range of 2000 to 20,000 Hz. This is a result of the APAC event, which results in the increasing spectra at the leg F location above 1000 Hz (see Table 3).

The transient response which results from the spacecraft V-band release is caused by the rapid release of the stored energy in the compressed (by V-band with 2500 lb of tension) spacecraft structure.

Table 2. M67-1 summary of pyro event and peak-g levels

General location	Component code (24 total)	Sensitive spacecraft axis	Event						
			Umbilical door slam peak-g	Shroud V-band peak-g	Spacecraft V-band peak-g	Solar panel deploy peak-g	PIPS 1 peak-g	PIPS 2 peak-g	APAC peak-g
Upper bus leg B (flight location)	B3	Z	4.3	33.0	125.0	25.0	82.0	51.0	7.0
Adapter-bay II (flight location)	F4	Z	26.0	485.0	100.0	2.1	23.0	12.0	3.4
Adapter foot G	F1	Radial	8.0	370.0	850.0	3.5	4.3	3.2	12.2
Adapter foot C	F3	Tangential	27.0	380.0	410.0	3.7	>50.0	45.0	5.4
Adapter near F4	F4A	Z	27.0	520.0	70.0	2.1	19.0	9.5	3.0
Bus top leg B	B1A	X	3.4	26.0	88.0	24.0	70.0	75.0	7.8
Bus top leg B	B2A	Y	3.5	21.0	90.0	21.0	—	94.0	7.8
Bus top leg B	B3A	Z	4.8	38.0	155.0	18.0	77.0	61.0	7.0
Bus top leg F	B4	X	1.0	15.0	67.0	21.0	7.0	4.5	150.0
Bus top leg F	B5	Y	0.8	13.0	54.0	26.0	4.5	2.7	135.0
Bus top leg F	B6	Z	1.3	25.0	83.0	72.0	3.0	2.2	175.0
Bus bottom leg B	BB1	X	6.8	43.0	440.0	5.4	55.0	47.0	2.4
Bus bottom leg B	BB2	Y	4.9	53.0	440.0	4.0	47.0	37.0	< 5.0
Bus bottom leg B	BB3	Z	—	73.0	430.0	18.0	37.0	45.0	5.1
Secondary structure (near bay IV)	SS4A	Z	—	≈ 5.0	8.2	9.1	12.0	7.5	36.0
Secondary structure (near bay IV)	SS5A	Bay VIII axis	—	≈ 5.0	5.5	11.0	11.0	7.5	39.0
Secondary structure (near bay IV)	SS6A	Bay II axis	—	≈ 5.0	40.0	9.0	11.0	7.5	22.0
Antenna superstructure	AS1	⊥ antenna axis	—	17.0	35.0	18.0	2.4	1.8	5400.0
Antenna superstructure	AS2	antenna axis	2.8	31.0	62.0	33.0	3.8	2.4	2500.0
Solar panel 1 (lower center)	1C4	X	6.2	29.0	24.0	100.0	4.3	3.5	<15.0
Solar panel 3 (right tip)	3T3	Y	10.5	48.0	29.0	230.0	23.0	17.0	20.0
PIPS nitrogen valve	MCV1	Bay II axis	2.3	≈10.0	48.0	2.3	7300.0	6500.0	< 2.0
PIPS fuel valve	MCV4	Bay II axis	2.0	9.5	38.0	1.8	6500.0	6500.0	< 2.0
PIPS frame	MC4	Bay II axis	3.0	22.0	130.0	8.0	800.0	470.0	< 5.0

## B. M67-2 Results

The M67-2 test was an abbreviated test both in pyro events performed and recording instrumentation. Response measurements were recorded only at the two flight locations (B3 and F4) and three other adapter locations (F1, F4A, and F3). Similar to the M67-1 data presentation, Figs. 47–51 are the composite shock spectra recorded at each accelerometer location for all the pyro events performed during the M67-2 test. Included in

each figure are curves of the significant transient-response-time histories at these accelerometer locations. As expected, the spacecraft V-band event produced the maximum shock spectra response at the flight transducer locations and in the adapter.

Table 4 is a tabulation of the accelerometers mounted on the spacecraft and peak-g levels recorded for all pyro events for the M67-2 test.

**Table 3. M67-1 summary of accelerometer locations and predominant pyro events**

General location	Component code	Sensitive spacecraft axis	Predominant pyro events and comments
Adapter bay II (flight accelerometer)	F4	Z	Shroud V-band (Fig. 20)
Adapter foot G	F1	Radial	Spacecraft V-band (Fig. 21)
Adapter foot C	F3	Tangential	Shroud V-band and spacecraft V-band (Fig. 22)
Adapter bay II (rear F4)	F4A	Z	Shroud V-band (Fig. 23)
Upper bus leg B (flight accelerometer)	B3	Z	Spacecraft V-band for $100 < f < 3000$ (Fig. 19)
			Midcourse pyros and spacecraft V-band for $f > 3000$ and $f < 100$
Top of bus leg B	B1A	X	Spacecraft V-band for $100 < f < 3000$ (Fig. 24)
			Midcourse pyros and spacecraft V-band for $f > 3000$ and $f < 100$
Top of bus leg B	B2A	Y	Spacecraft V-band for $100 < f < 3000$ (Fig. 25)
			Midcourse pyros and spacecraft V-band for $f > 3000$ and $f < 100$ B3
Top of bus leg B	B3A	Z	Spacecraft V-band for $100 < f < 3000$ (Fig. 26)
			Midcourse pyros and spacecraft V-band for $f > 3000$ and $f < 100$ B3
Top of bus leg F	B4	X	APAC pyro for $f > 1000$ Hz
			Spacecraft V-band pyro for $f < 1000$ Hz (Fig. 27)
Top of bus leg F	B5	Y	APAC pyro for $f > 1000$ Hz
			Spacecraft V-band pyro for $f < 1000$ Hz (Fig. 28)
Top of bus leg F	B6	Z	APAC pyro for $f > 1000$ Hz
			Spacecraft V-band pyro for $f < 1000$ Hz (Fig. 29)
Bottom of bus leg B	BB1	X	Spacecraft V-band (Fig. 30)
Bottom of bus leg B	BB2	Y	Spacecraft V-band (Fig. 31)
Bottom of bus leg B	BB3	Z	Spacecraft V-band (Fig. 32)
Secondary structure	SS4A	Z	Spacecraft V-band (Fig. 33)
Secondary structure	SS5A	Bay VIII axis	Spacecraft V-band (Fig. 34)
Secondary structure	SS6A	Bay II axis	Spacecraft V-band (Fig. 35)
Antenna superstructure	AS1	⊥ antenna axis	APAC pyro (Fig. 36)
Antenna superstructure	AS2	antenna axis	APAC pyro (Fig. 37)
Solar panel 1 (lower center)	1C4	X	Solar panel deploy pyro (Fig. 38)
Solar panel 3 (right tip)	3T3	Y	Solar panel deploy pyro (Fig. 39)
PIPS nitrogen valve	MCV1	Bay II axis	Midcourse pyros (Fig. 40)
PIPS fuel valve	MCV4	Bay II axis	Midcourse pyros (Fig. 41)
PIPS frame	MC1	Bay II axis	Midcourse pyros (Fig. 42)

**Table 4. M67-2 pyro test peak-g level tabulation**

General location	Component code <sup>a</sup>	Sensitive spacecraft axis	Pyro events		
			Spacecraft V-band release, peak-g	Solar panel release, peak-g	APAC, peak-g
Upper bus leg B (flight transducer)	B3	Z	128	52.0	6.4
Adapter bay II (flight transducer)	F4	Z	111	—	10.5
Adapter foot G	F1	Radial	1,200	3.2	8.1
Adapter foot C	F3	Tangential	390	3.6	4.1
Adapter near F4	F4A	Z	125	1.4	2.4
<sup>a</sup> These accelerometer codes correspond to the codes used for the M67-1 spacecraft.					

### C. Comparison of M67-1 and M67-2 Responses

Comparison of the response data for the M67-1 and M67-2 tests for the same pyro event at the same accelerometer locations shows similar response trends. This comparison is shown in Figs. 52-62, where each accelerometer location common to both spacecraft tests is composited for the same pyro event.

In general, the spacecraft V-band release event produces better agreement between like accelerometer locations than does the solar panel deploy or APAC pyro

events. However, the spectra variations from M67-1 to M67-2 tests were smaller than expected and are considered excellent.

High-speed movies of the V-band release were taken during the M67-1 and M67-2 pyro tests. Figure 63 shows a sequence of six frames taken during the M67-2 spacecraft V-band release. The photographs show the release device at the instant before release (Fig. 63) and five consecutive frames after release. As noted earlier, the film speed was approximately 5000 frames/s.



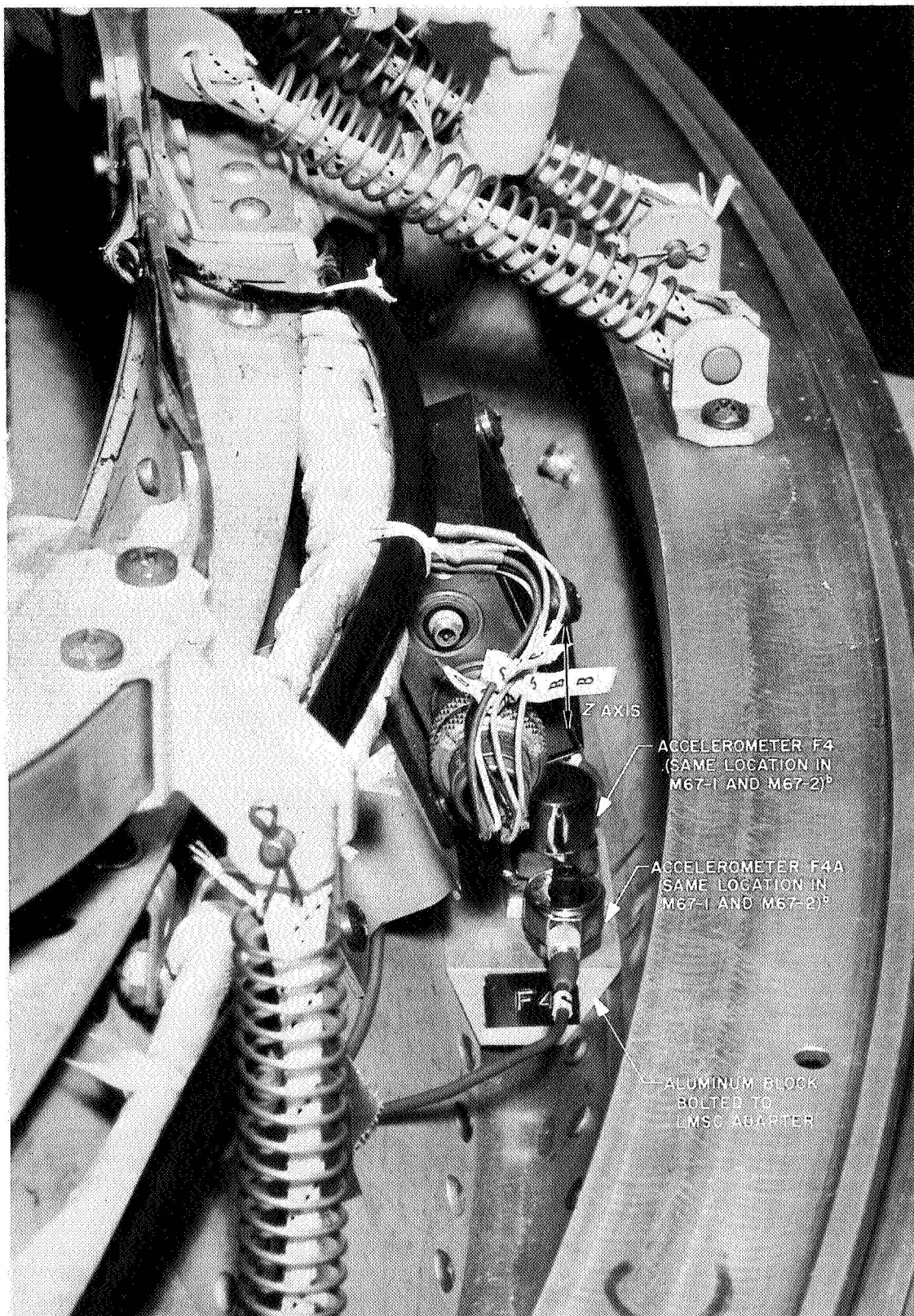


Fig. 1. Accelerometer locations F4 and F4A; adapter flight location

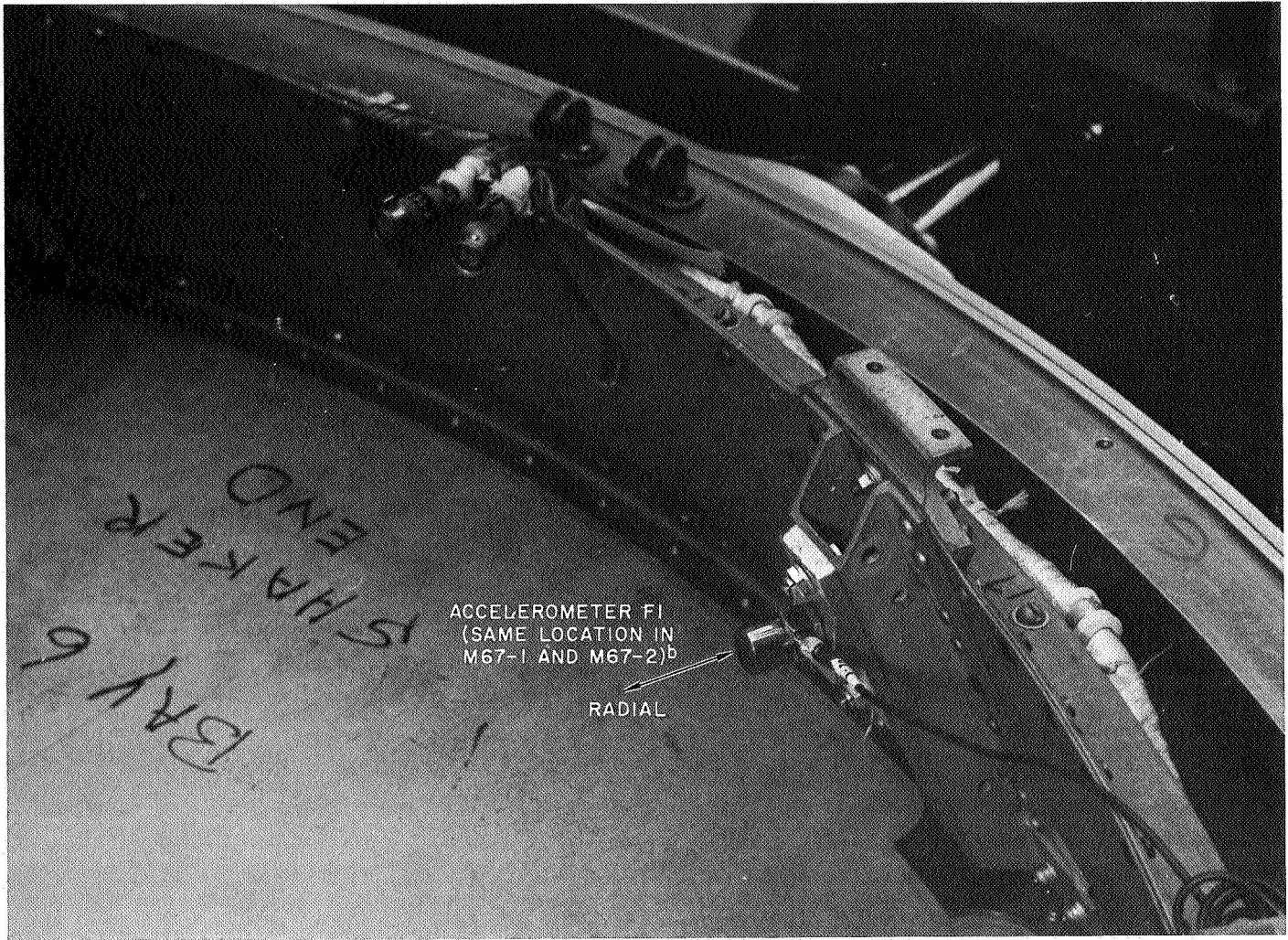
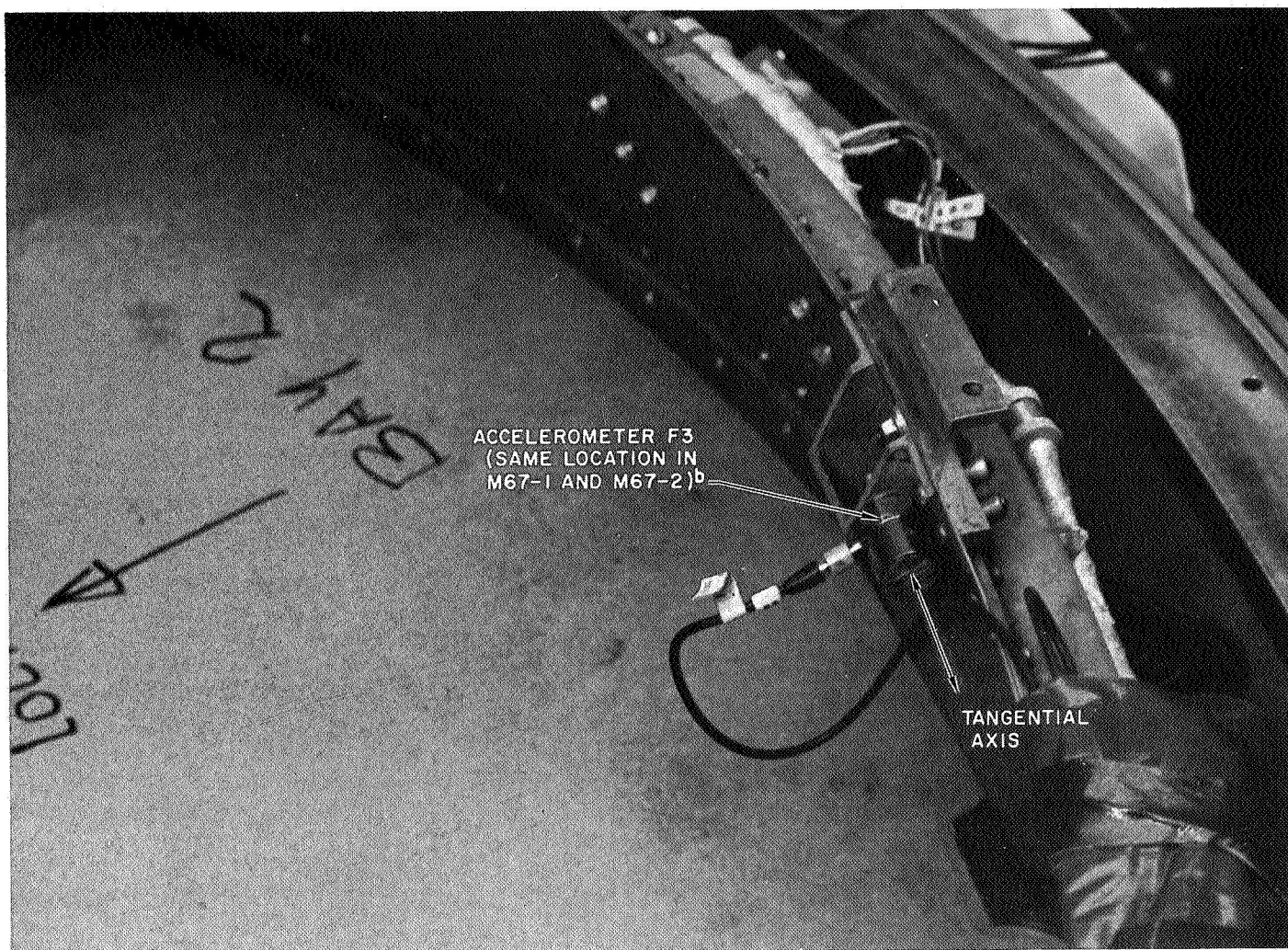


Fig. 2. Accelerometer location F1; adapter foot G





**Fig. 3. Accelerometer location F3; adapter foot C**

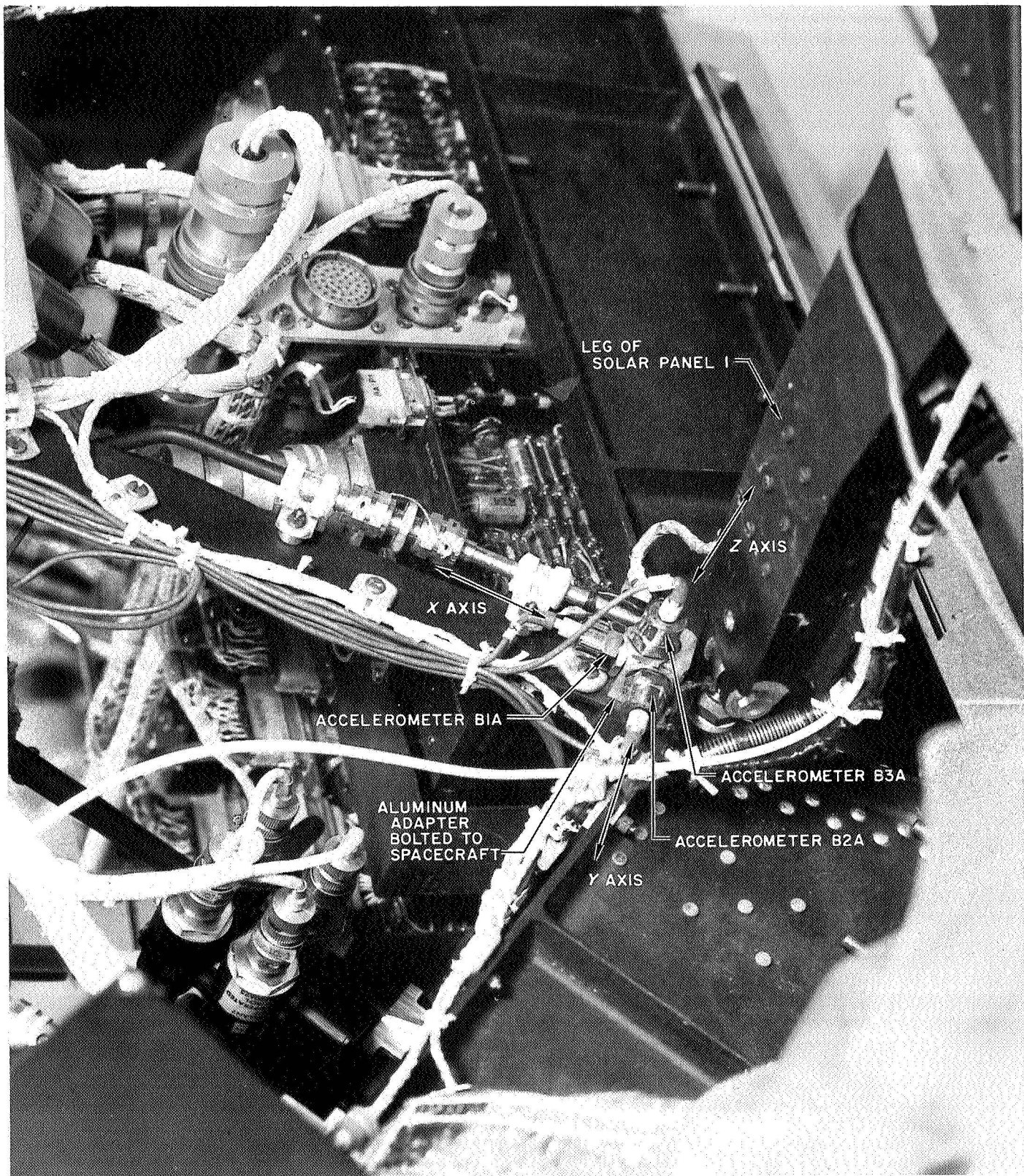
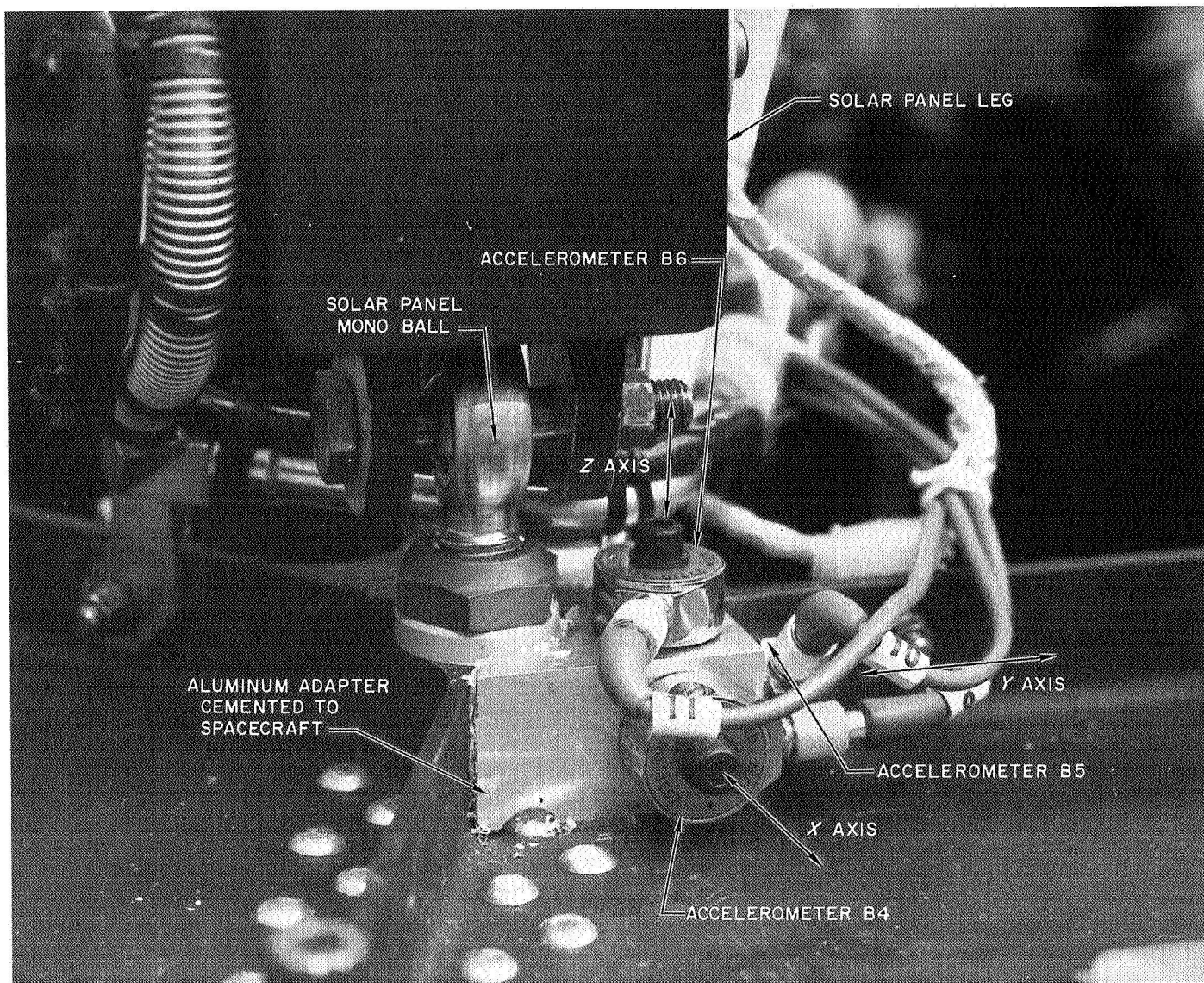
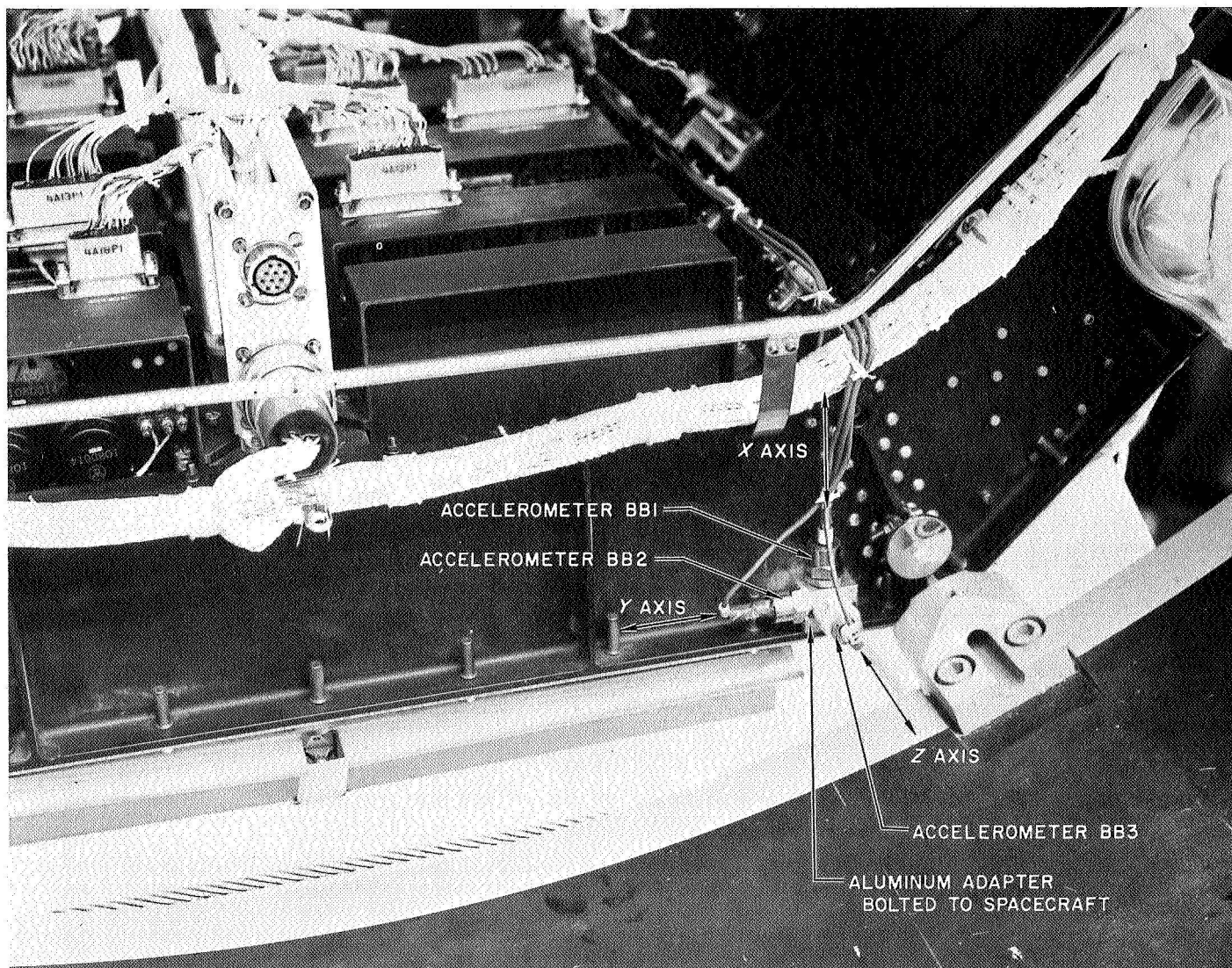


Fig. 4. Accelerometer locations B1A, B2A, and B3A; top of bus leg B





**Fig. 5. Accelerometer locations B4, B5, and B6; top of bus leg F**



**Fig. 6. Accelerometer locations BB1, BB2, and BB3; bottom of bus leg B**



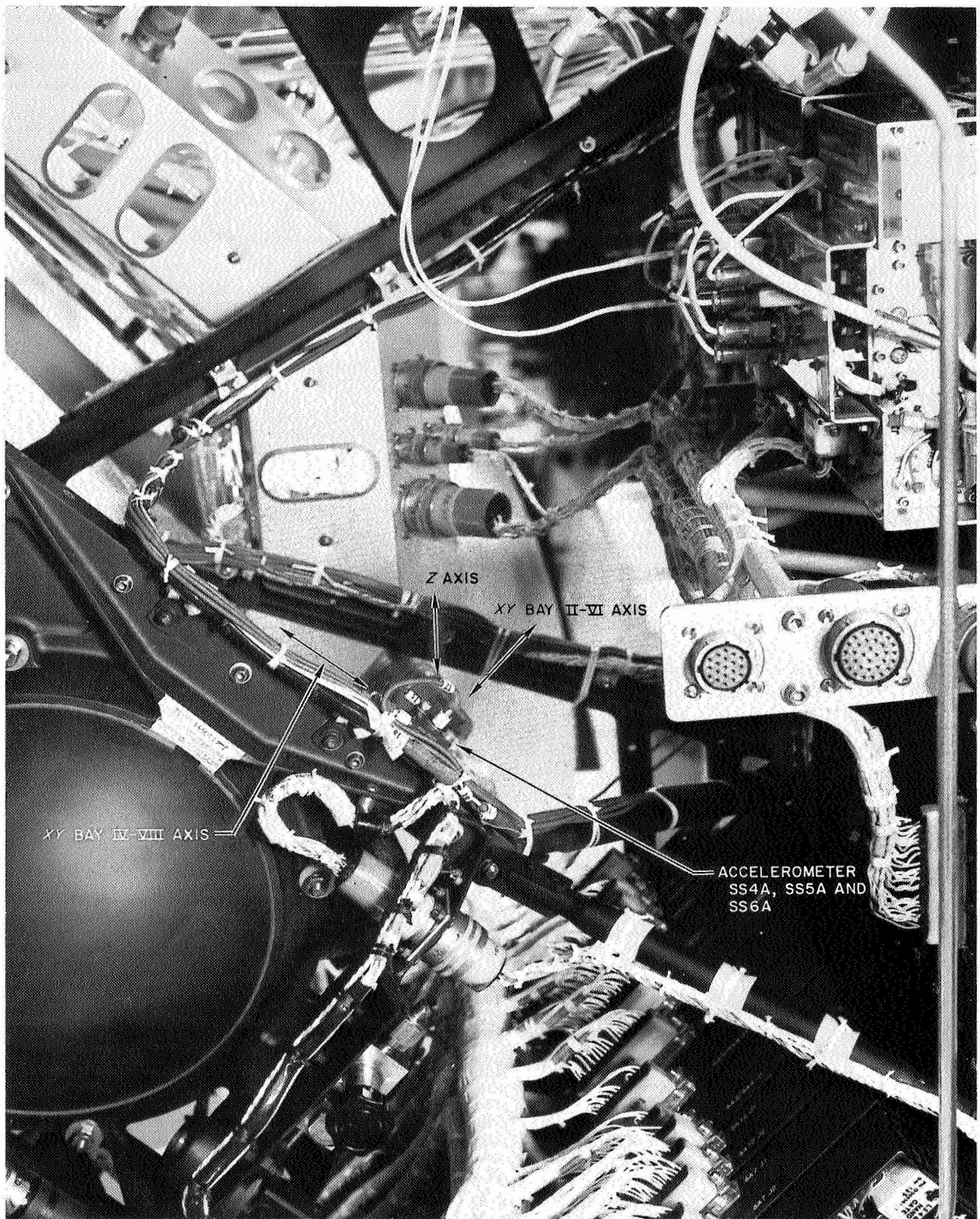


Fig. 7. Accelerometer locations SS4A, SS5A, and SS6A; secondary structure

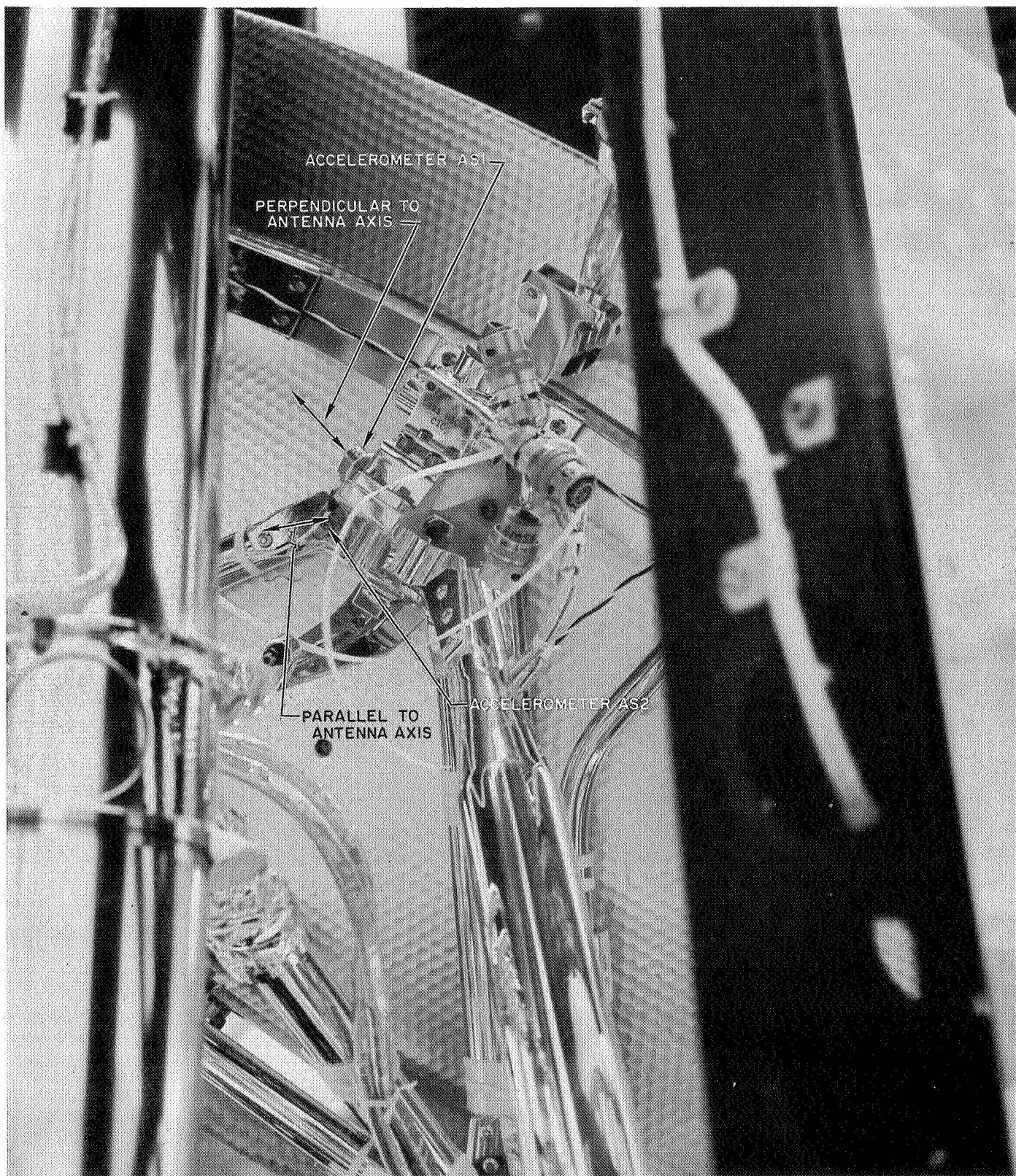


Fig. 8. Accelerometer locations AS1 and AS2; antenna superstructure



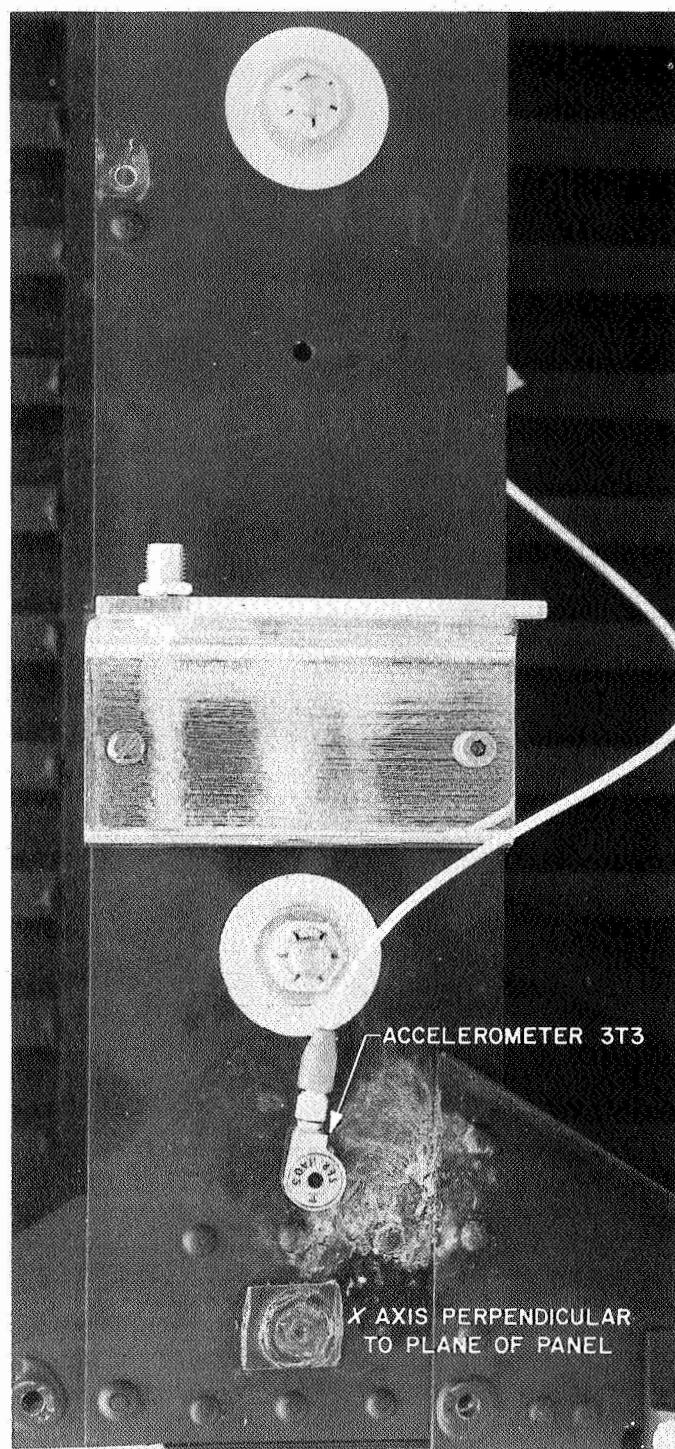
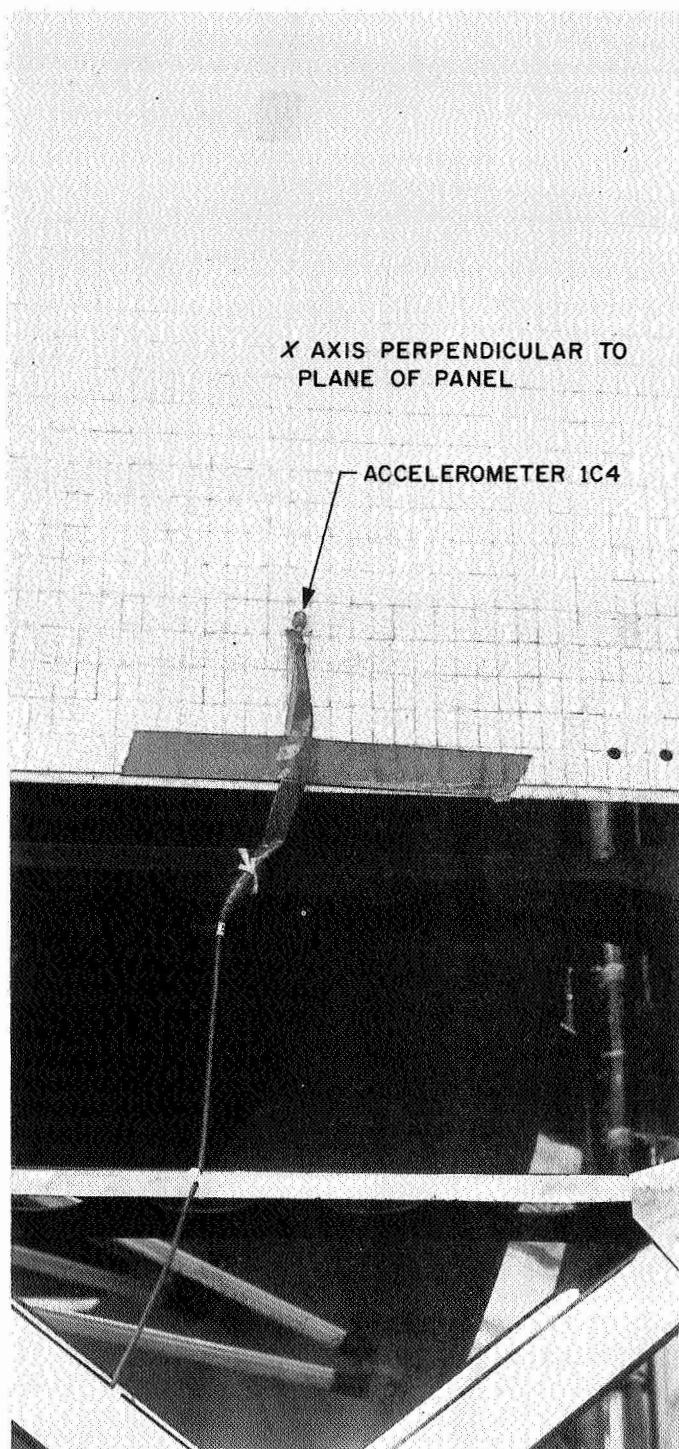


Fig. 9. Accelerometer location 1C4, solar panel 1 and 3T3 on panel 3

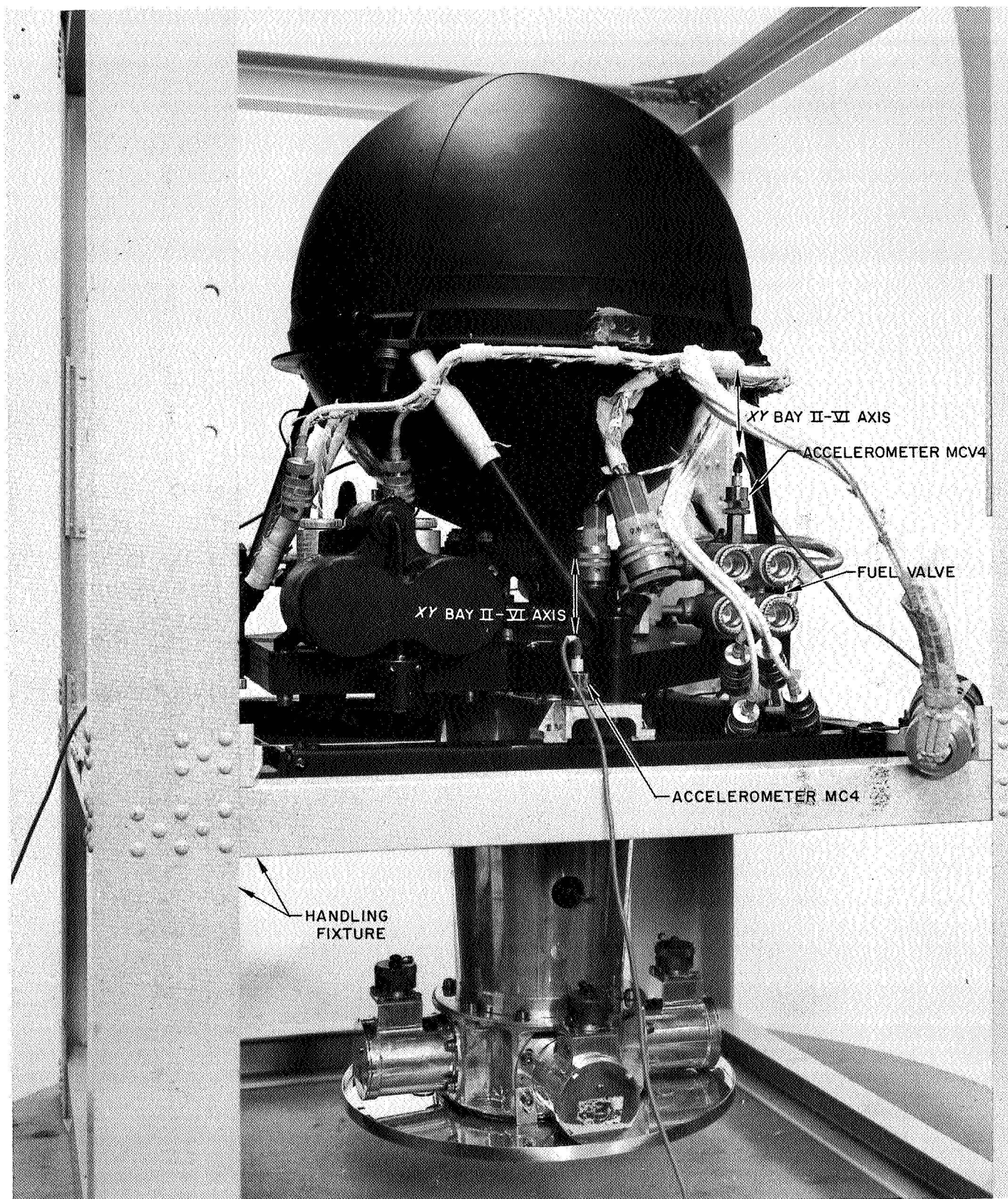


Fig. 10. Accelerometer locations MC4 and MCV4; midcourse motor



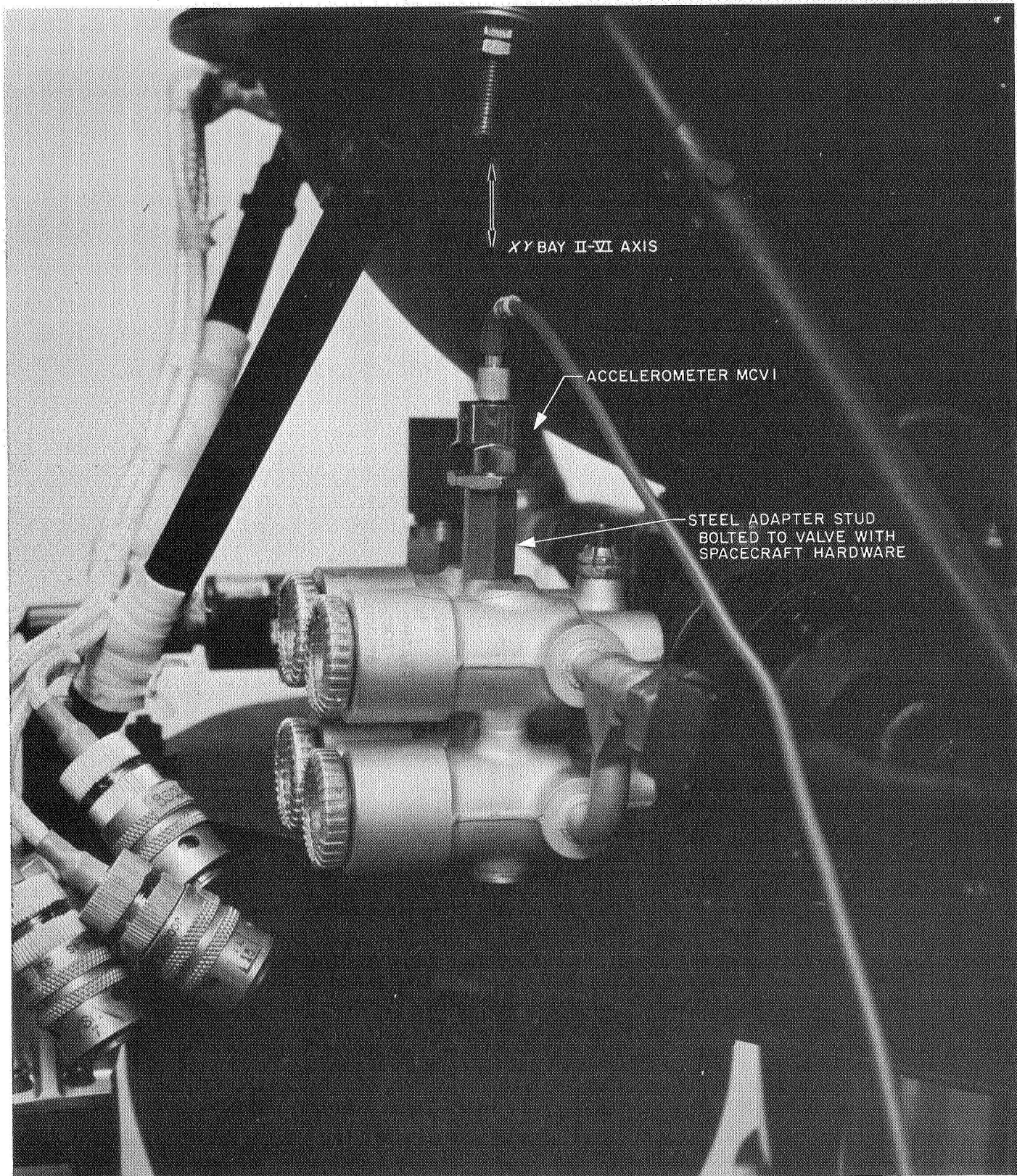


Fig. 11. Accelerometer location MCV1; midcourse motor nitrogen valve

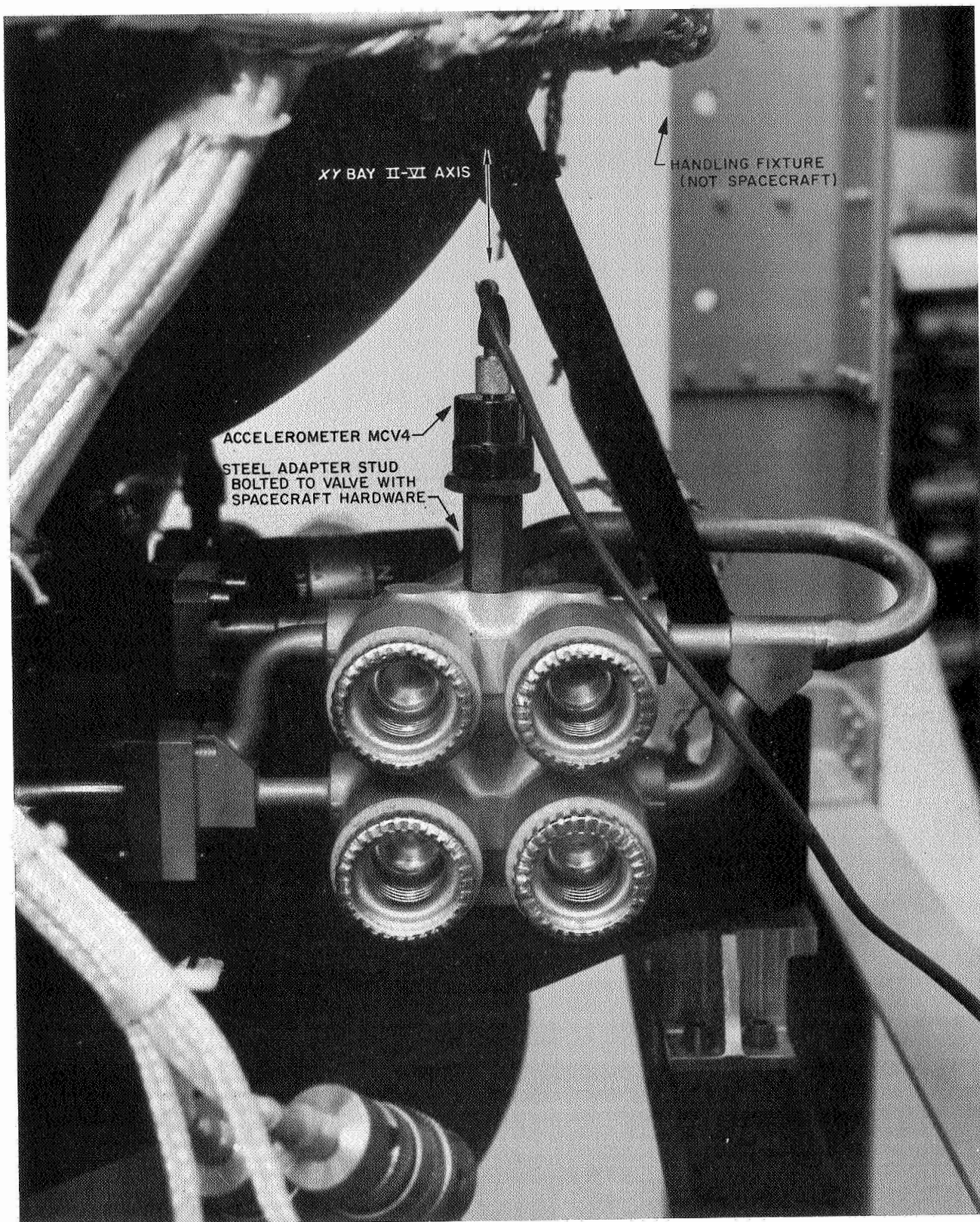
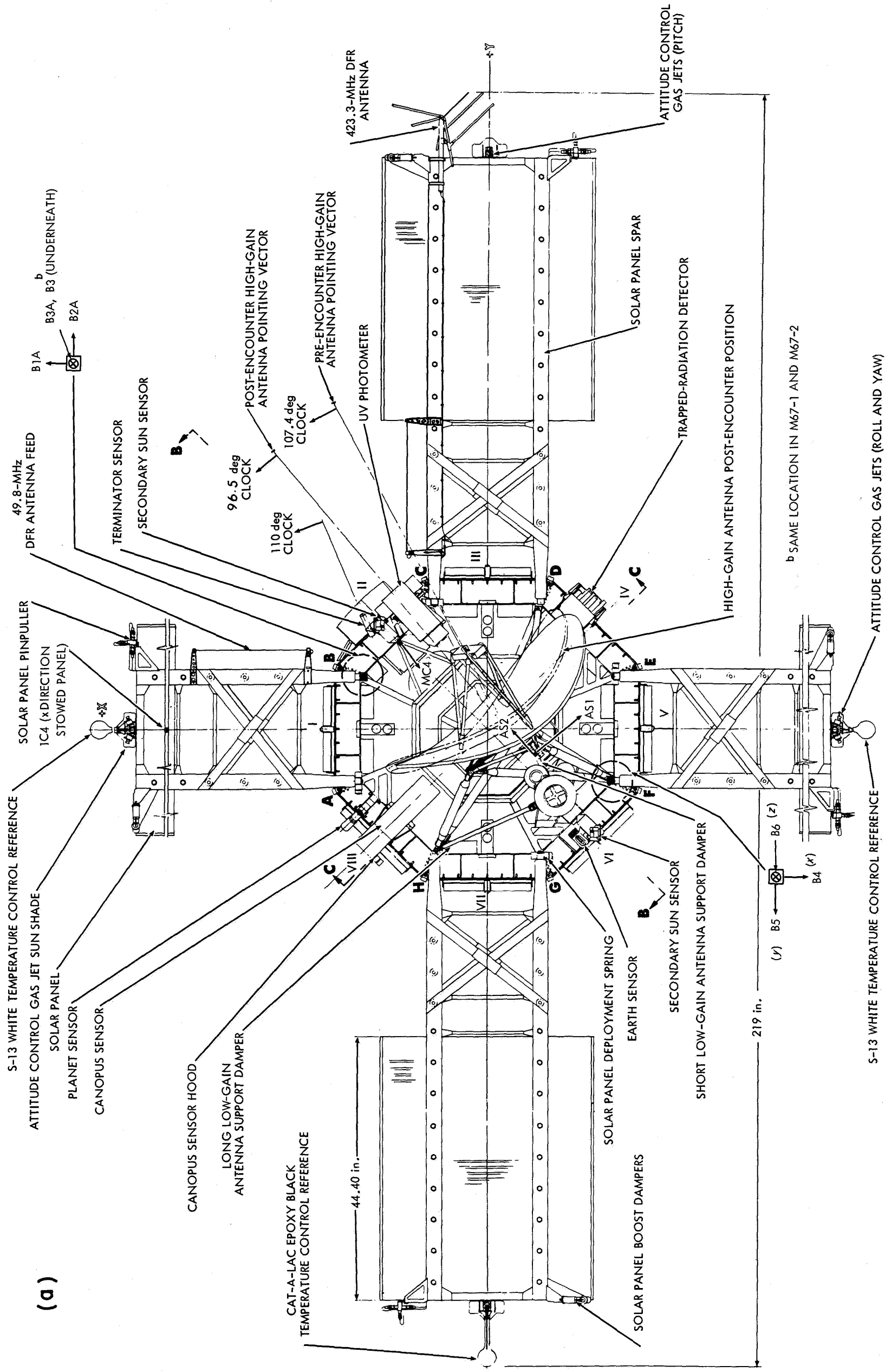


Fig. 12. Accelerometer location MCV4; midcourse motor fuel valve

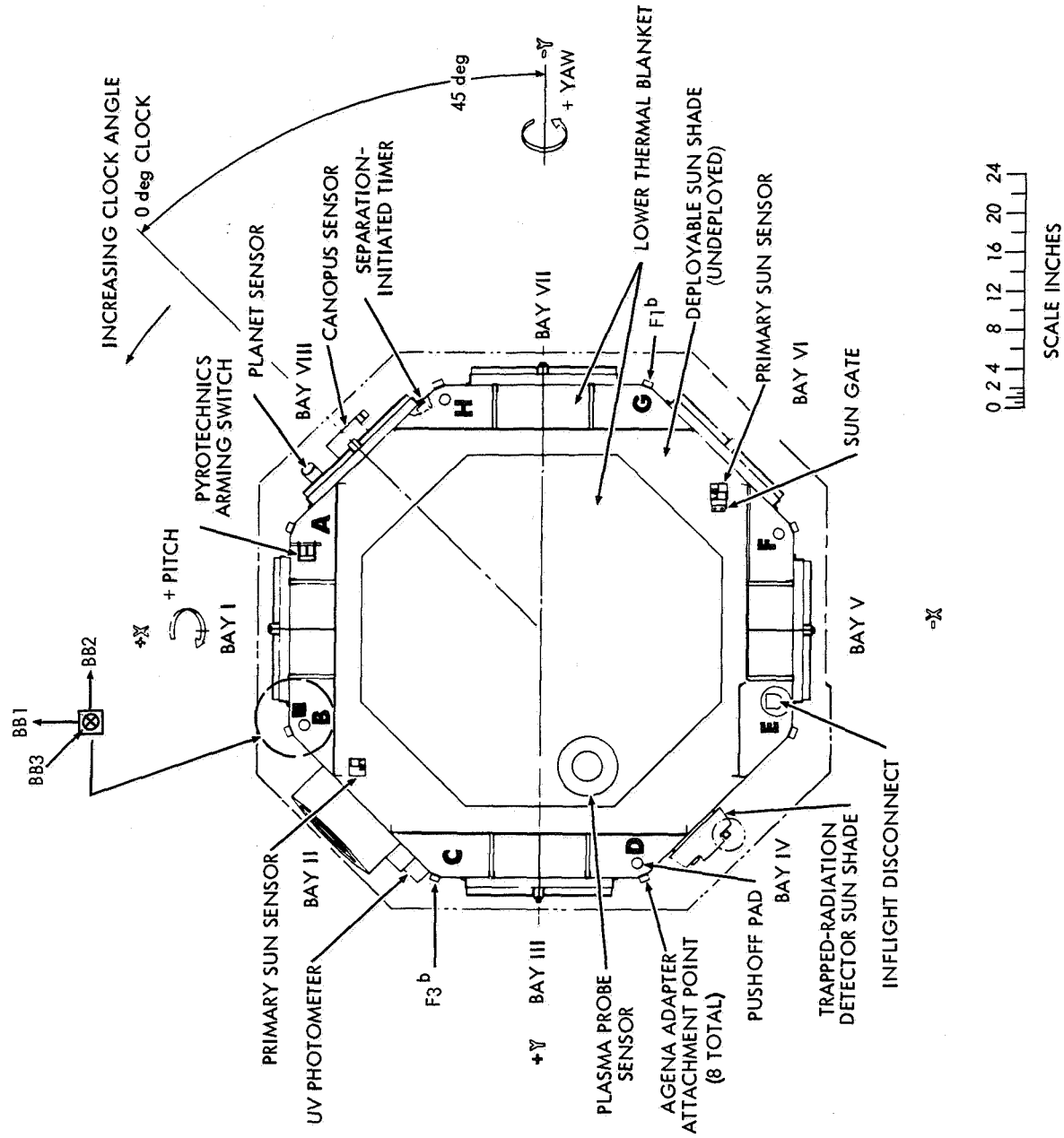




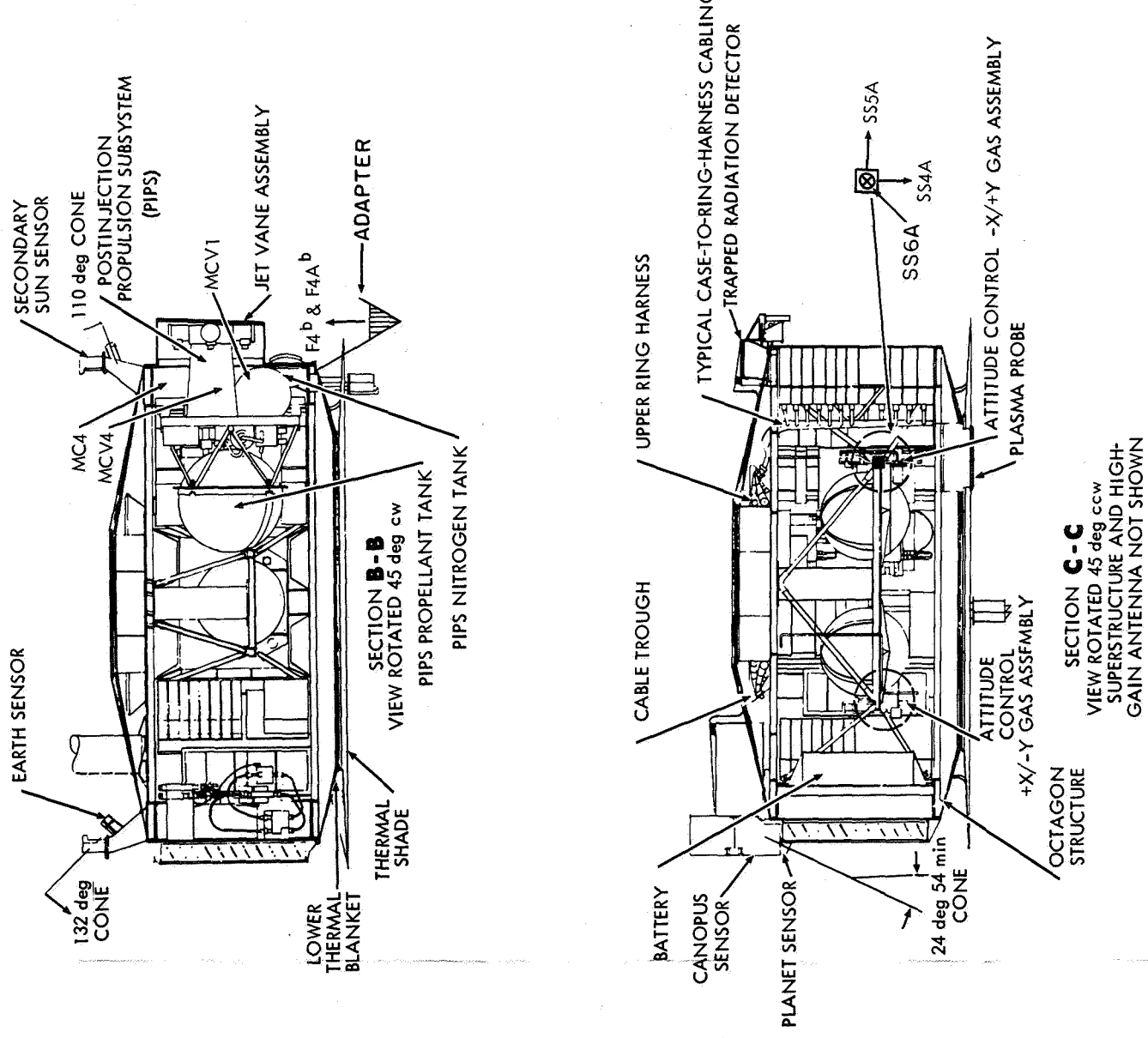


PRECEDING PAGE BLANK NOT FILMED.

(b)



(c)



FOLDOUT FRAME 23-C

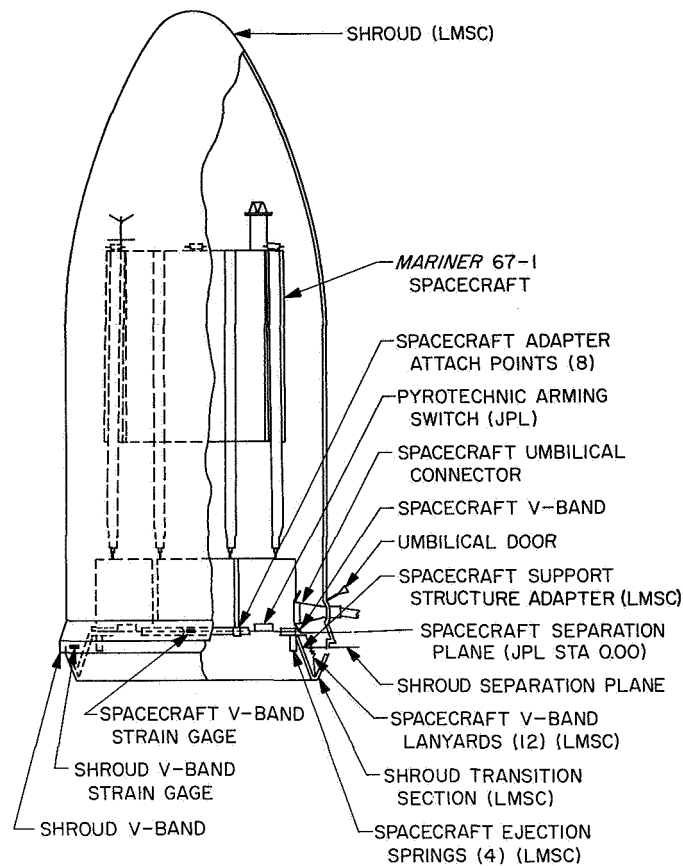
FOLDOUT FRAME

Fig. 13. M67-1 and M67-2 accelerometer locations

FOLDOUT FRAME







**Fig. 14. M67-1 spacecraft pyro test configuration showing shroud, spacecraft and adapter**

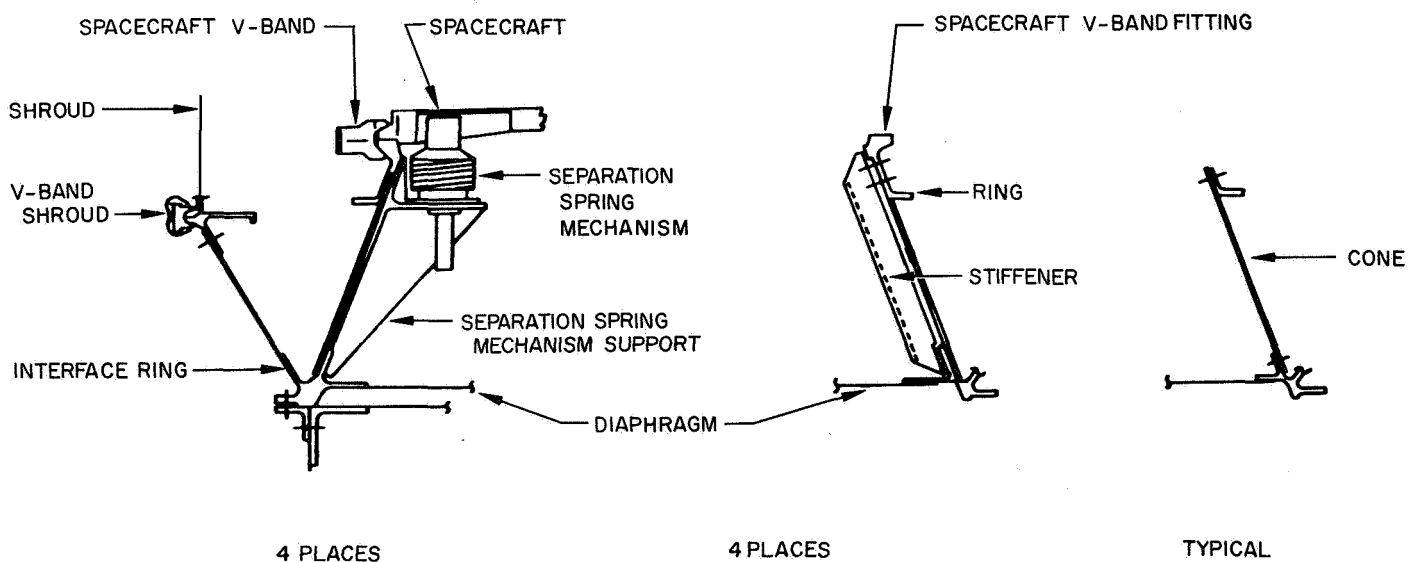


**Fig. 15. Spacecraft adapter**

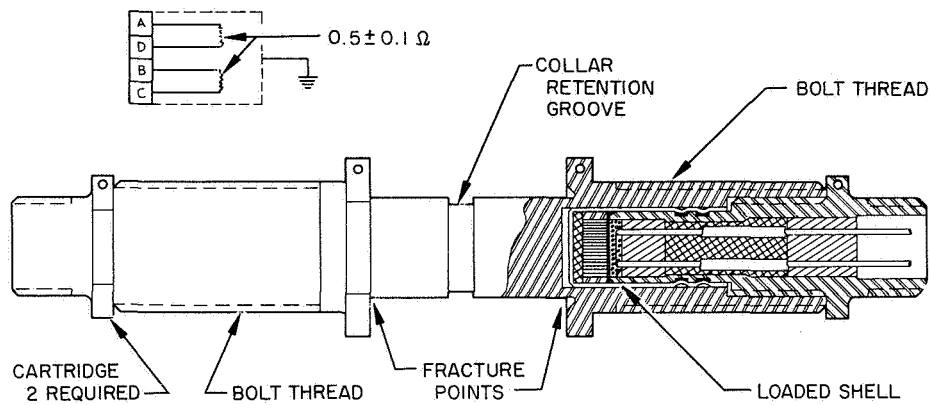


**Fig. 16. Shroud V-band explosive bolt release assembly**

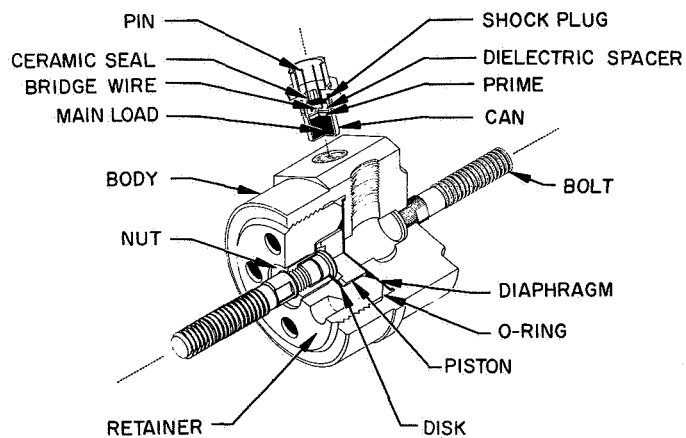


**Fig. 17. Spacecraft V-band release assembly**

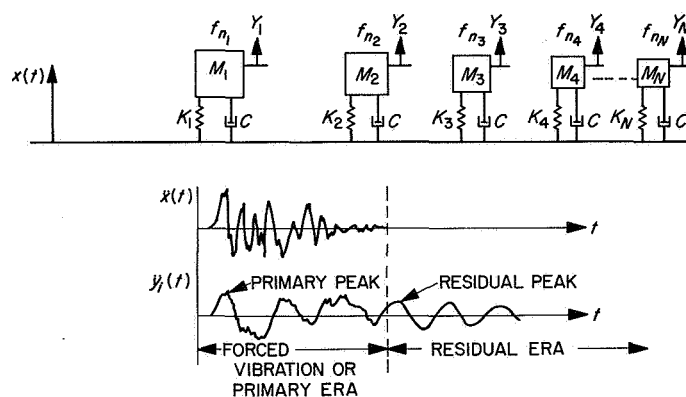


**Fig. 18. One-degree-of-freedom oscillator model for shock spectra representation**

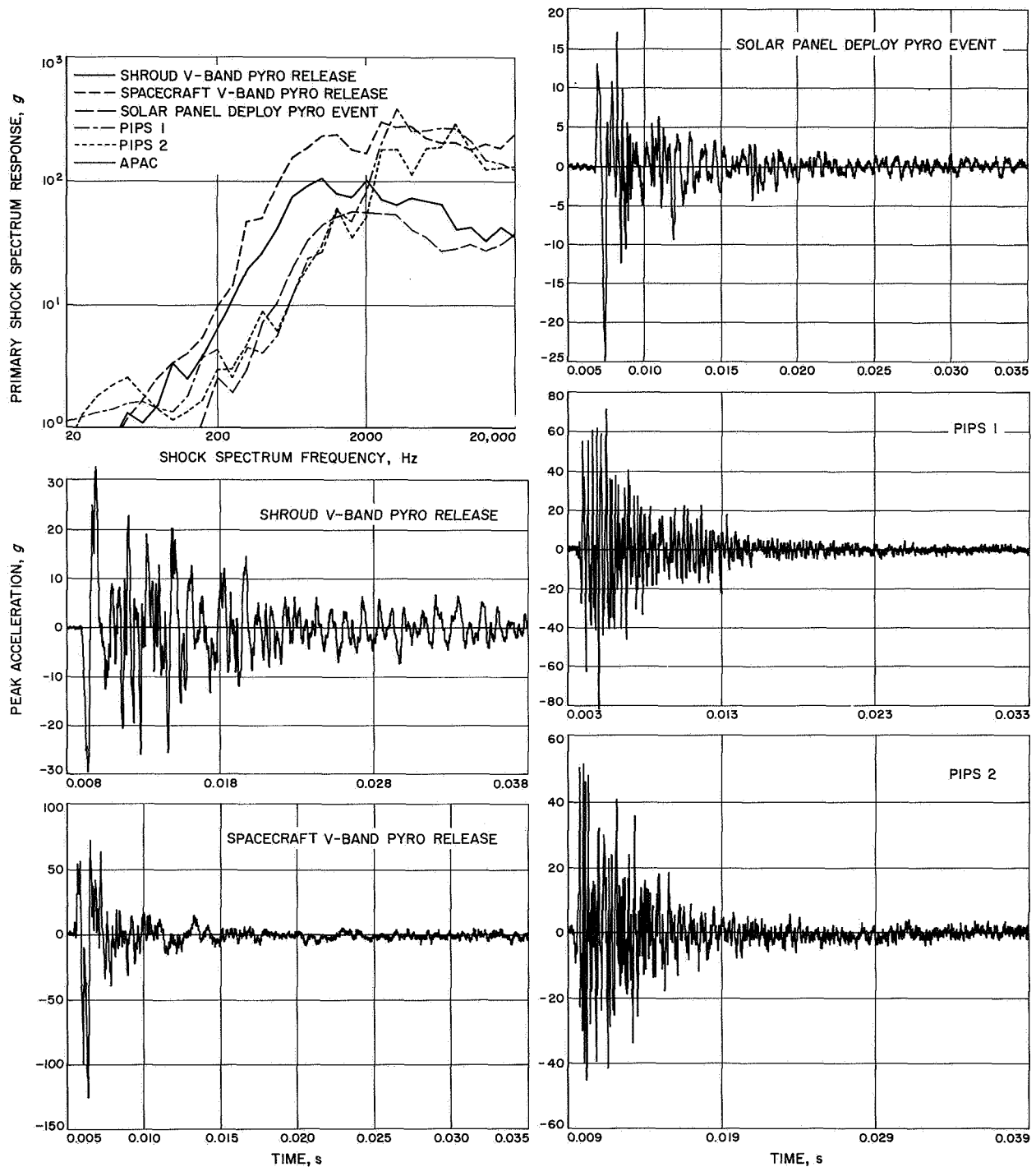


Fig. 19. M67-1 primary shock spectra composite and transient-time history at accelerometer B3

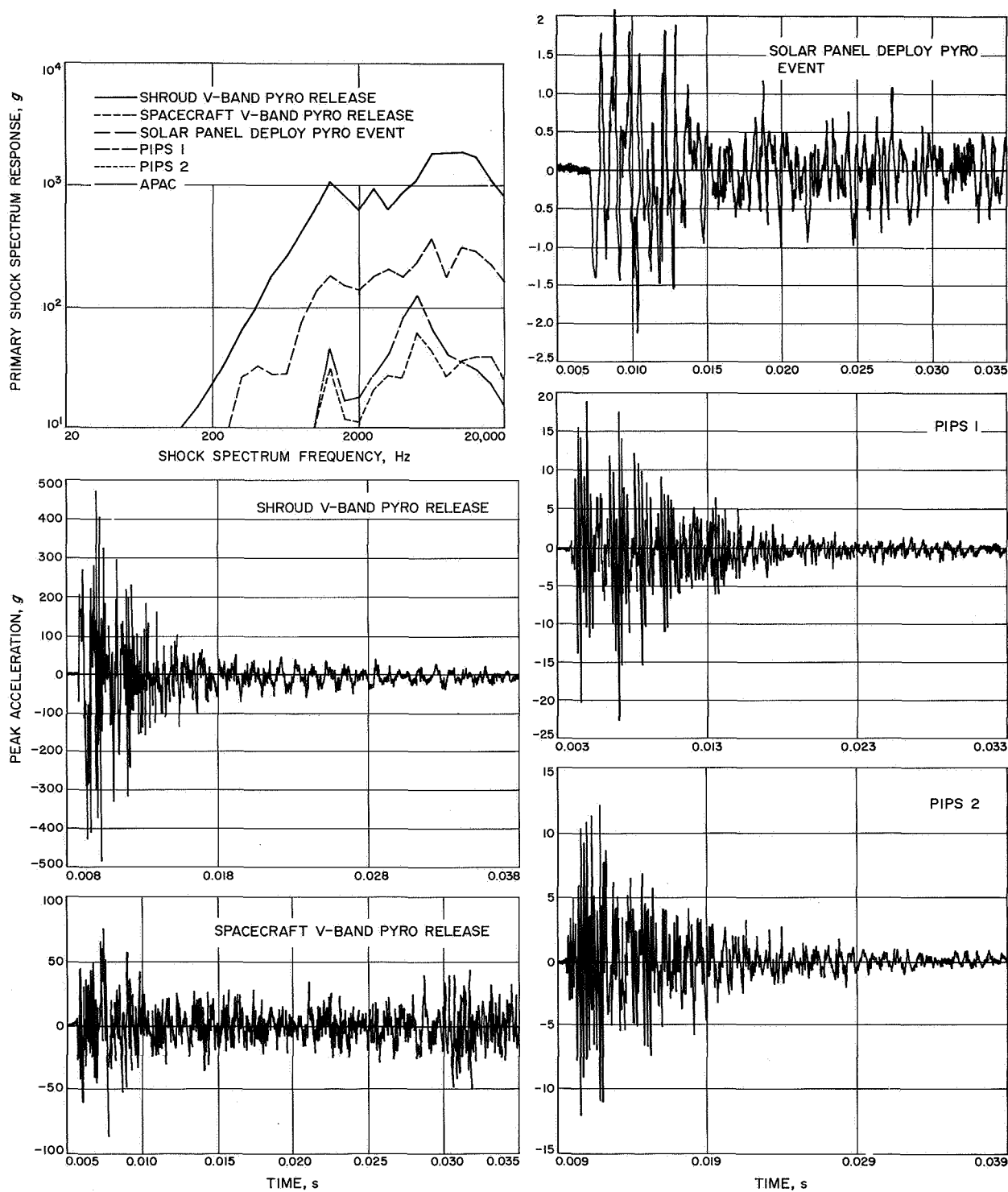


Fig. 20. M67-1 primary shock spectra composite and transient-time history at accelerometer F4

FOLDOUT FRAME 29-A

FOLDOUT FRAME

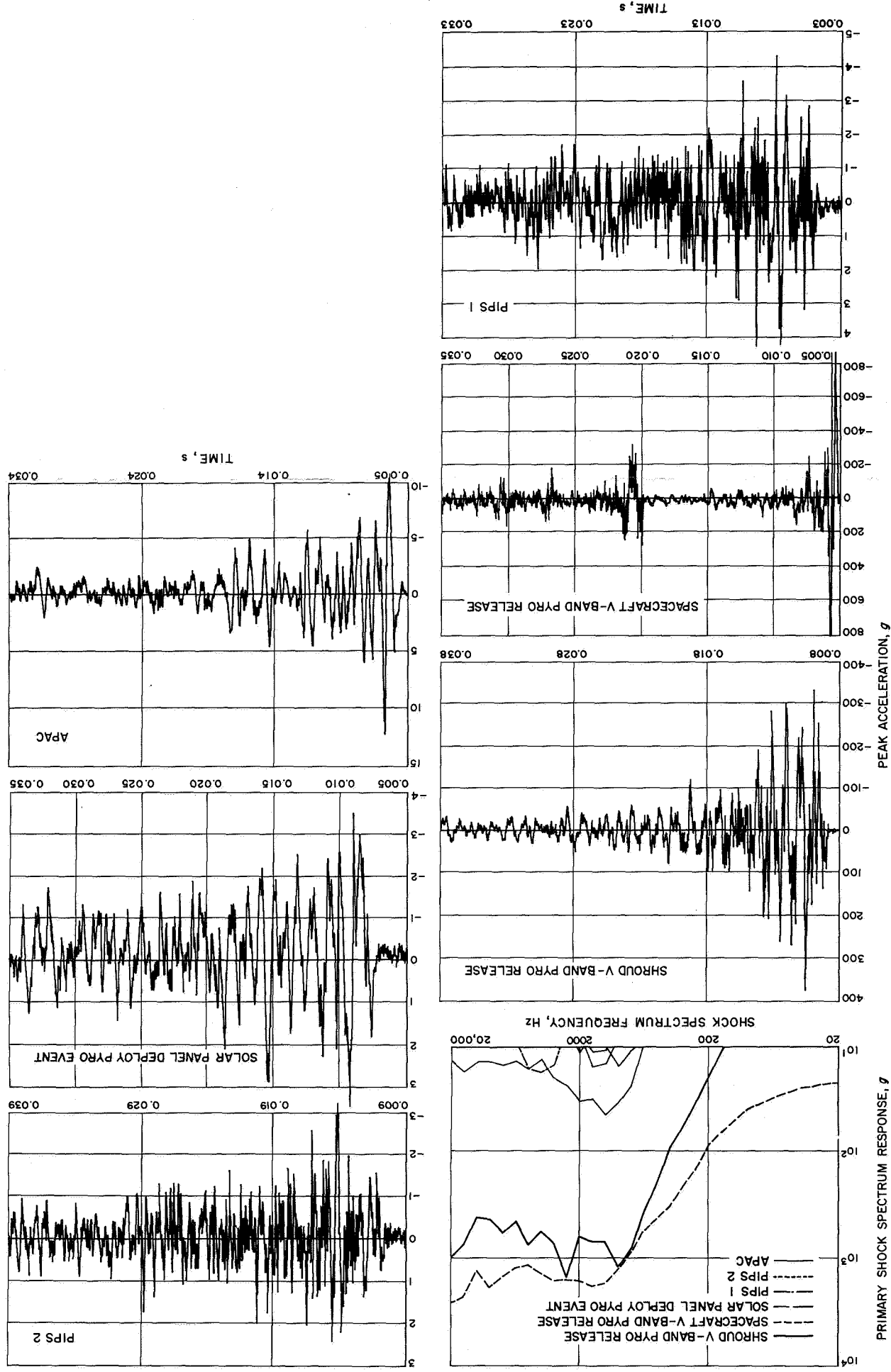


Fig. 21. M67-1 primary shock spectra composite and transient-time history at accelerometer F1



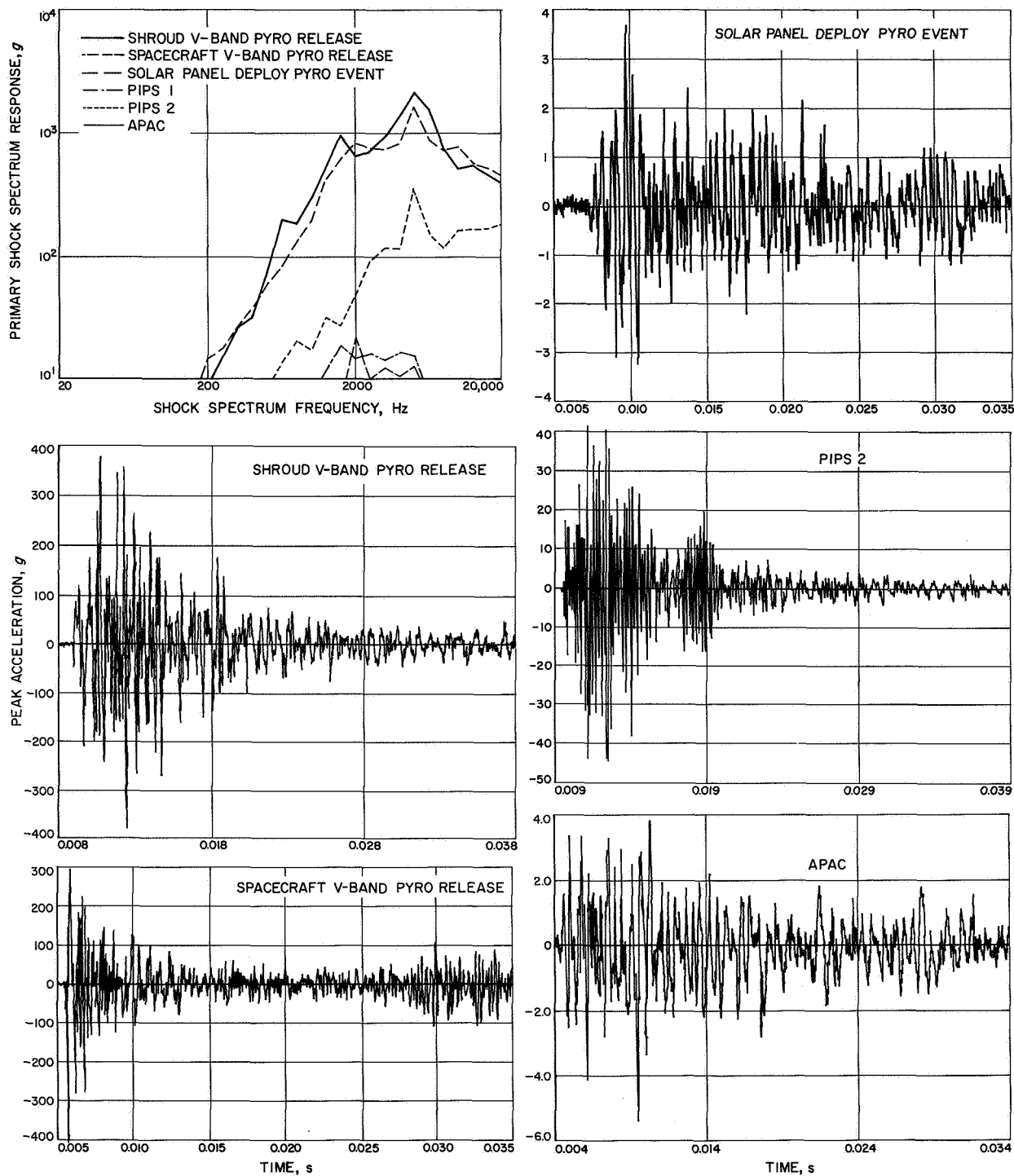


Fig. 22. M67-1 primary shock spectra composite and transient-time history at accelerometer F3

PRECEDING PAGE BLANK NOT FILMED.

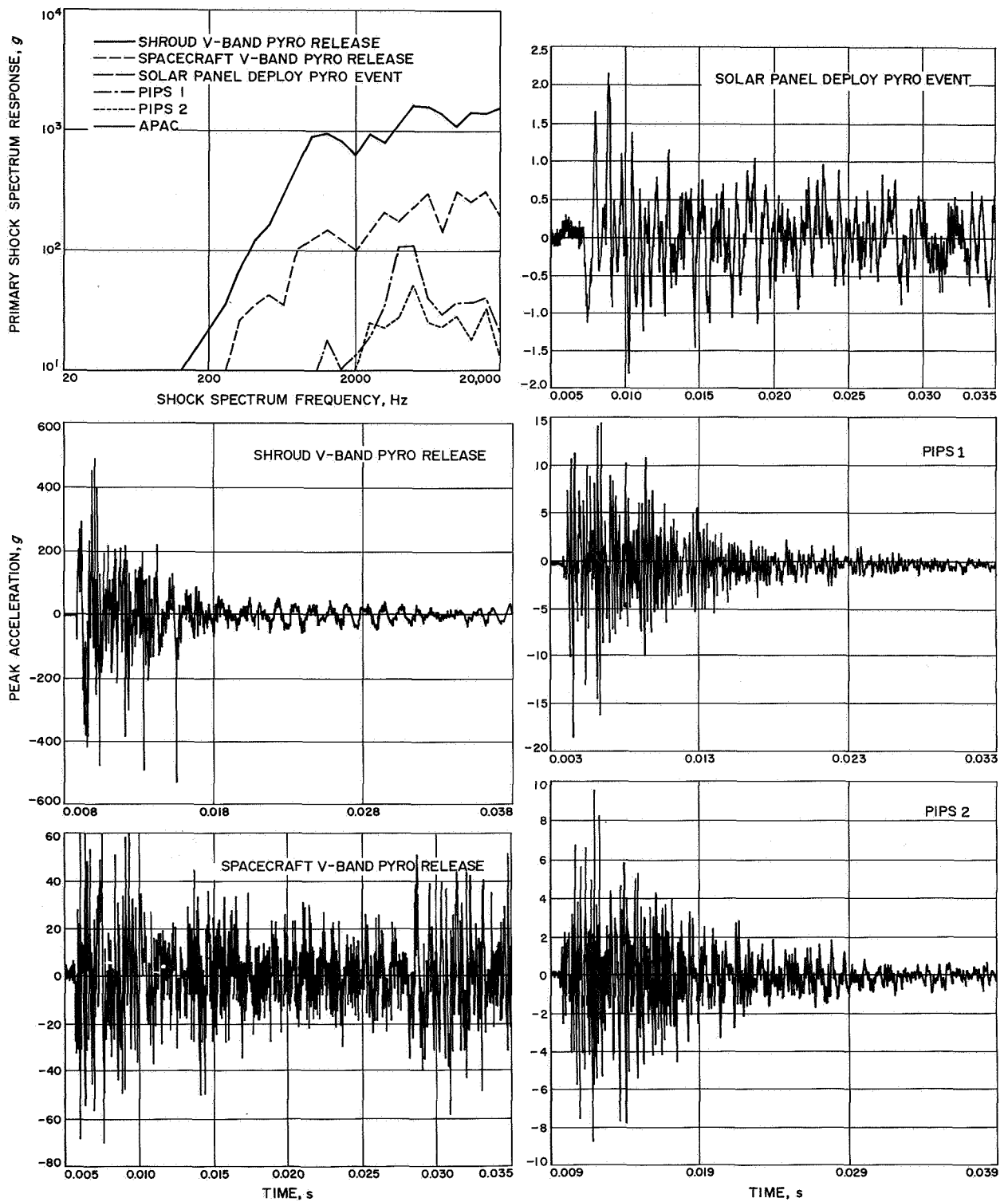


Fig. 23. M67-1 primary shock spectra composite and transient-time history at accelerometer F4A



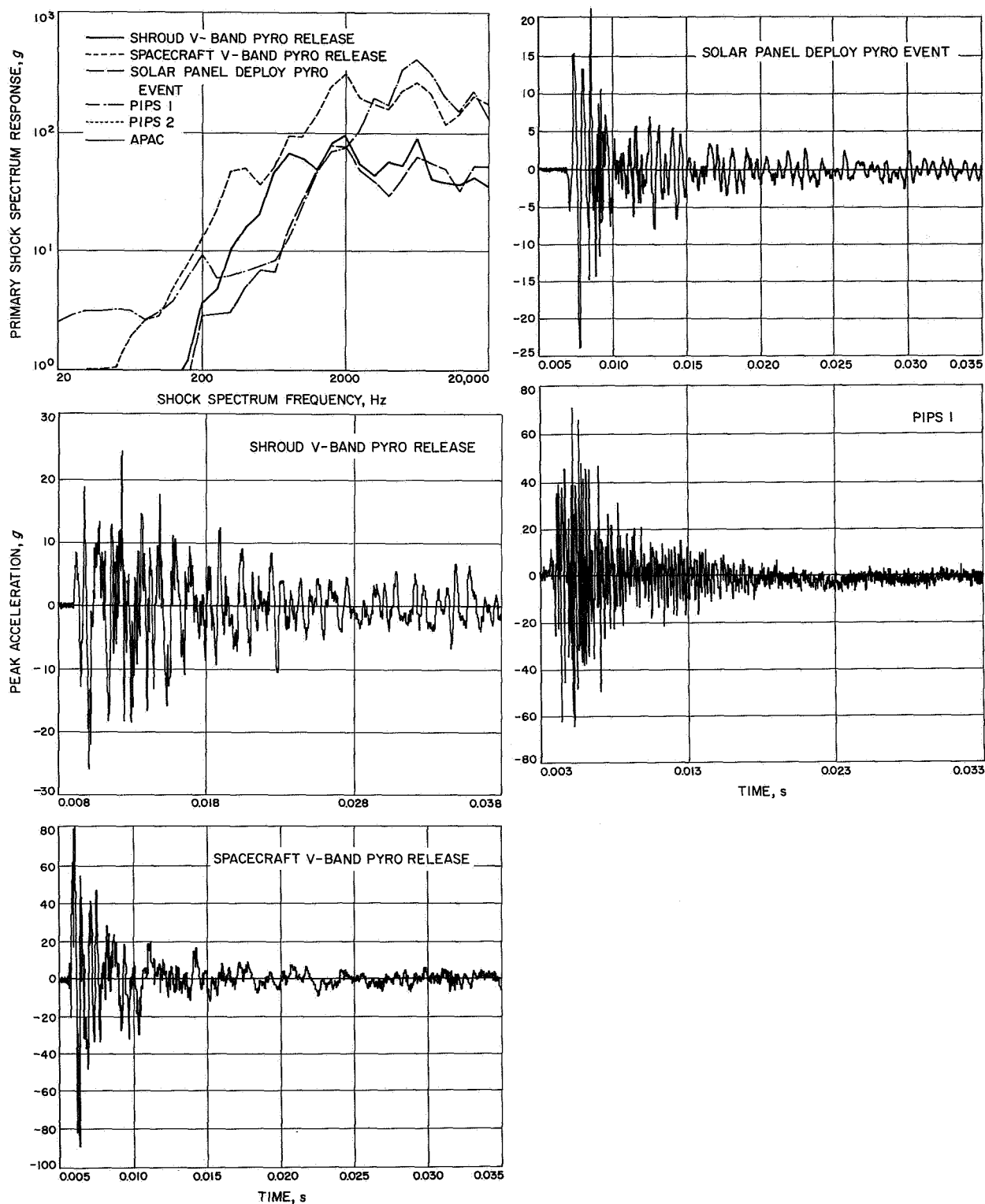


Fig. 24. M67-1 primary shock spectra composite and transient-time history at accelerometer B1A

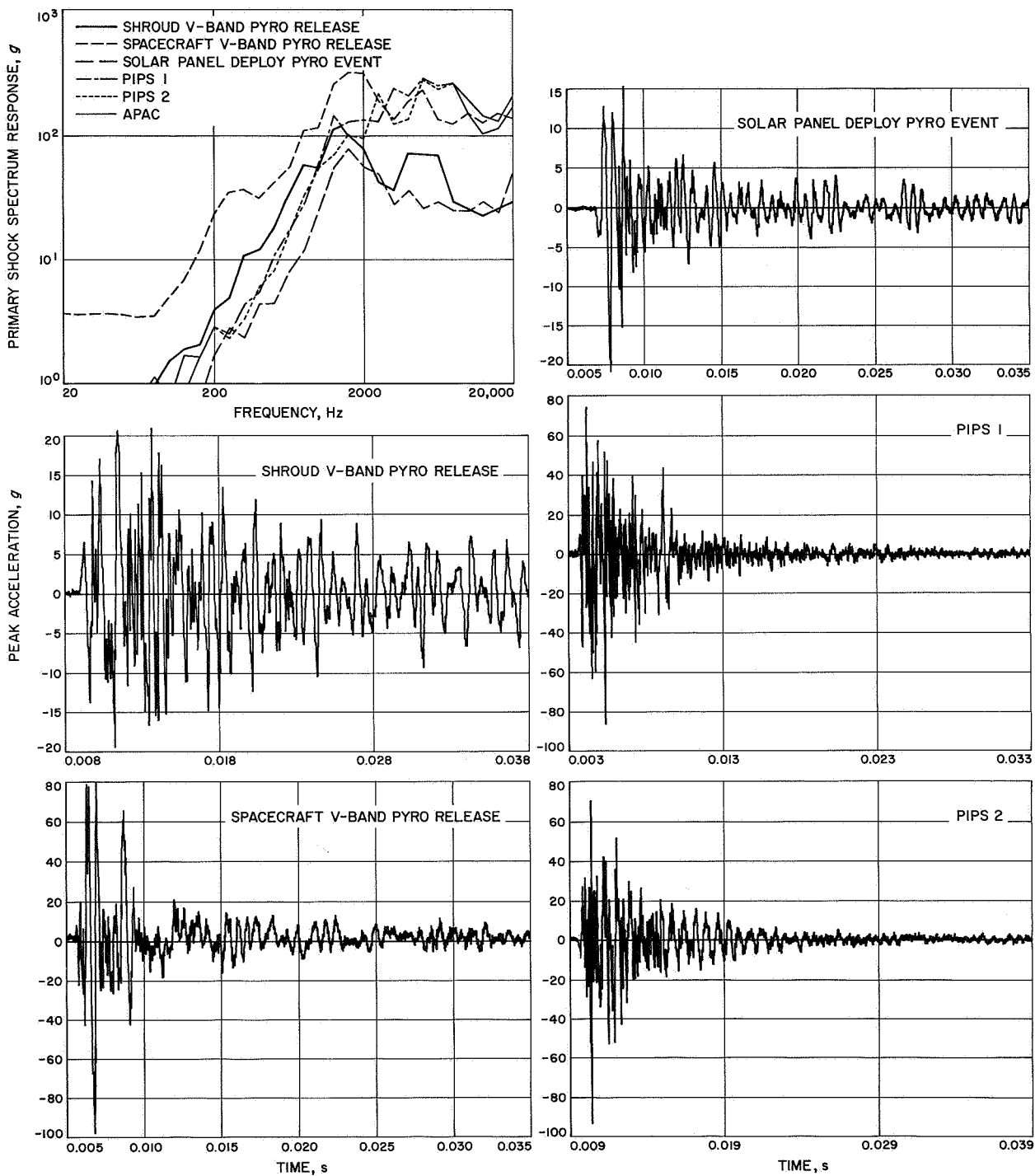


Fig. 25. M67-1 primary shock spectra composite and transient-time history at accelerometer B2A

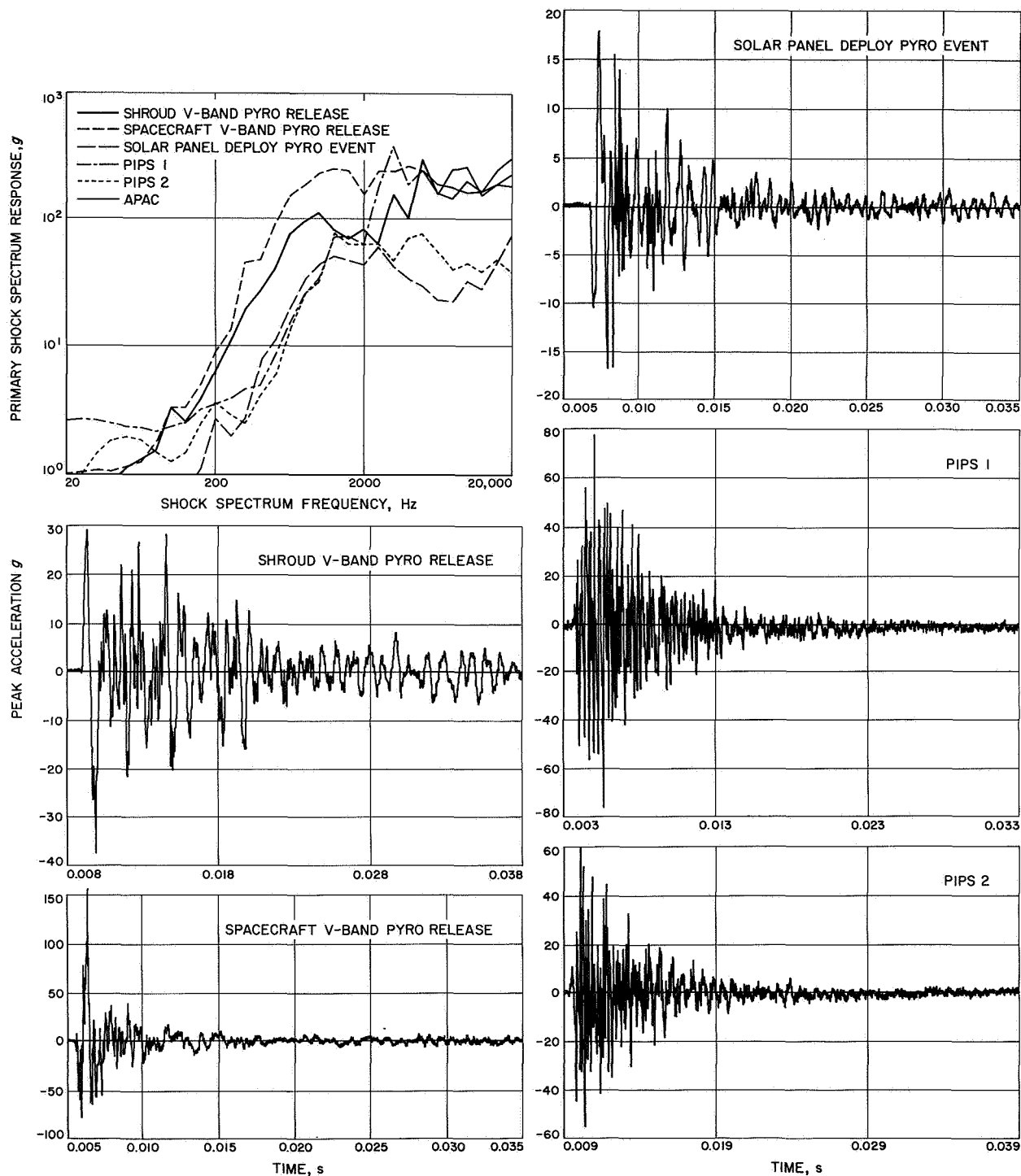


Fig. 26. M67-1 primary shock spectra composite and transient-time history at accelerometer B3A

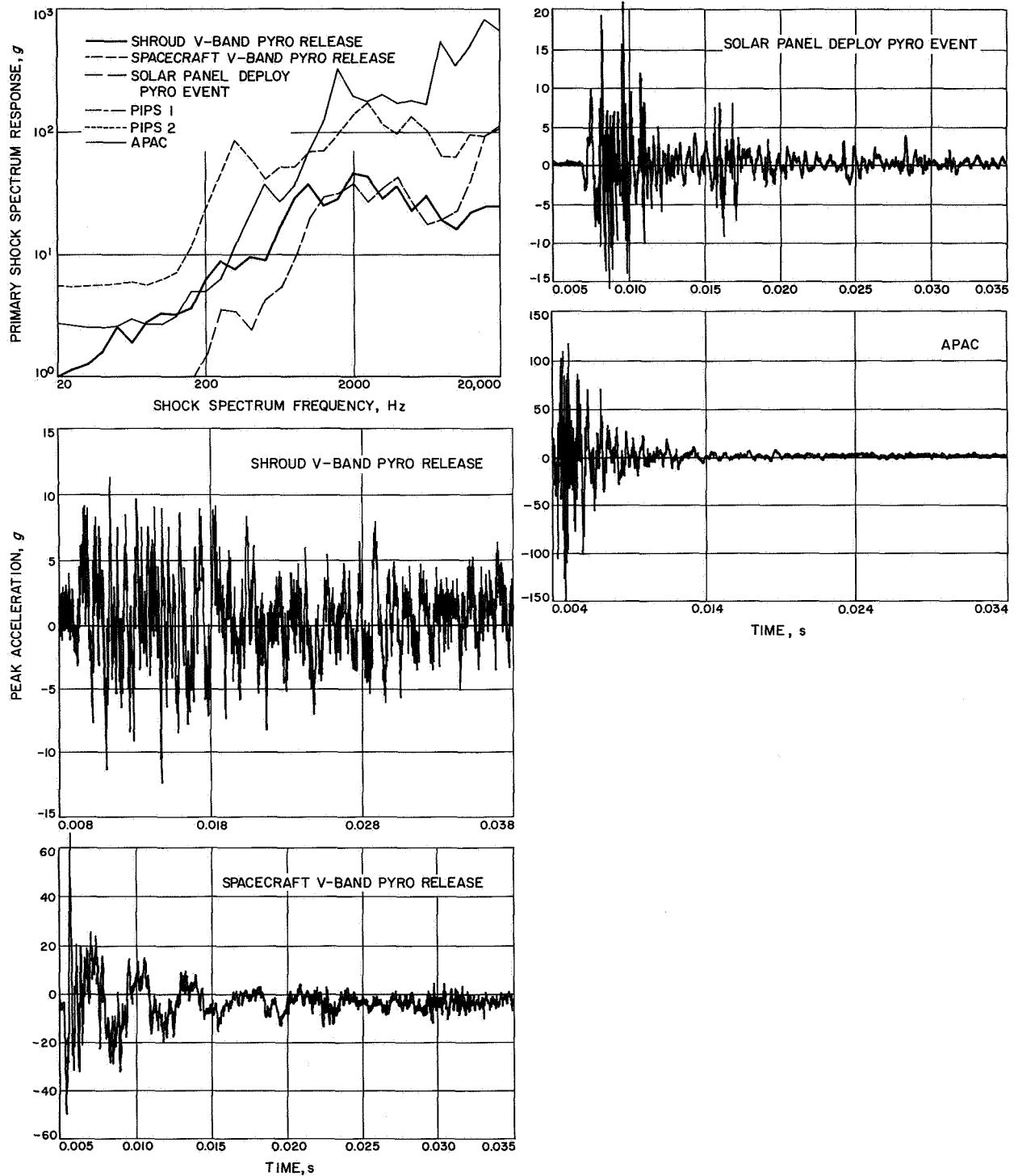


Fig. 27. M67-1 primary shock spectra composite and transient-time history at accelerometer B4

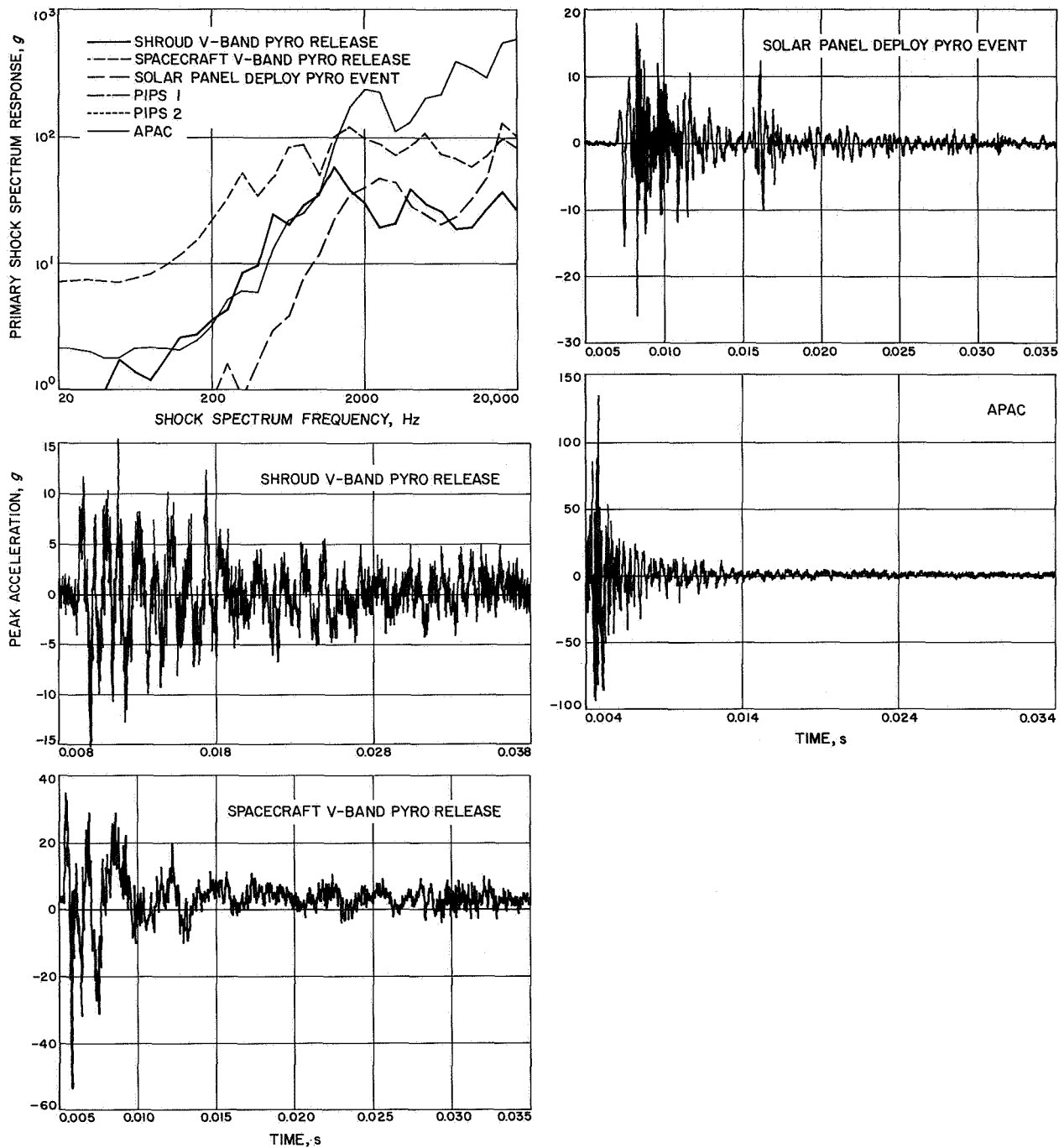


Fig. 28. M67-1 primary shock spectra composite and transient-time history at accelerometer B5

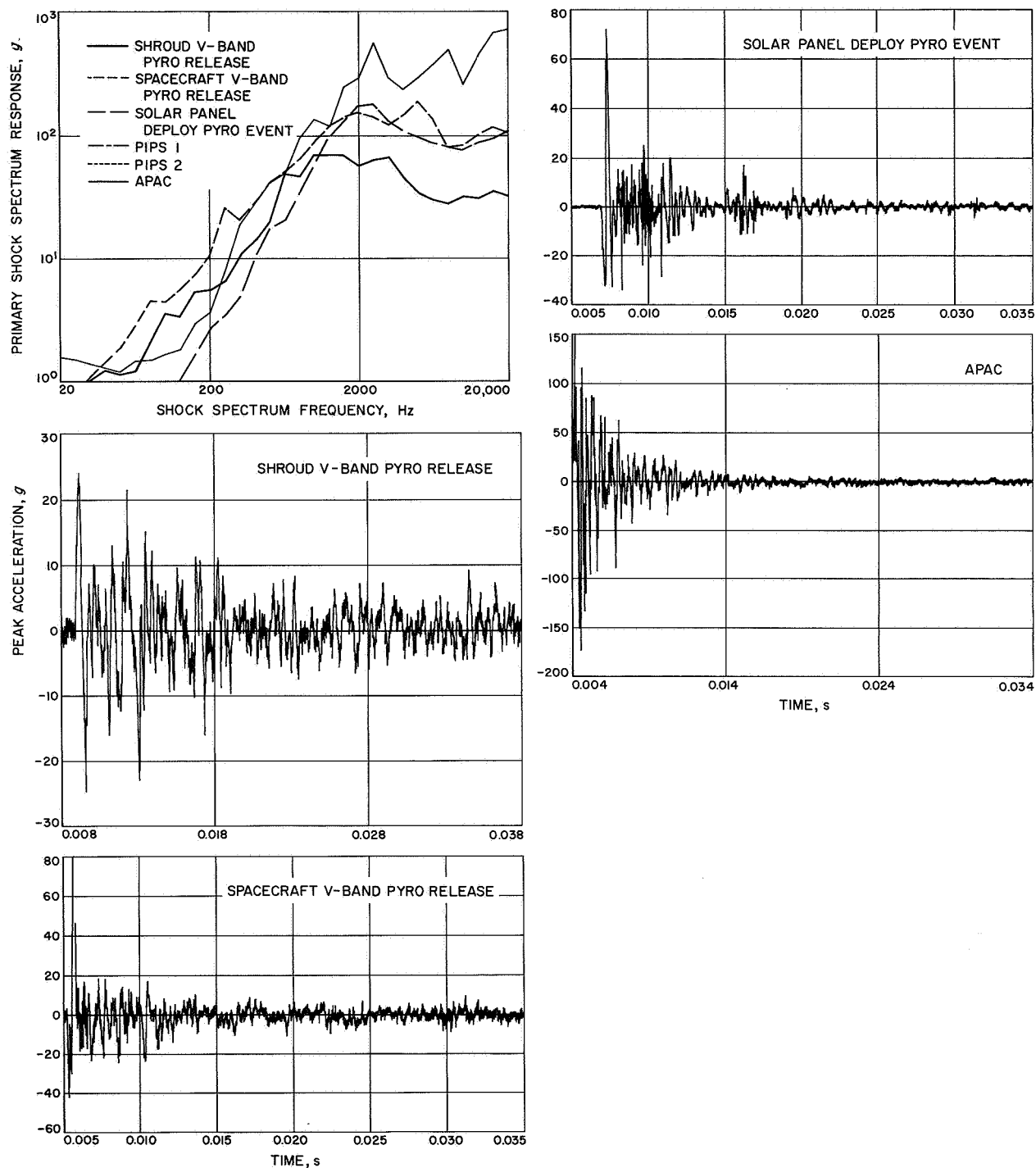


Fig. 29. M67-1 primary shock spectra composite and transient-time history at accelerometer B6

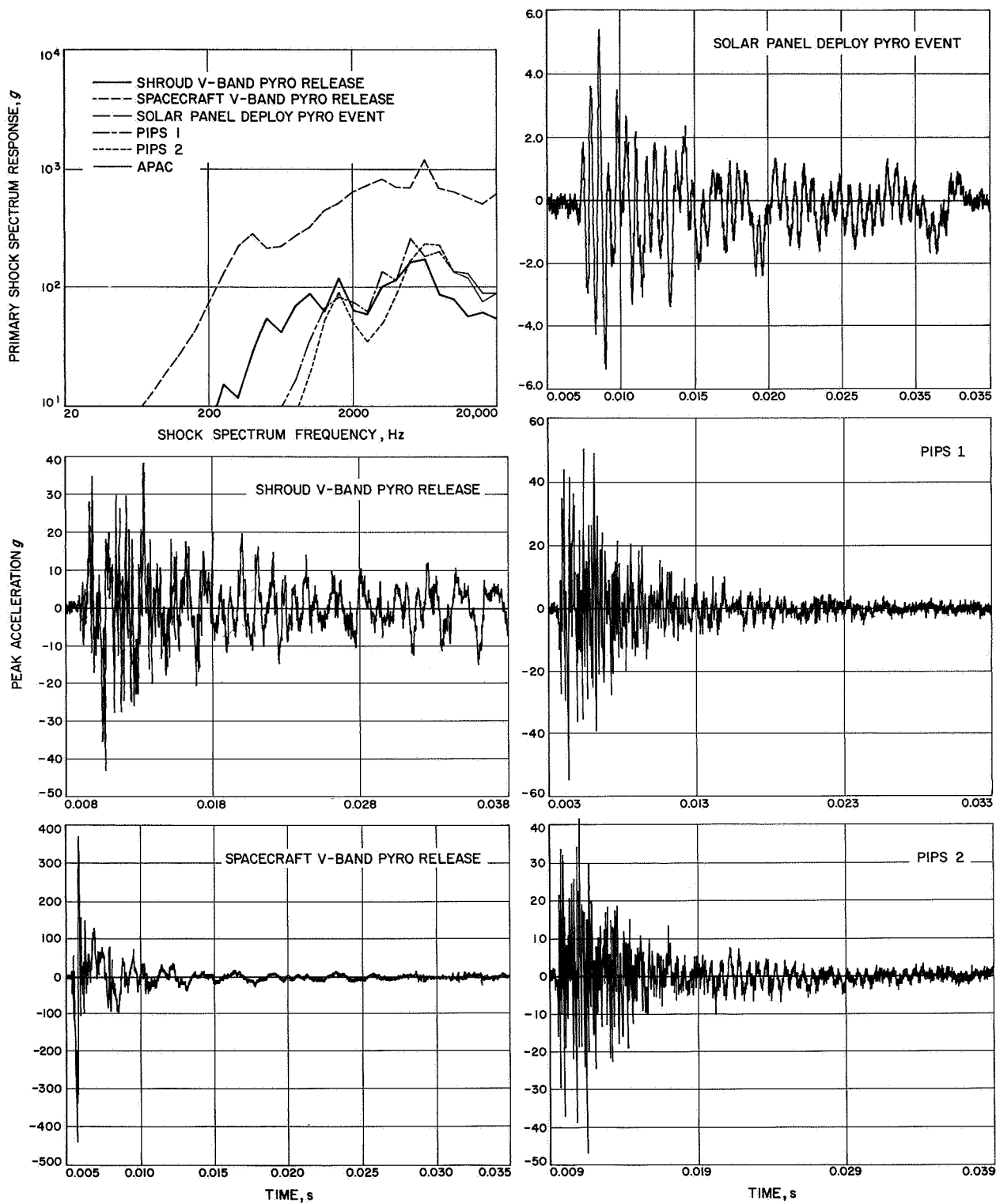


Fig. 30. M67-1 primary shock spectra composite and transient-time history at accelerometer BB1

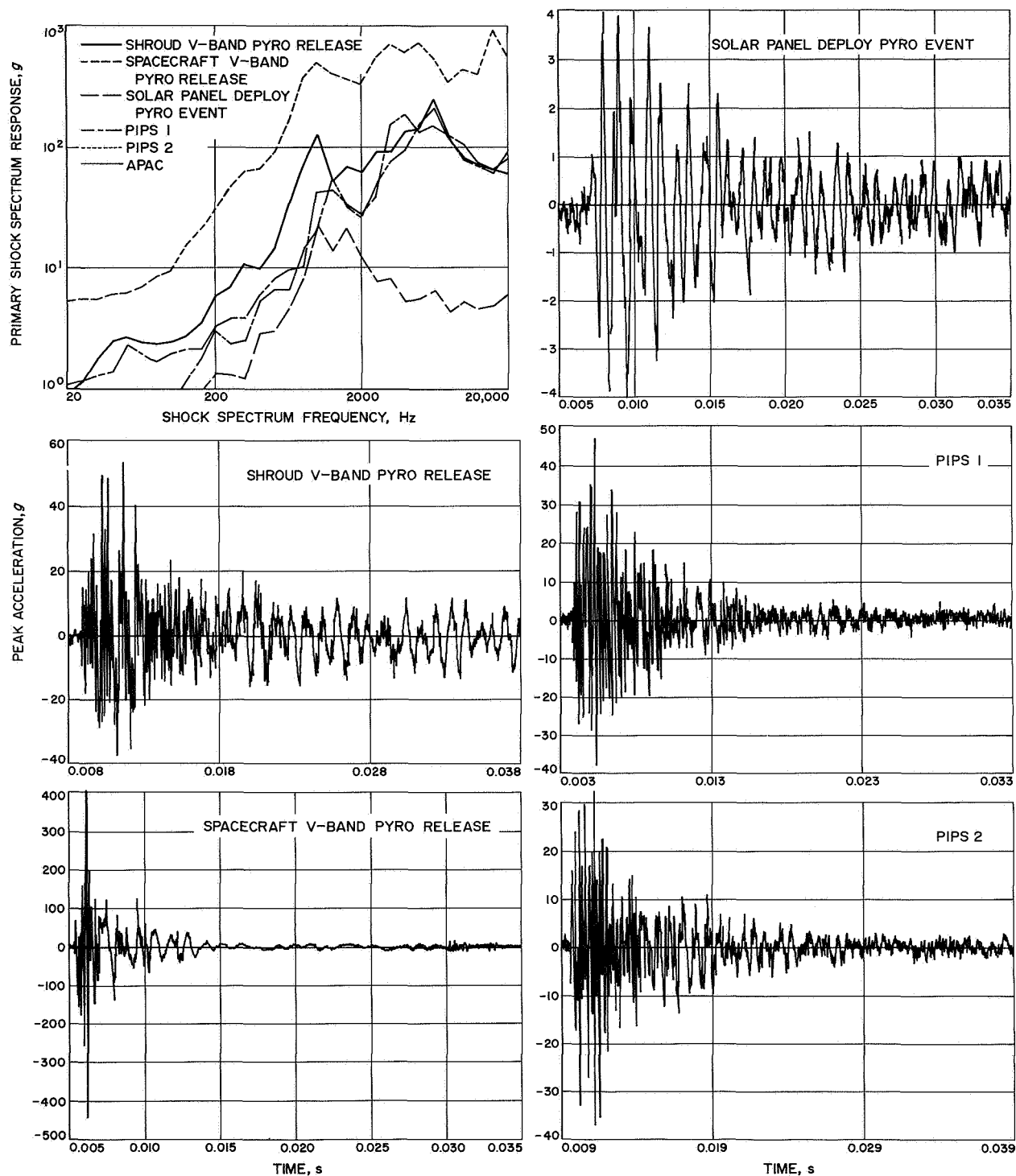


Fig. 31. M67-1 primary shock spectra composite and transient-time history at accelerometer BB2



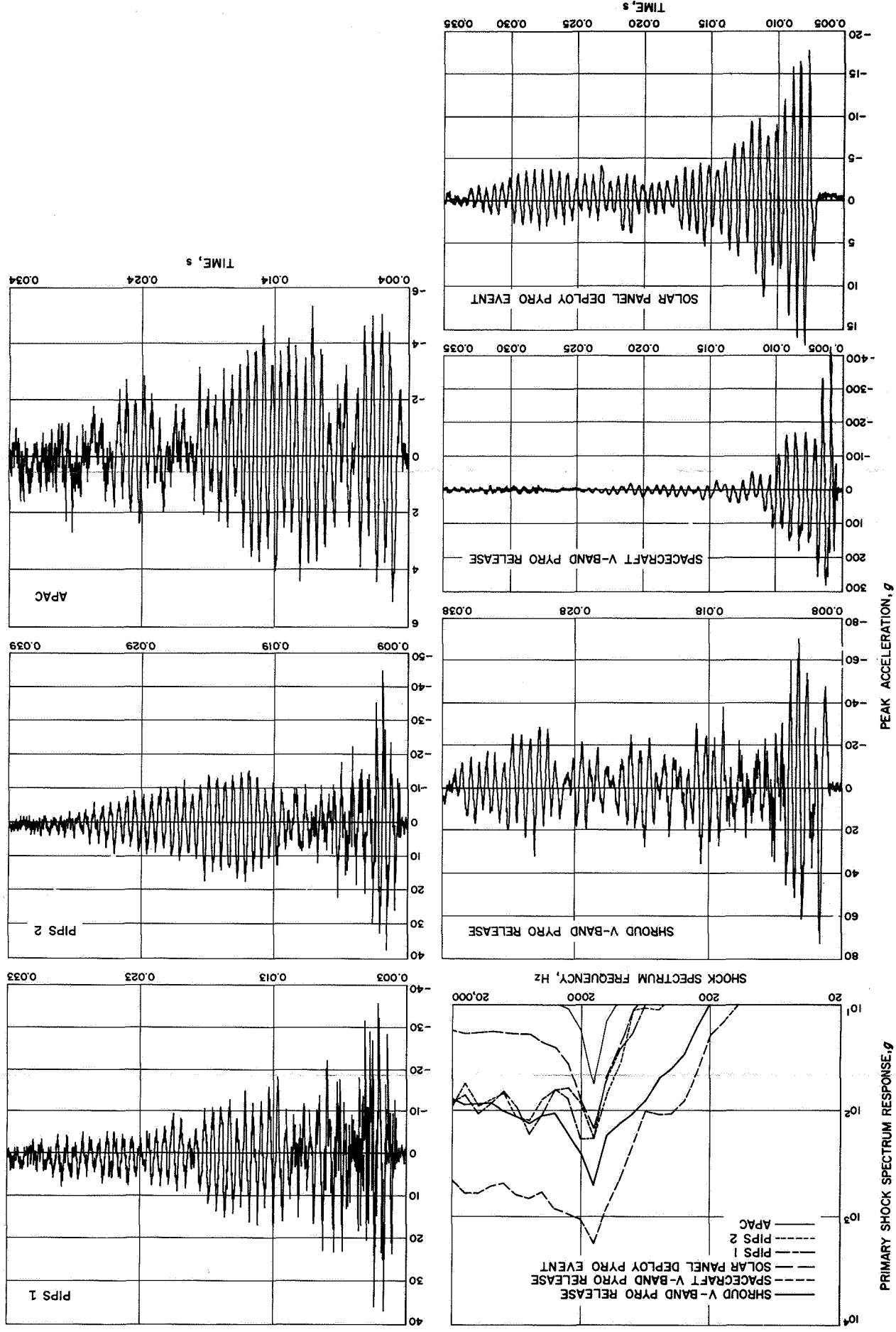


Fig. 32. M67-1 primary shock spectra composite and transient-time history at accelerometer BB3

FOLDOUT FRAME

JPL TECHNICAL REPORT 32-1218

FOLDOUT FRAME 41-A

41-B



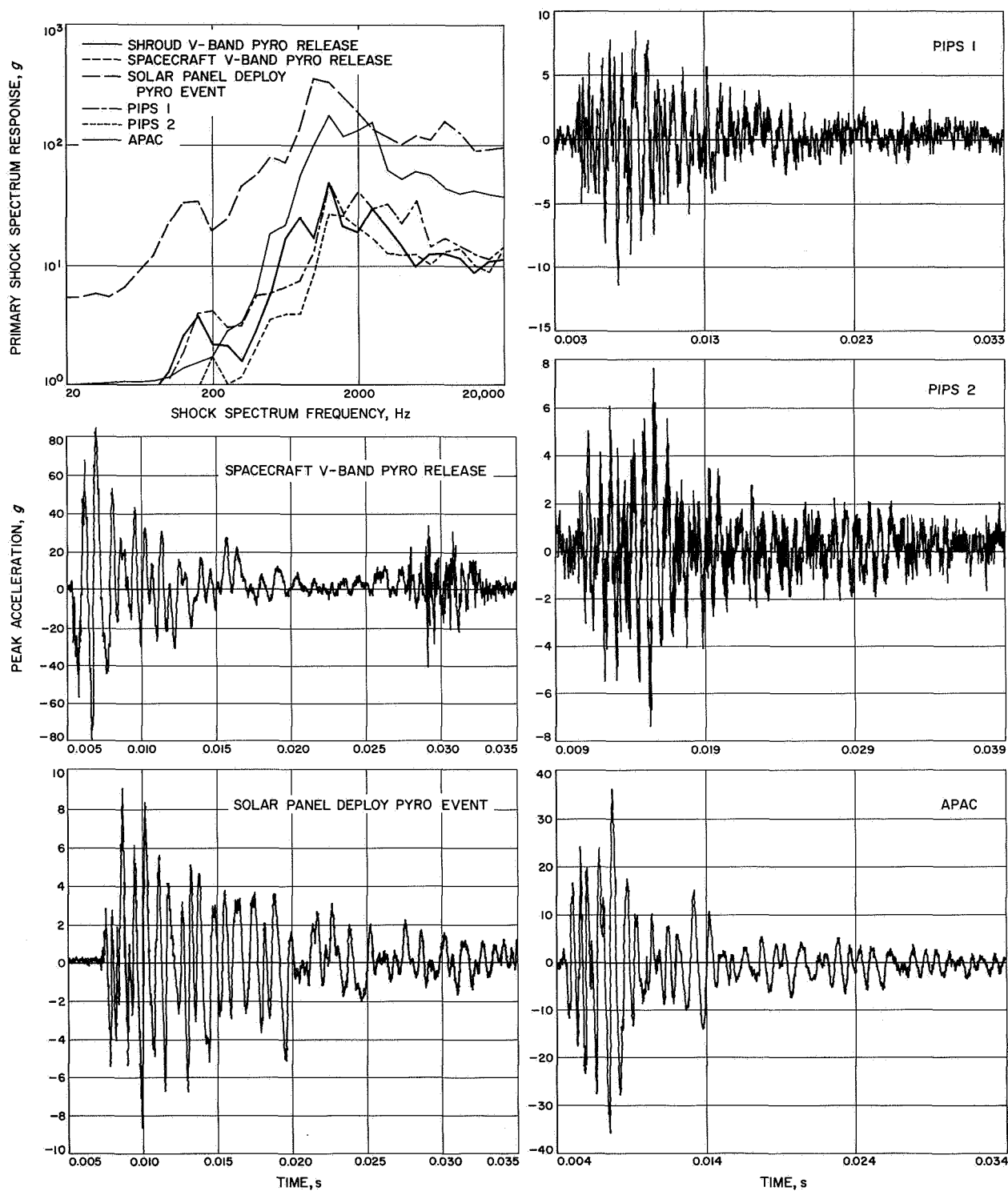


Fig. 33. M67-1 primary shock spectra composite and transient-time history at accelerometer SS4A

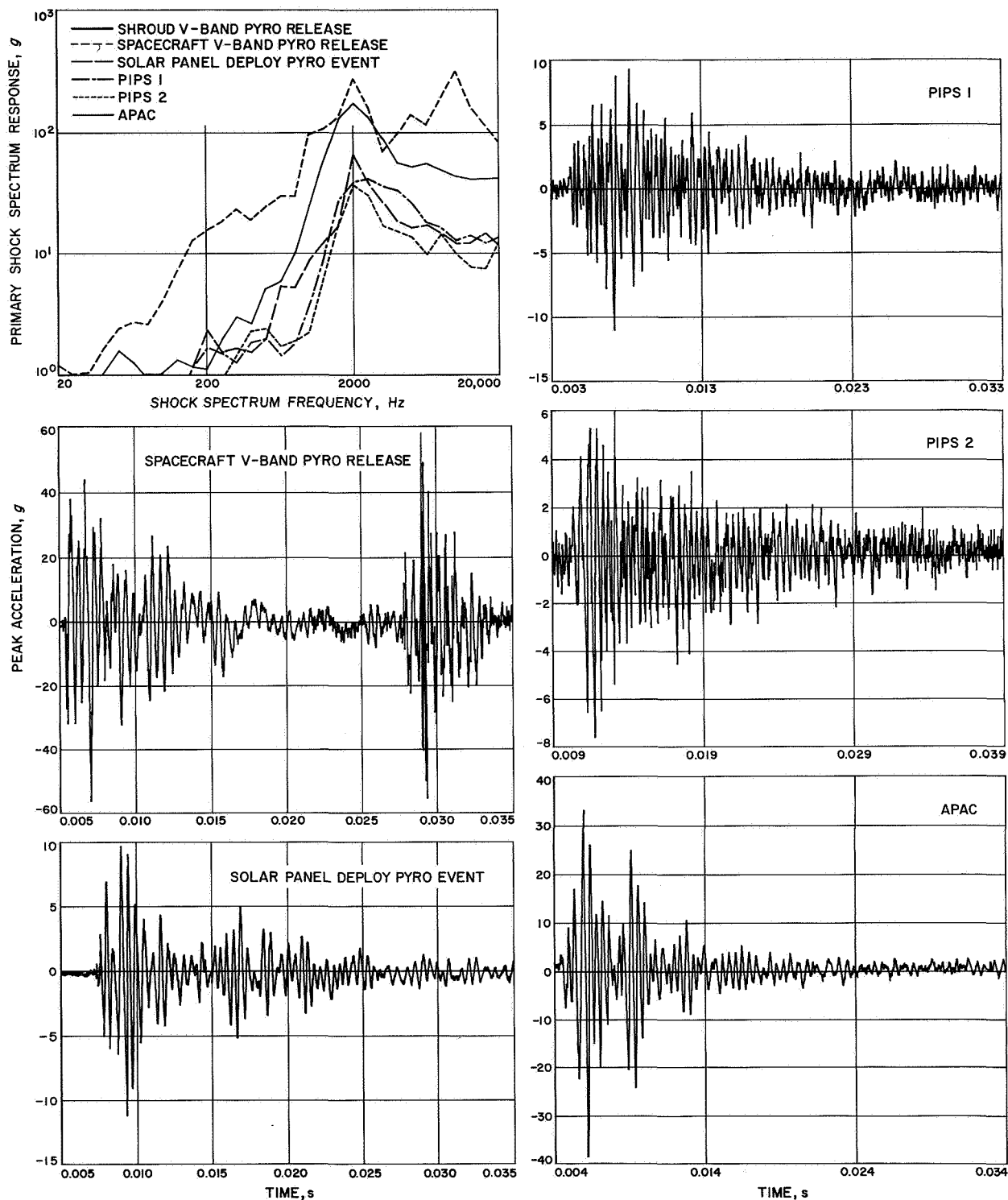


Fig. 34. M67-1 primary shock spectra composite and transient-time history at accelerometer SS5A

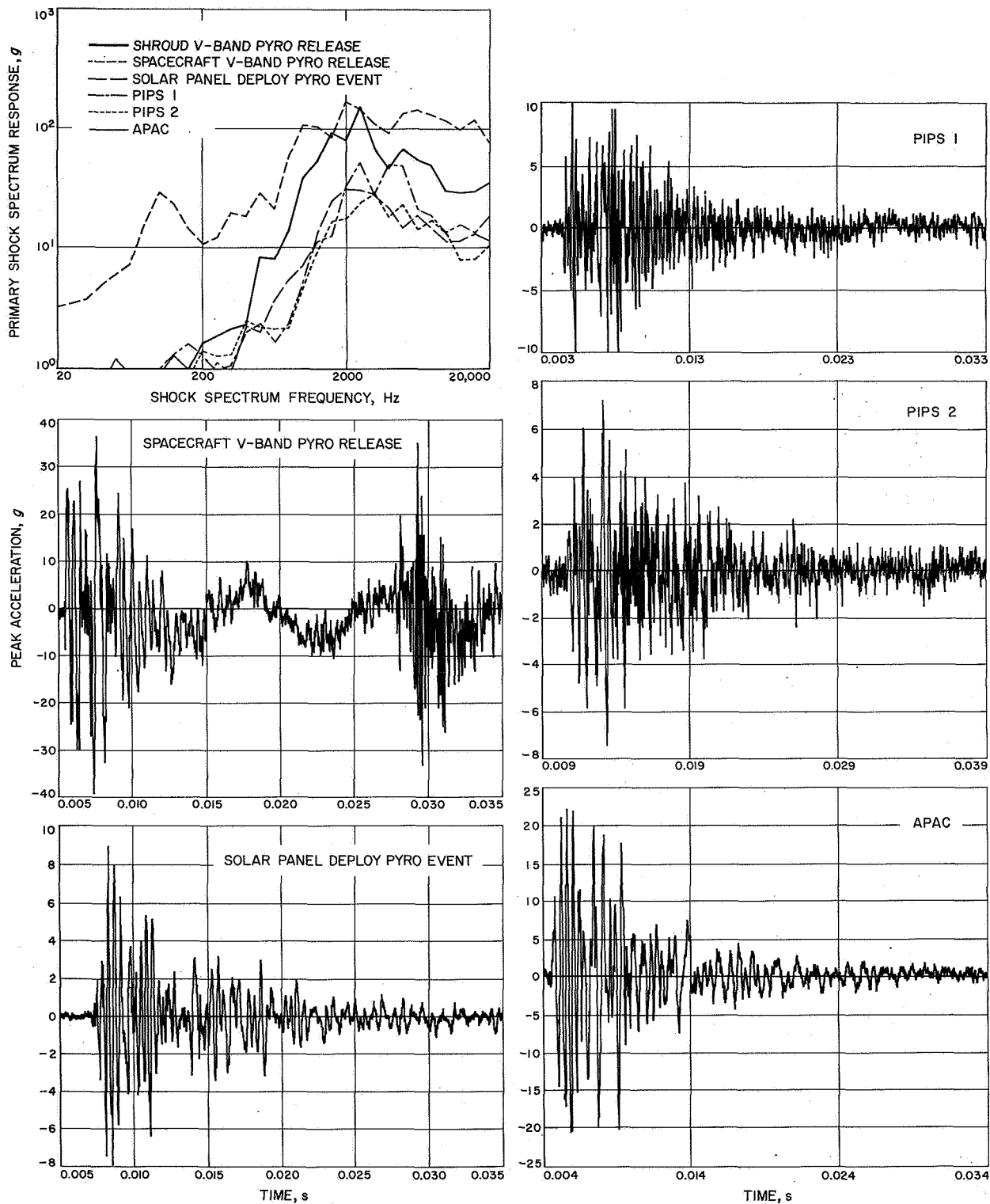
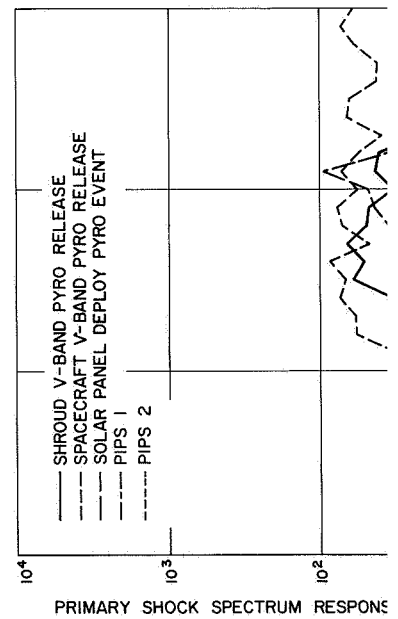
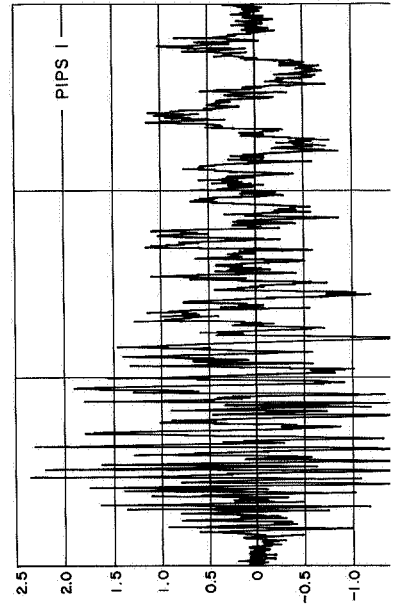


Fig. 35. M67-1 primary shock spectra composite and transient-time history at accelerometer SS6A





# PART A



FOLDOUT FRAME

PART B

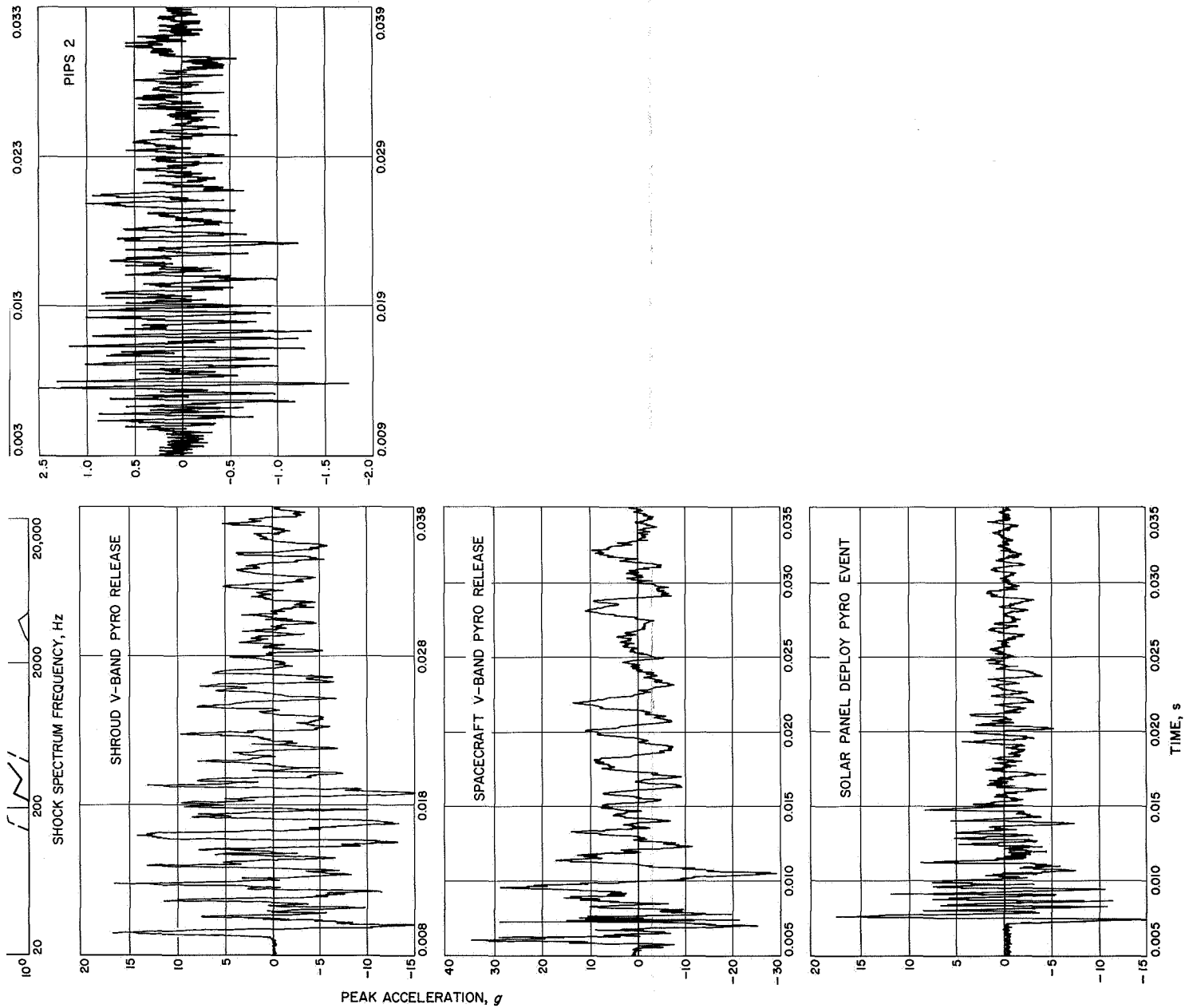


Fig. 36. M67-1 primary shock spectra composite and transient-time history at accelerometer ASI

FOLDOUT FRAME



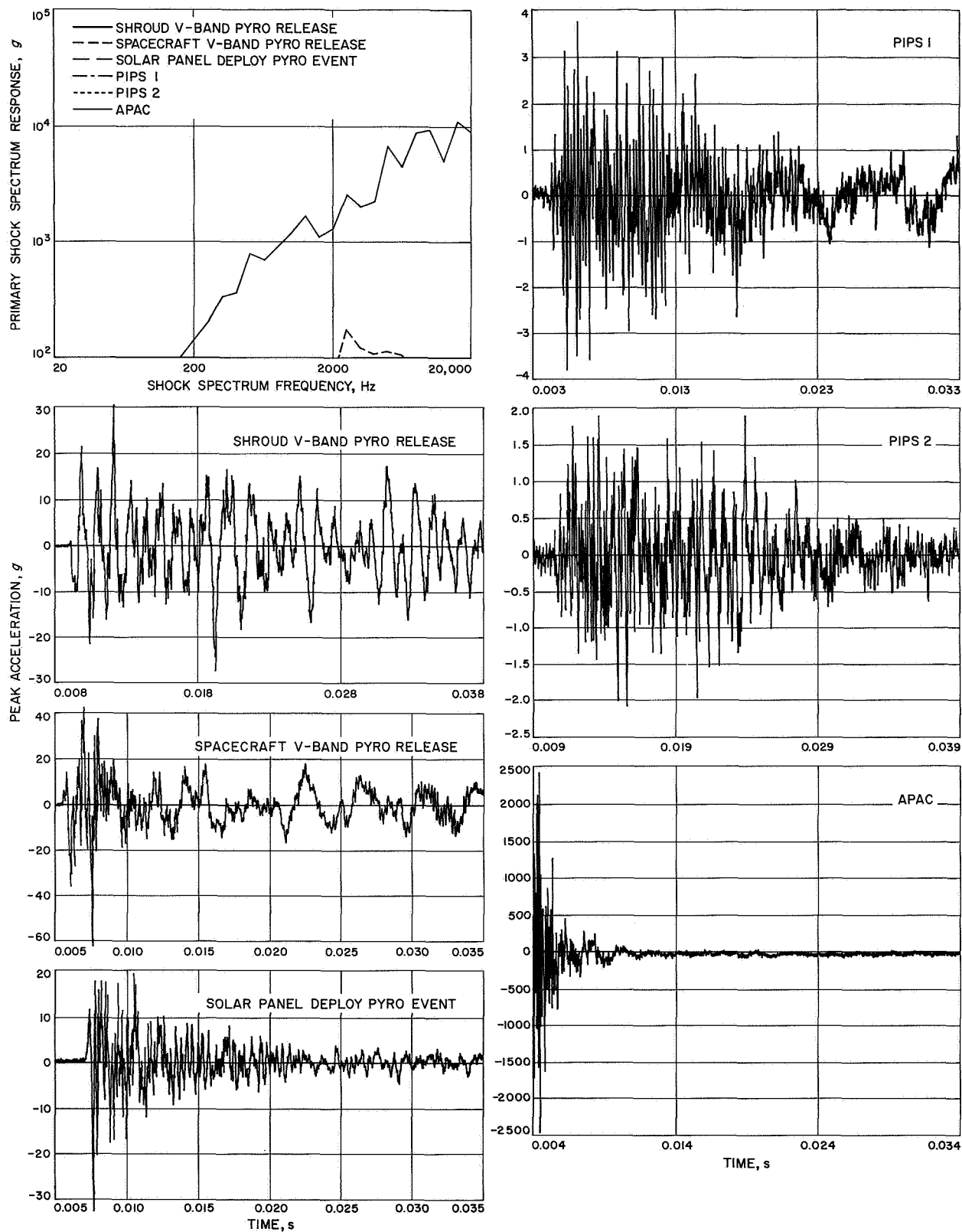


Fig. 37. M67-1 primary shock spectra composite and transient-time history at accelerometer AS2





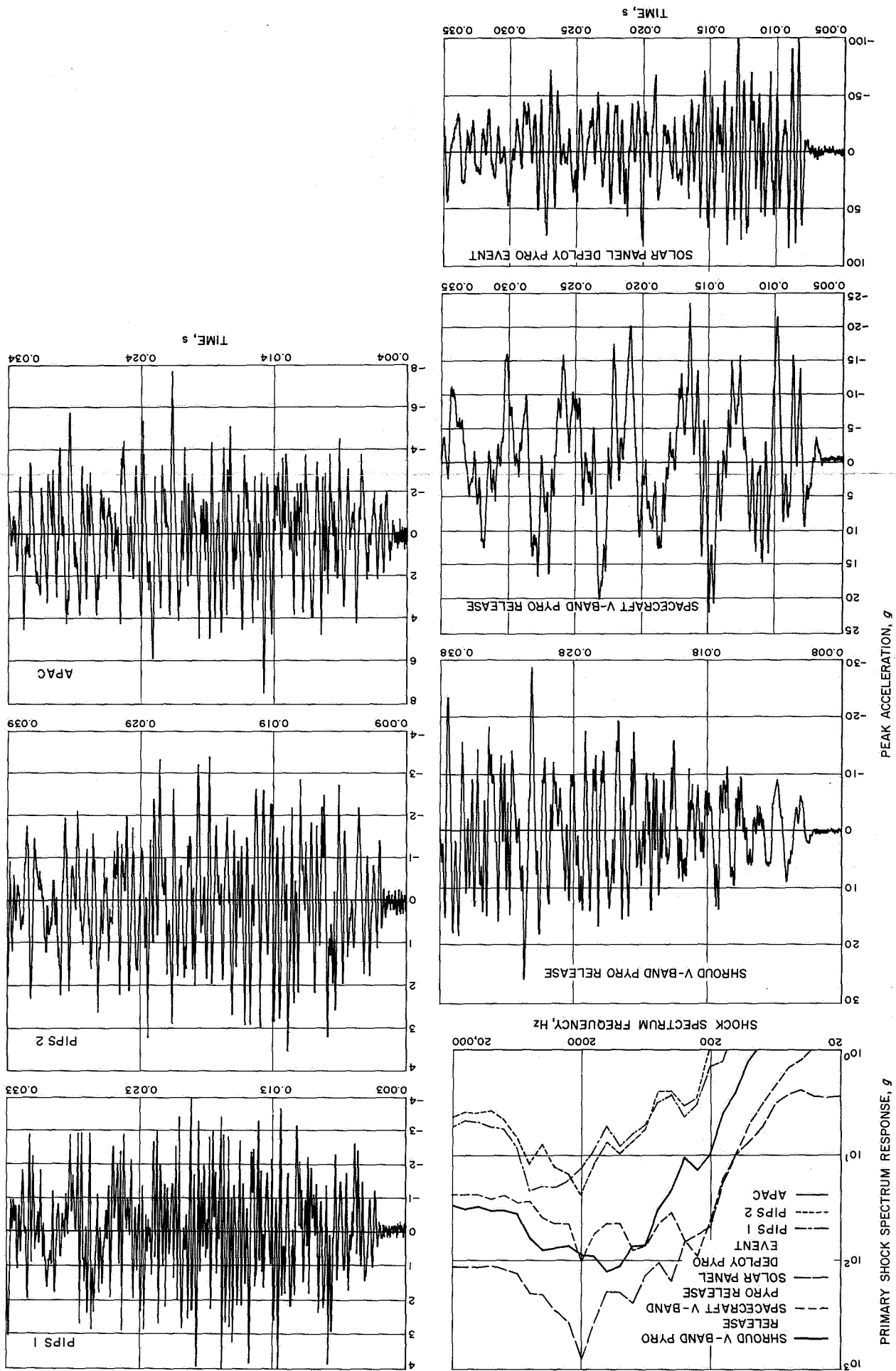


Fig. 38. M67-1 primary shock spectra composite and transient-time history at accelerometer IC4

FOLDOUT FRAME

FOLDOUT FRAME 51-A

52-B

1

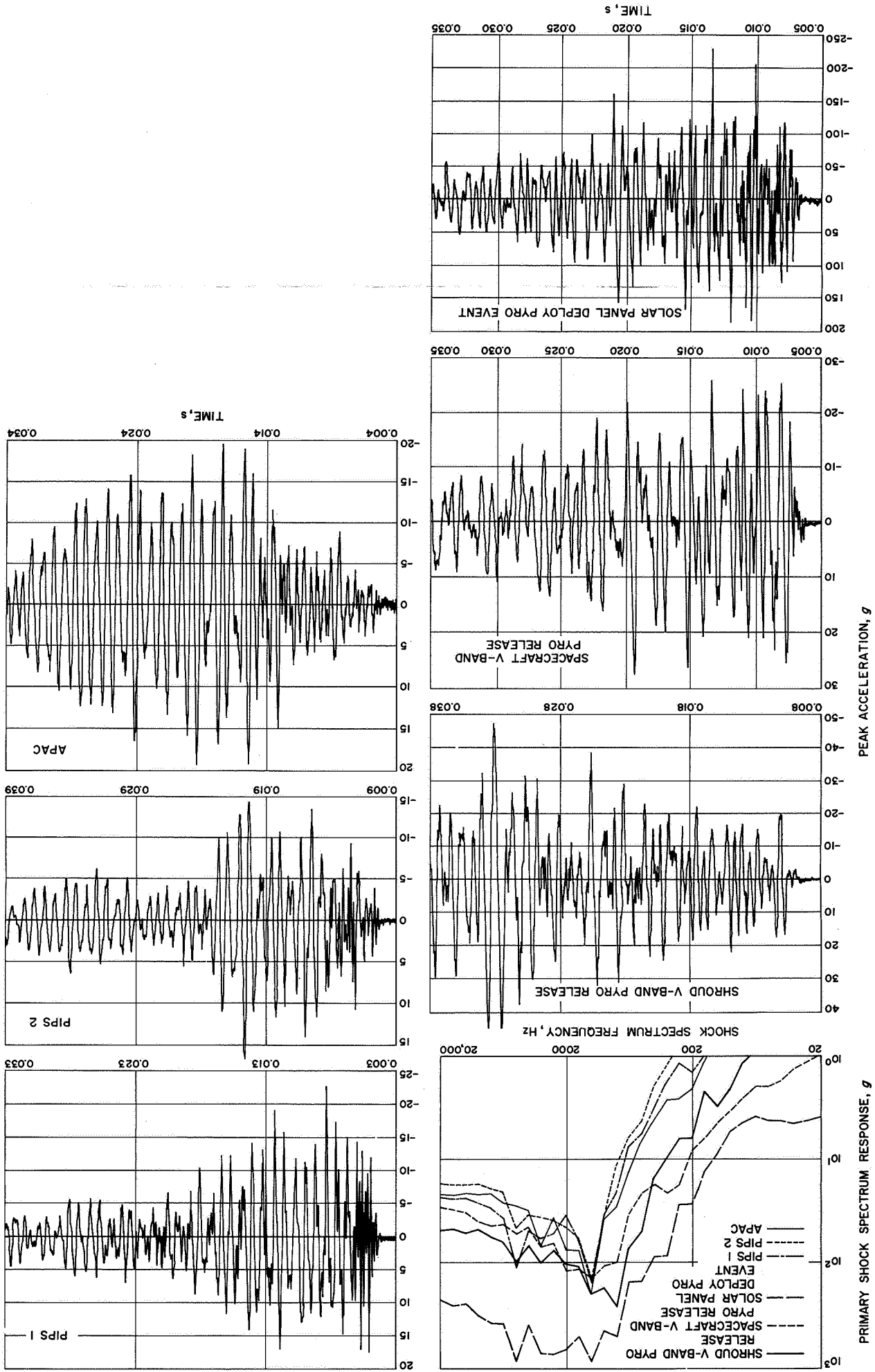


Fig. 39. M67-1 primary shock spectra composite and transient-time history at accelerometer 313

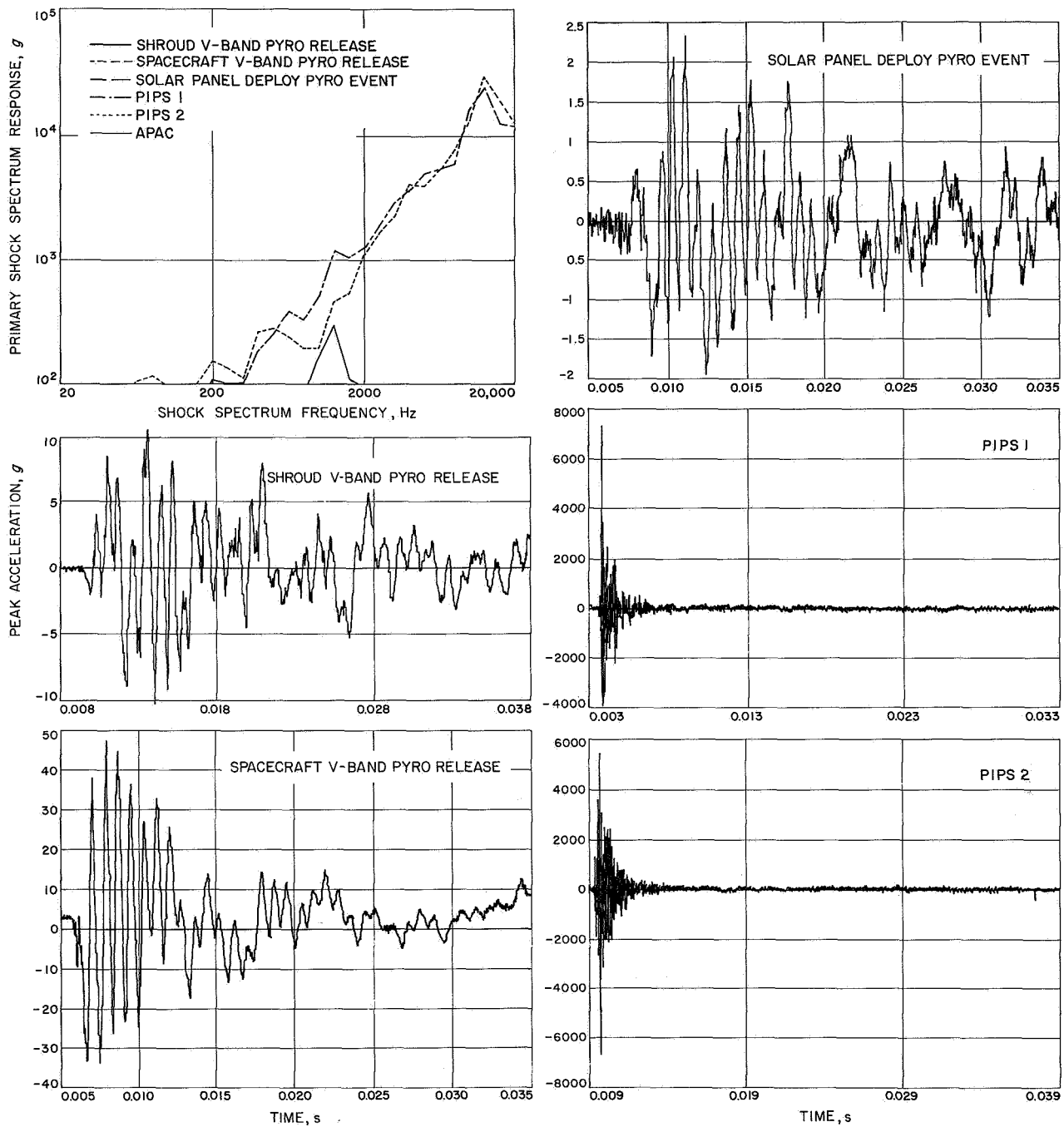


Fig. 40. M67-1 primary shock spectra composite and transient-time history at accelerometer MCV1

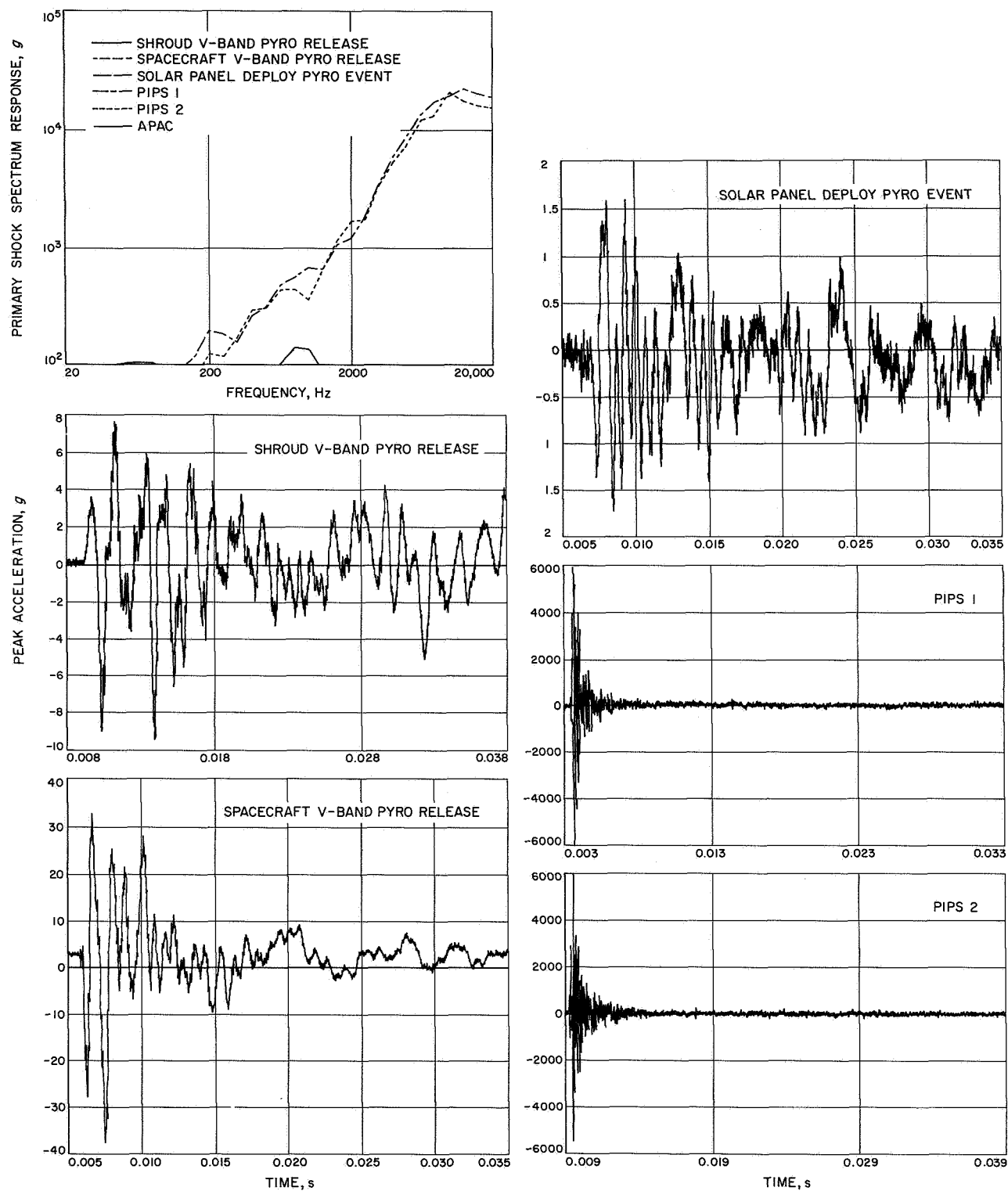


Fig. 41. M67-1 primary shock spectra composite and transient-time history at accelerometer MCV4

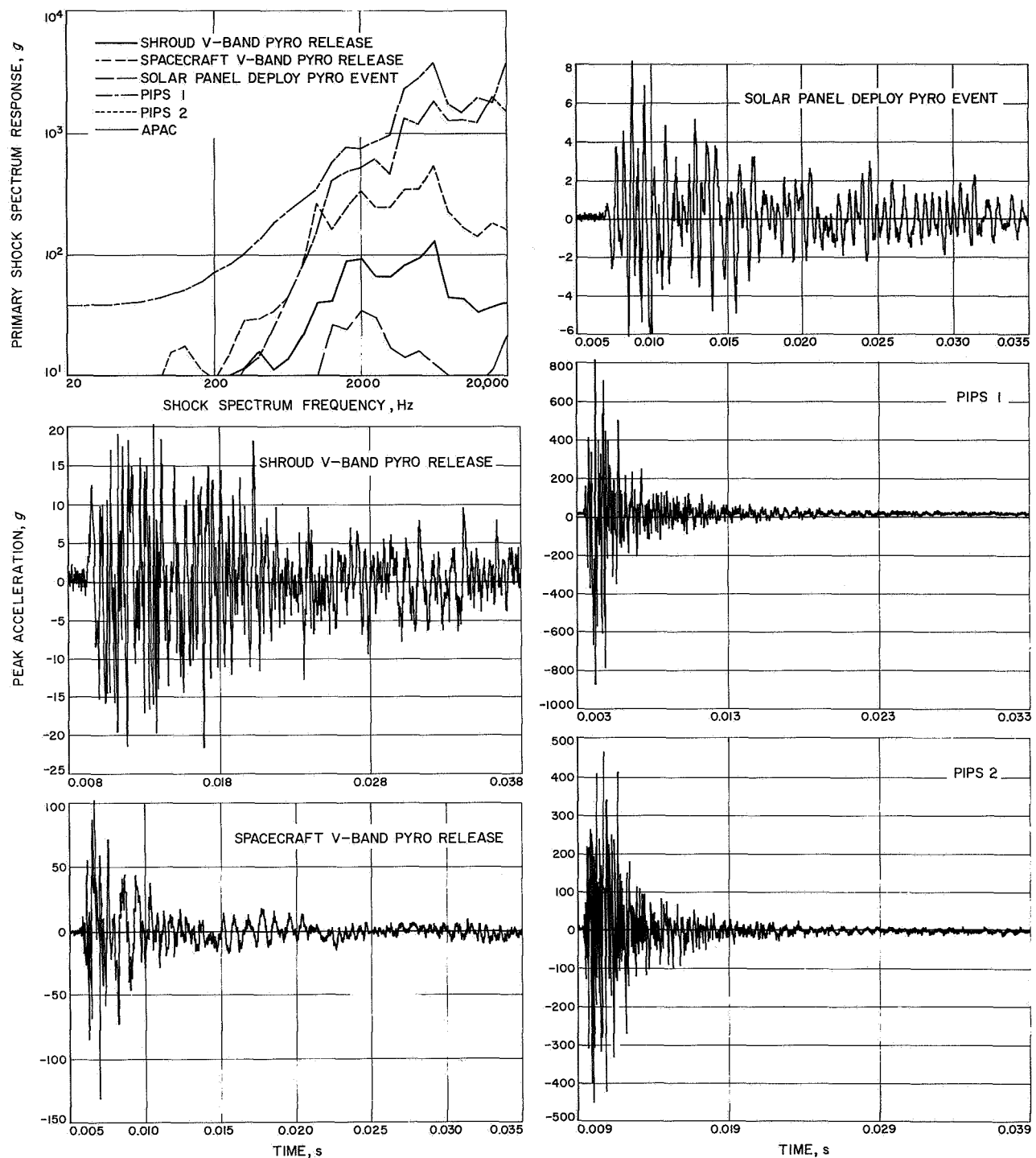
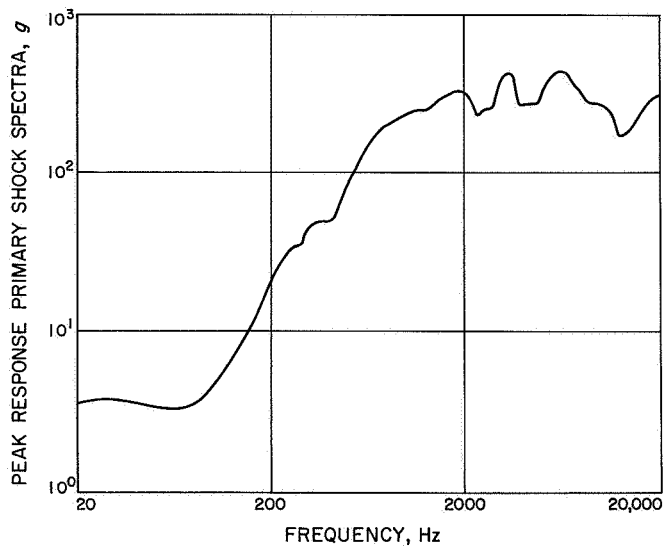
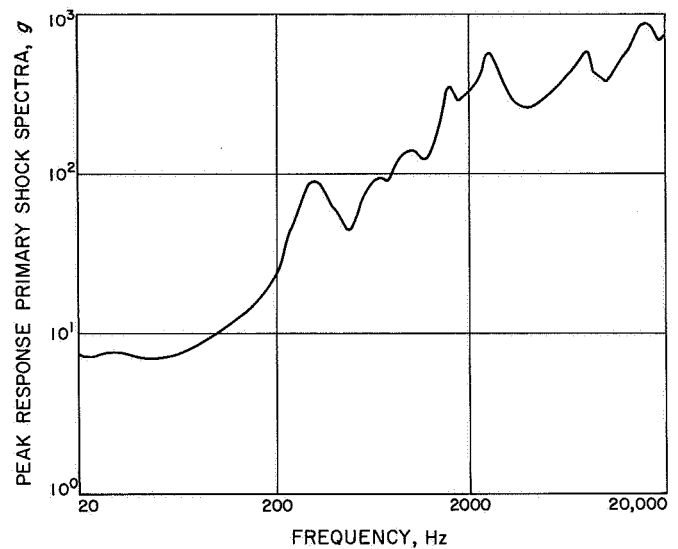


Fig. 42. M67-1 primary shock spectra composite and transient-time history at accelerometer MC4





**Fig. 43. M67-1 maximum enveloping primary shock spectra from accelerometers B1A, B2A, and B3A for all pyro events**



**Fig. 44. M67-1 maximum enveloping primary shock spectra from accelerometers B4, B5, and B6 for all pyro events**

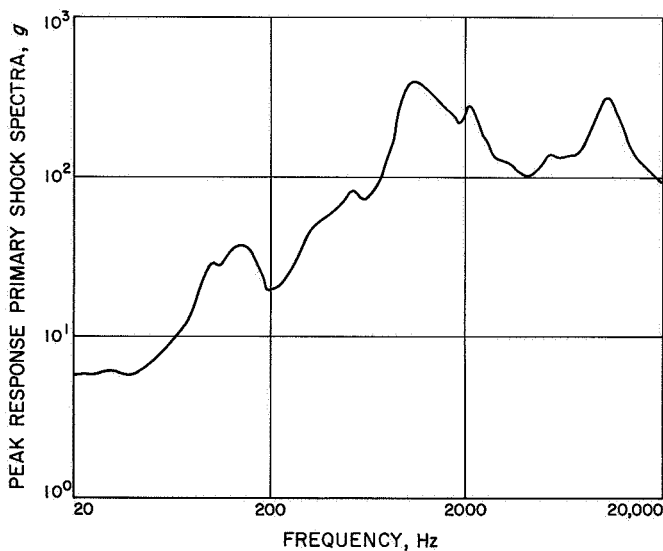


**Fig. 45. M67-1 maximum enveloping primary shock spectra from accelerometers SS4A, SS5A, and SS6A for all pyro events**

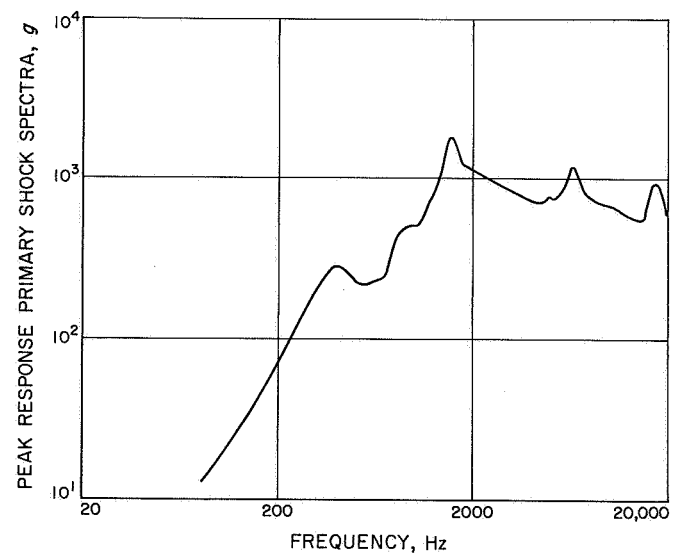


**Fig. 46. M67-1 maximum enveloping primary shock spectra from accelerometers BB1, BB2, and BB3 for all pyro events**

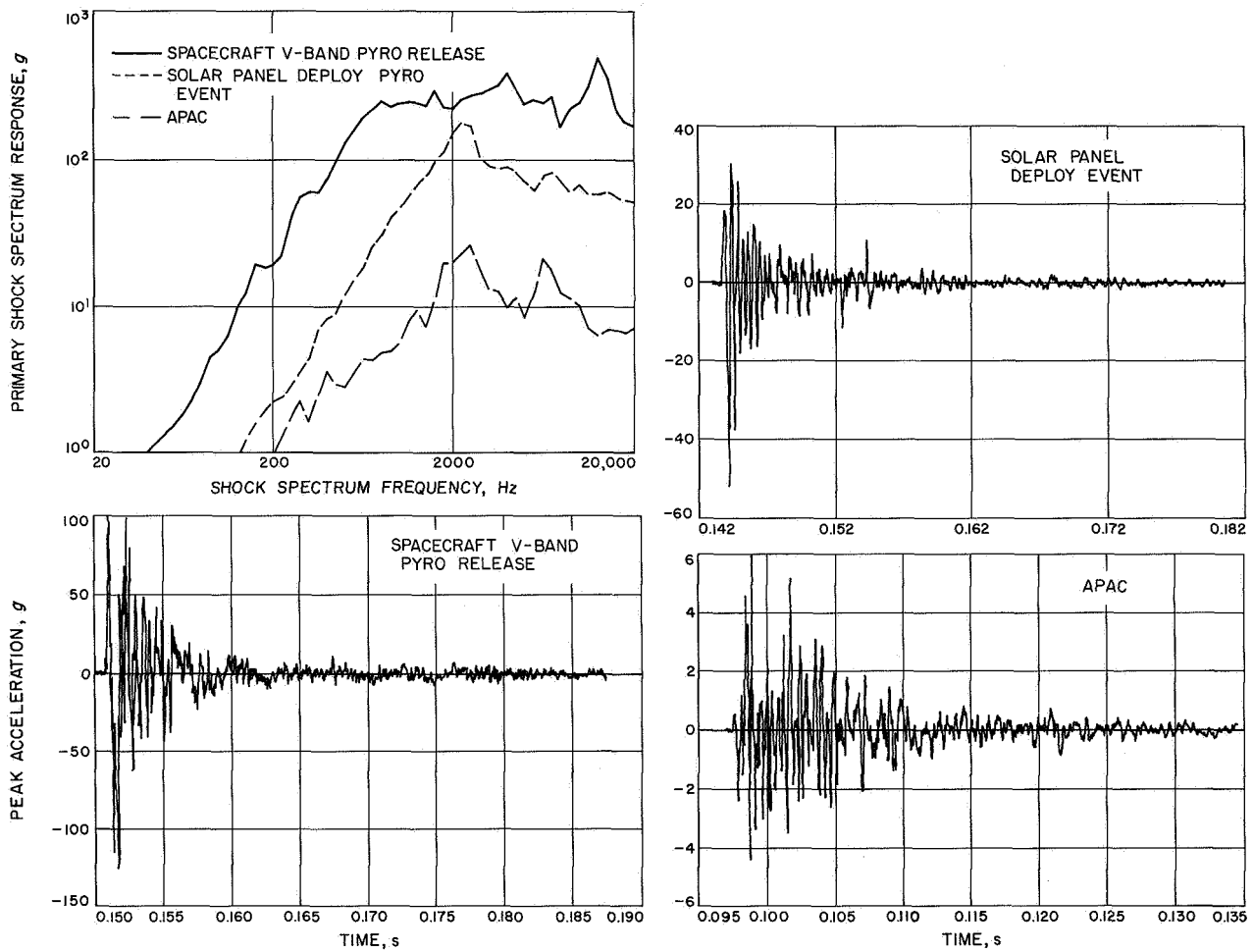
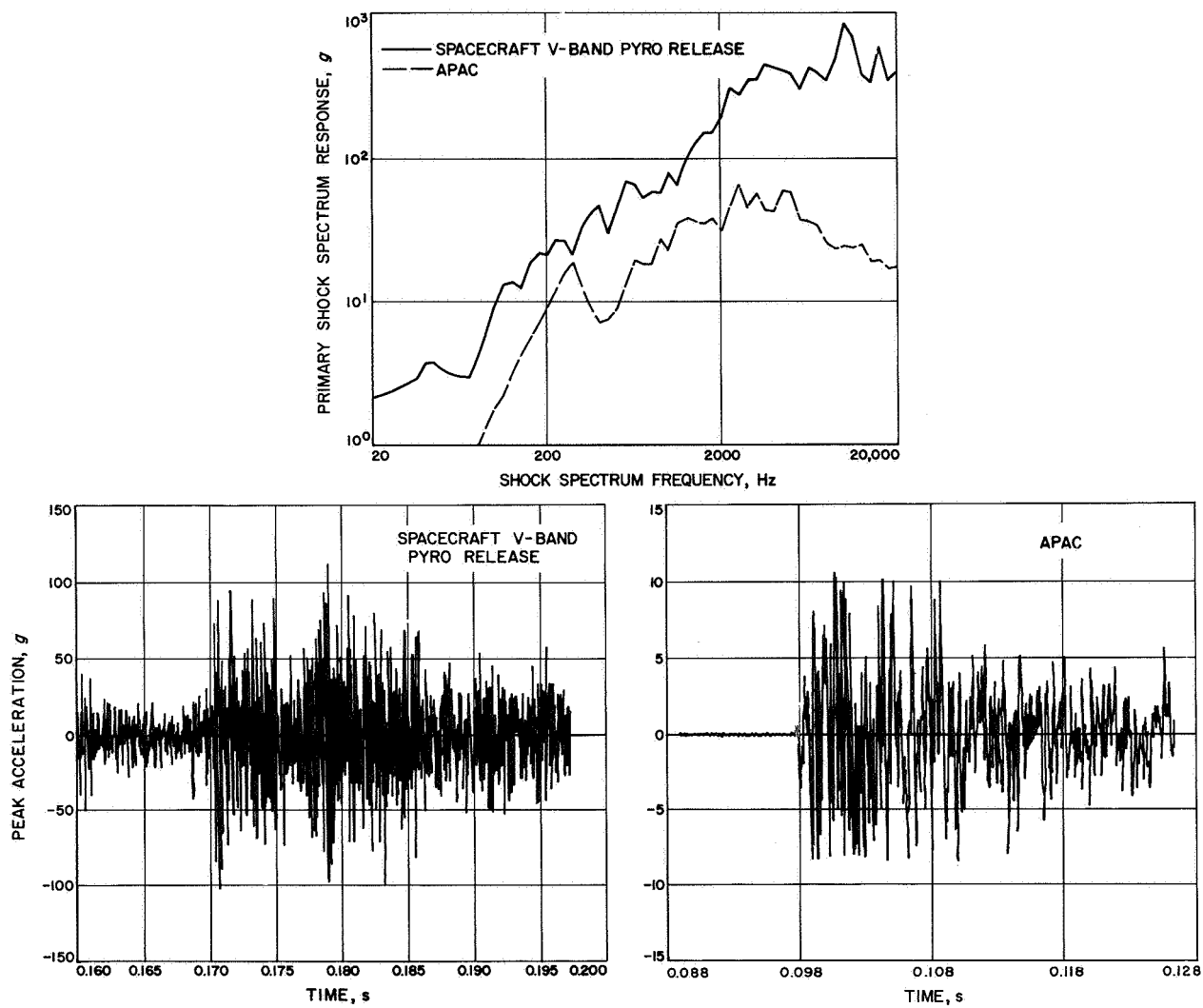


Fig. 47. M67-2 primary shock spectra composite and transient-time history at accelerometer B3



**Fig. 48. M67-2 primary shock spectra composite and transient-time history at accelerometer F4**

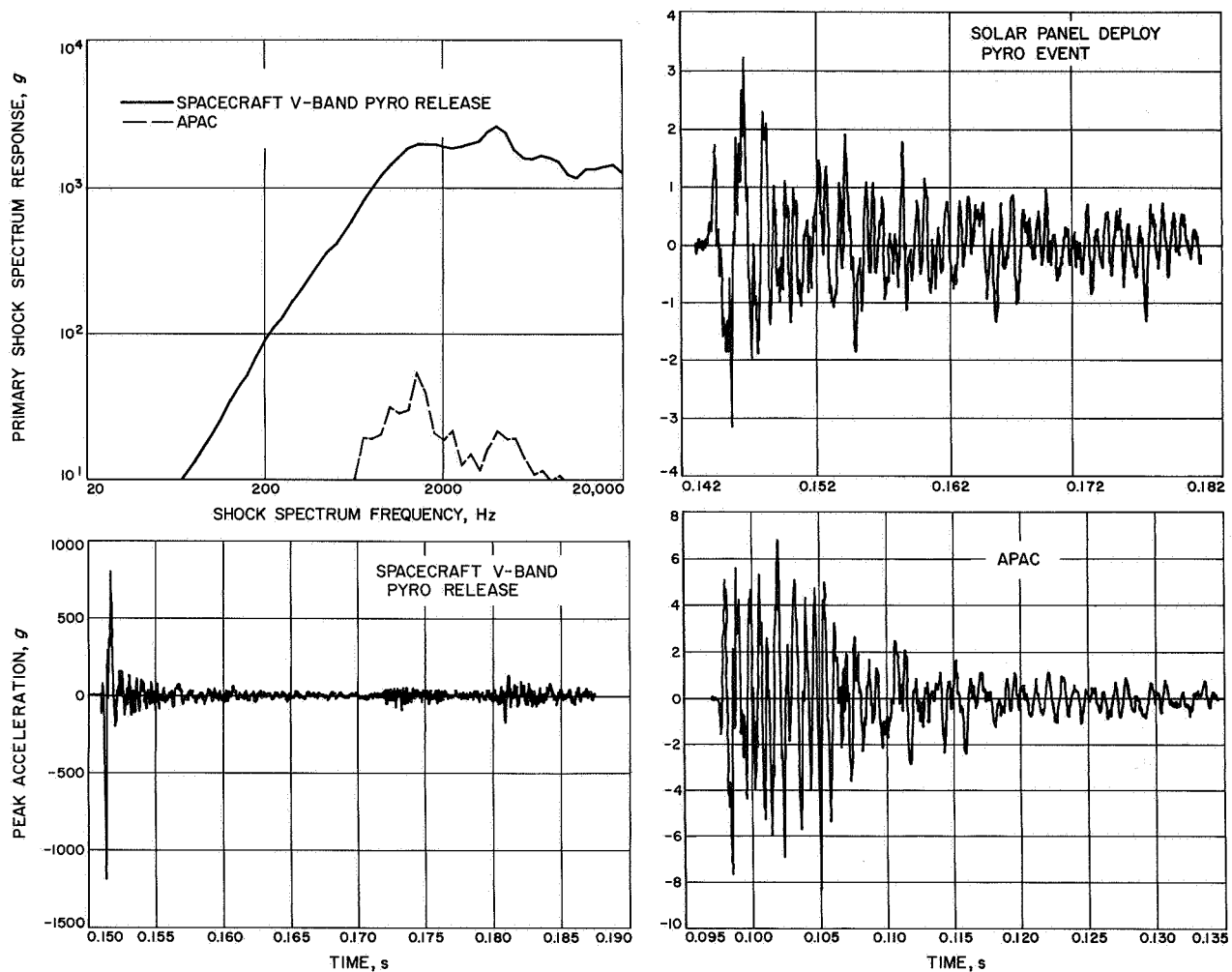


Fig. 49. M67-2 primary shock spectra composite and transient-time history at accelerometer F1

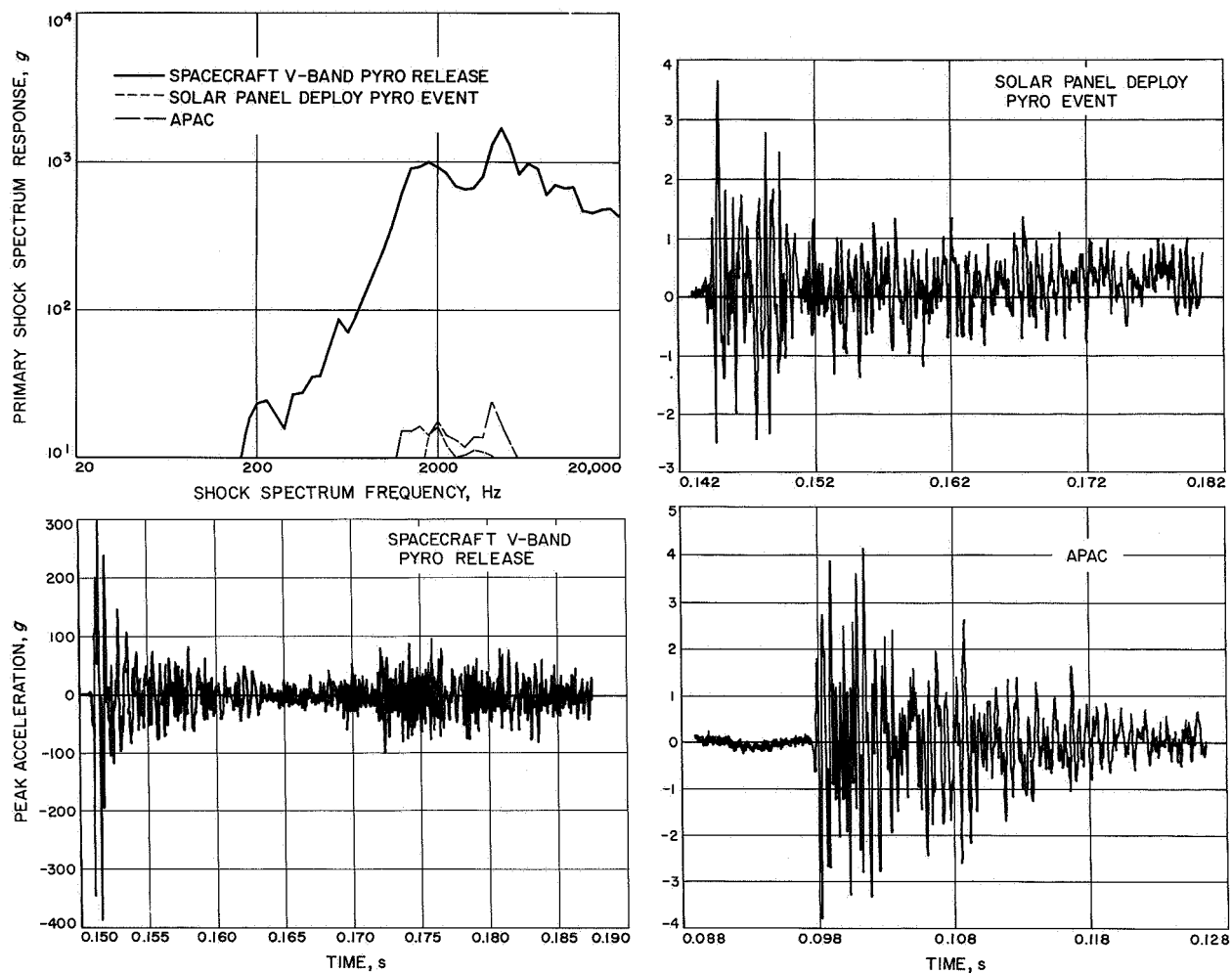


Fig. 50. M67-2 primary shock spectra composite and transient-time history at accelerometer F3

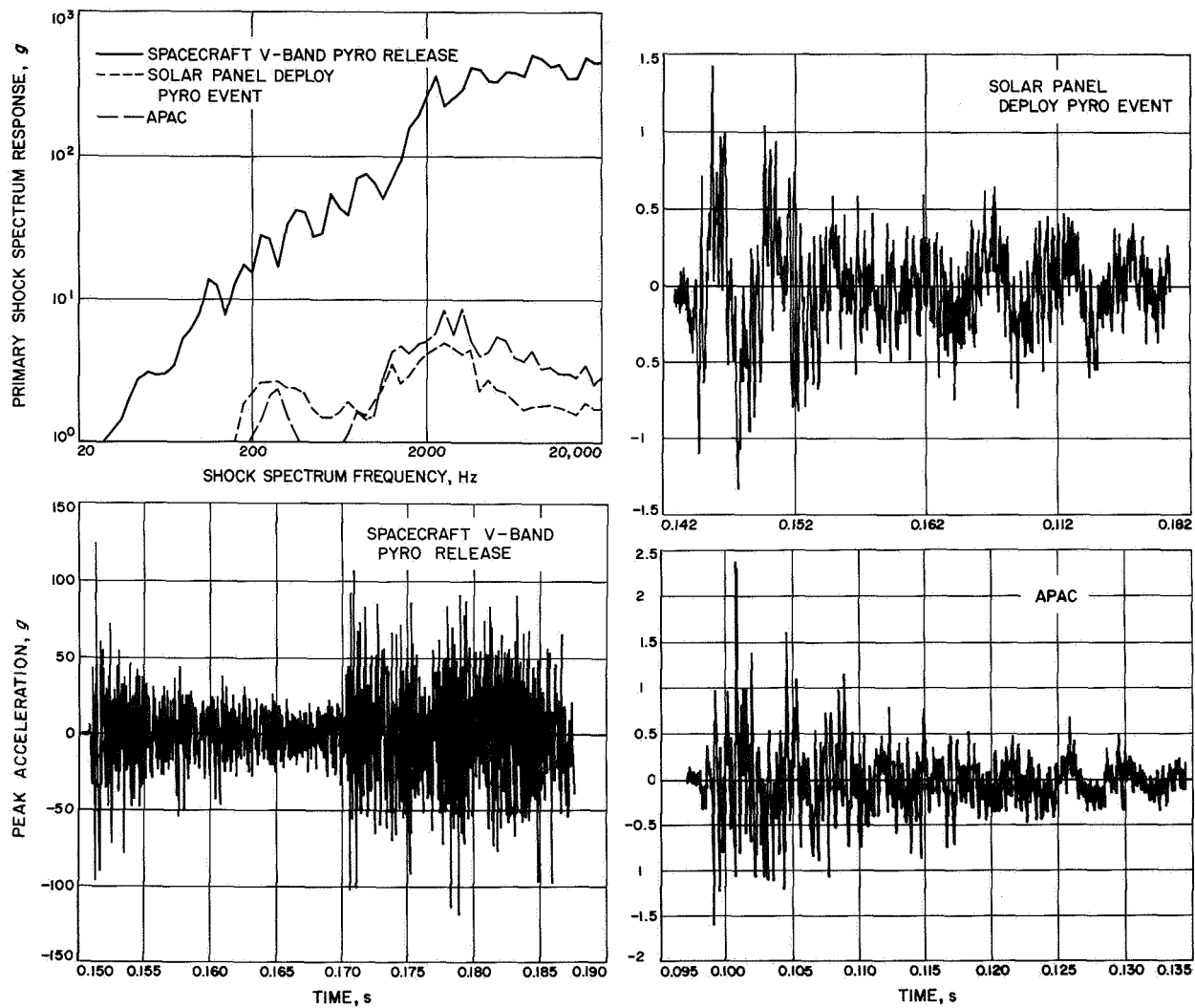
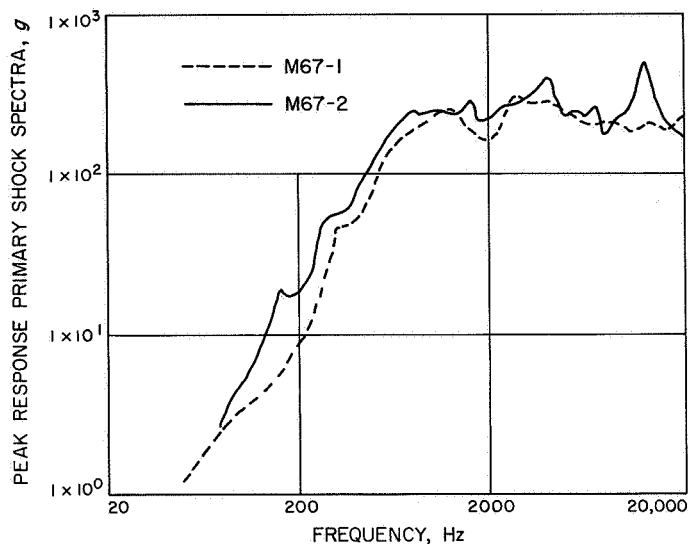
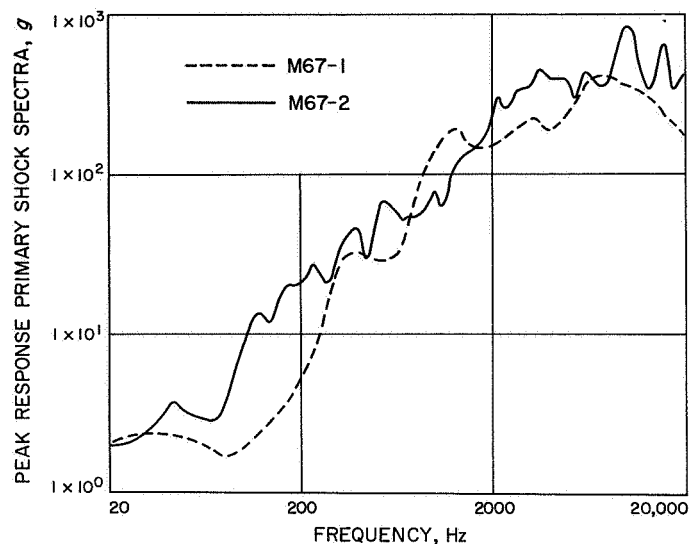


Fig. 51. M67-2 primary shock spectra composite and transient-time history at accelerometer F4A



**Fig. 52. M67-1 and M67-2 comparison of primary shock spectra for spacecraft V-band release at accelerometer B3**



**Fig. 53. M67-1 and M67-2 comparison of primary shock spectra for spacecraft V-band release at accelerometer F4**

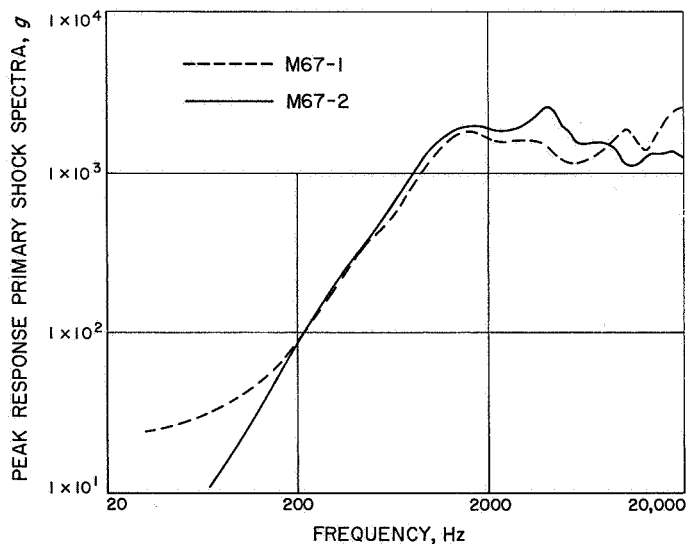


**Fig. 54. M67-1 and M67-2 comparison of primary shock spectra for spacecraft V-band release at accelerometer F1**

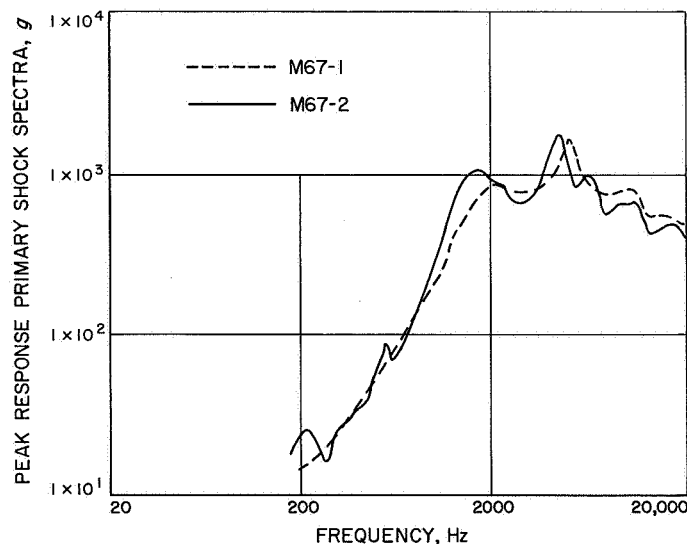


**Fig. 55. M67-1 and M67-2 comparison of primary shock spectra for spacecraft V-band release at accelerometer F3**



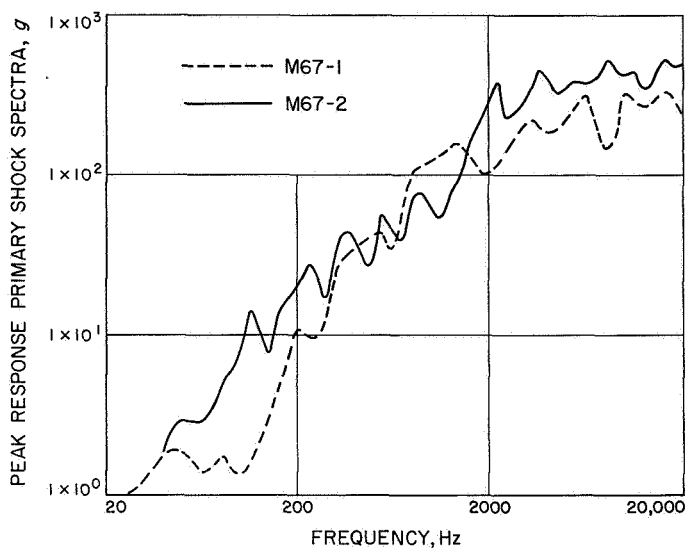


**Fig. 56. M67-1 and M67-2 comparison of primary shock spectra for spacecraft V-band release at accelerometer F4A**

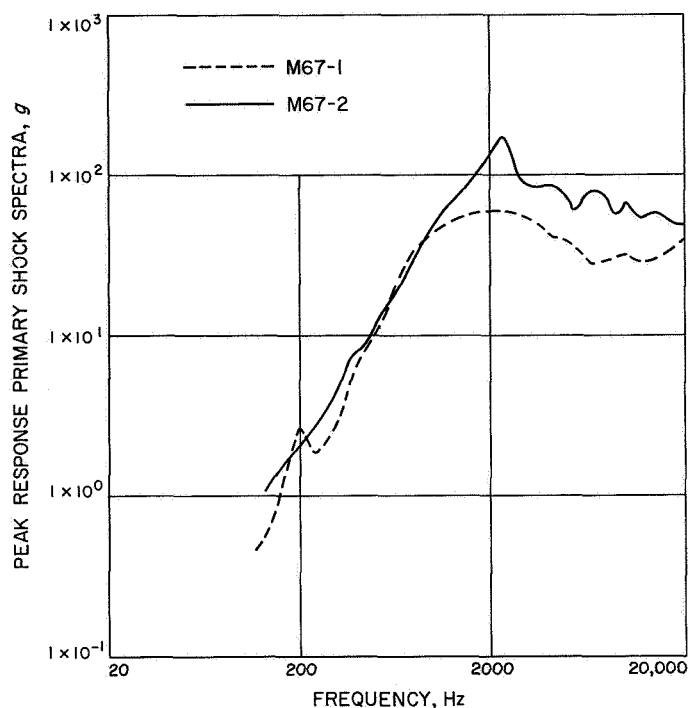


**Fig. 57. M67-1 and M67-2 comparison of primary shock spectra for solar panel deploy pyro at accelerometer B3**

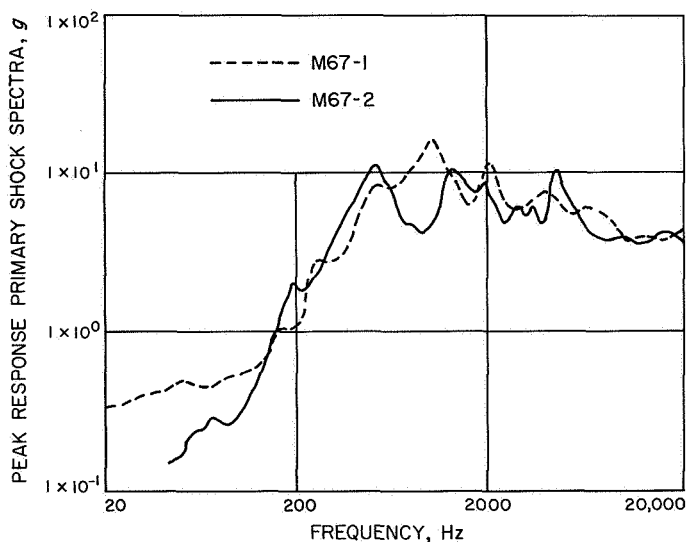


**Fig. 58. M67-1 and M67-2 comparison of primary shock spectra for solar panel deploy pyro at accelerometer F1**

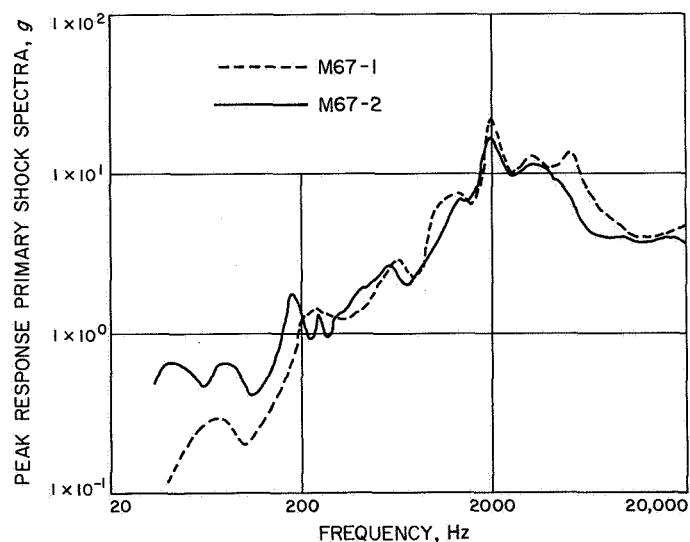


**Fig. 59. M67-1 and M67-2 comparison of primary shock spectra for solar panel deploy pyro at accelerometer F3**

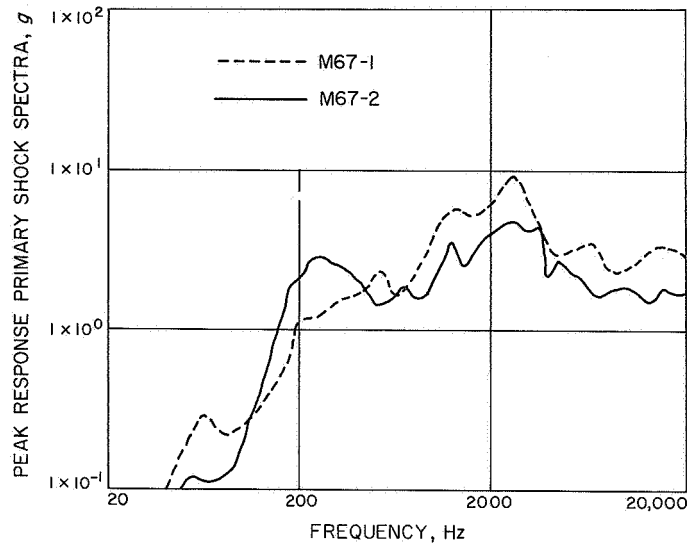


**Fig. 60. M67-1 and M67-2 comparison of primary shock spectra for solar panel deploy pyro at accelerometer F4A**

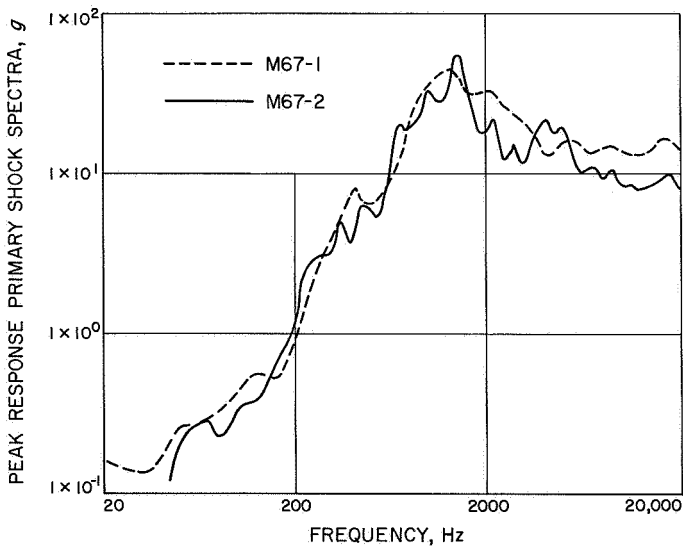


**Fig. 61. M67-1 and M67-2 comparison of primary shock spectra for APAC pyro event at accelerometer F1**

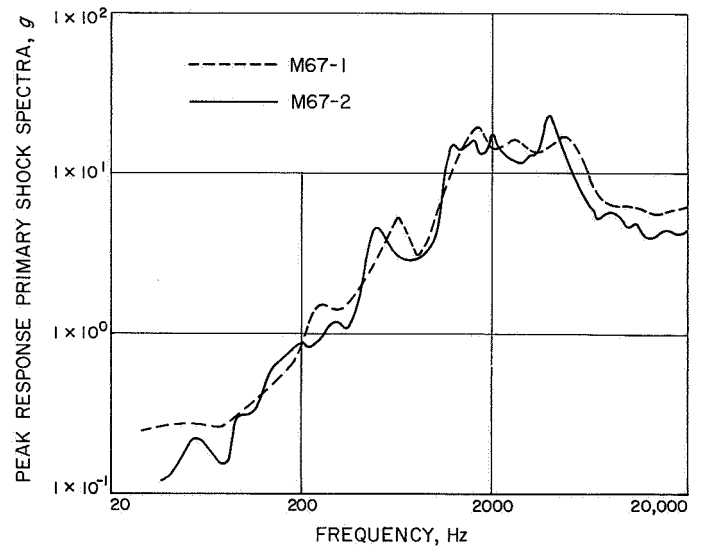


**Fig. 62. M67-1 and M67-2 comparison of primary shock spectra for APAC pyro event at accelerometer F3**

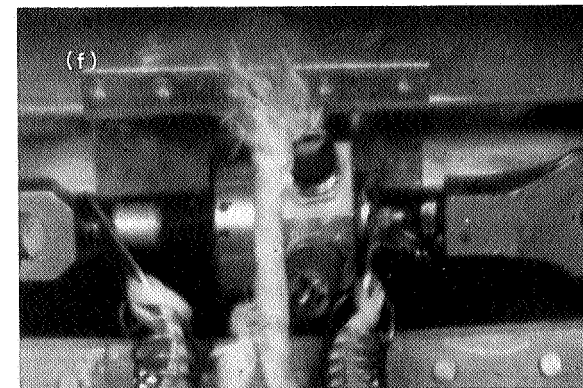
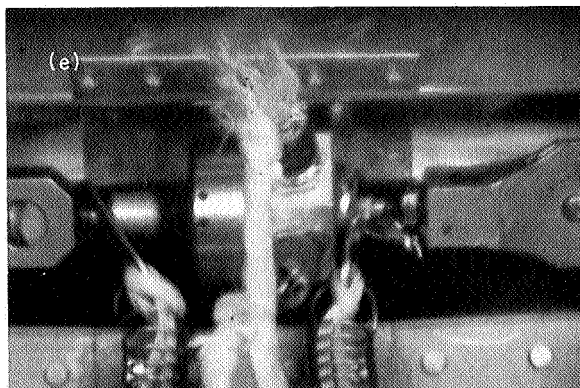
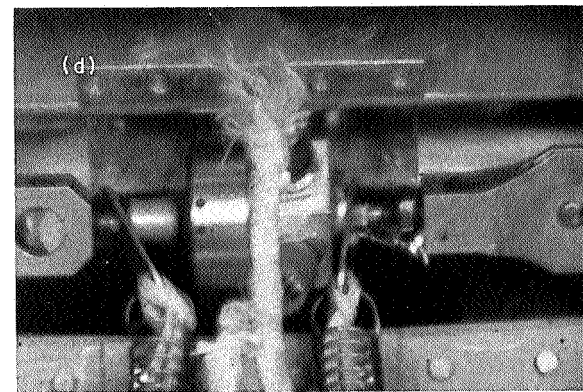
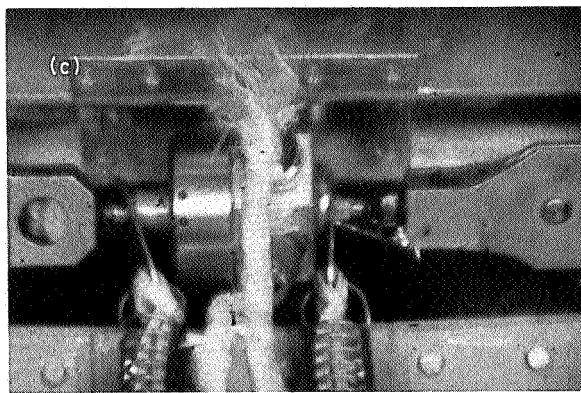
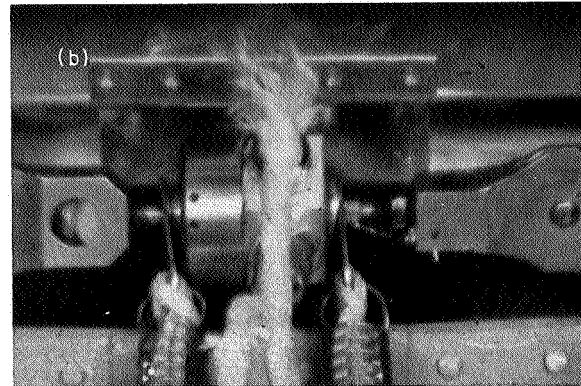
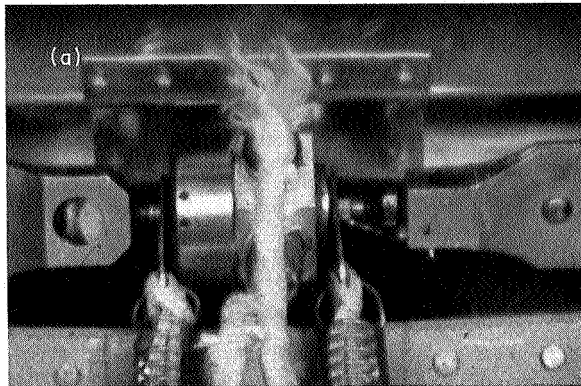


**Fig. 63. M67-2 spacecraft V-band release device during pyro firing (sequence of six photographs taken from high-speed movies)**



## Appendix

### Transient Response of Umbilical Door Slam Recorded Prior to M67-1 Pyro Test

Prior to the M67-1 FA test, questions arose concerning the severity of the shock transient resulting from the slamming of the umbilical door in the LMSC shroud prior to liftoff.

The M67-1 spacecraft pyro test setup offered the opportunity to measure and record the spacecraft transient response to the umbilical door slam. Prior to the start of the test, the umbilical door was opened fully and allowed to slam shut while recording all the transducers noted in Table 1. This procedure was followed twice.

All the response data were reduced and analyzed in the manner described in Section IV. The significant results are presented in Figs. A-1 through A-17 of this appendix in the form of time history and shock spectra (both primary and residual). Table 2 earlier presented a tabulation of the peak-g levels recorded during these door-slam runs. The door slam event was shown to produce an insignificant transient response throughout the spacecraft. In addition, the door slam served the additional and most useful purpose of allowing all transducers to be checked one last time prior to the actual pyro test.

PRECEDING PAGE BLANK NOT FILMED.

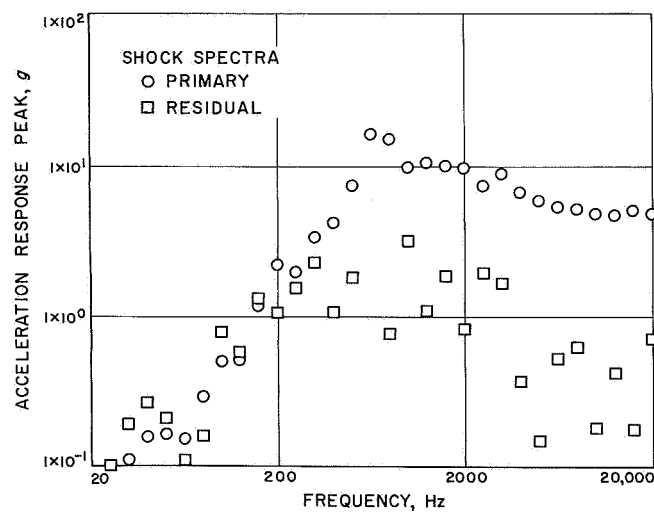
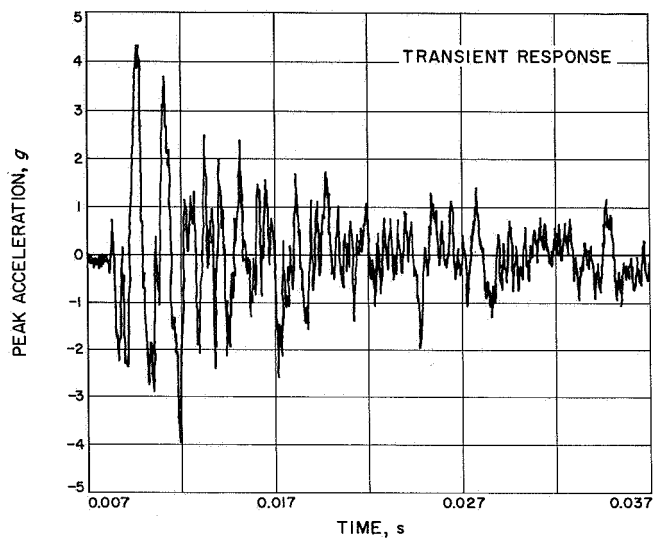


**Fig. A-1. Transient response and shock spectra at accelerometer B3 (flight transducer, umbilical door slam event)**

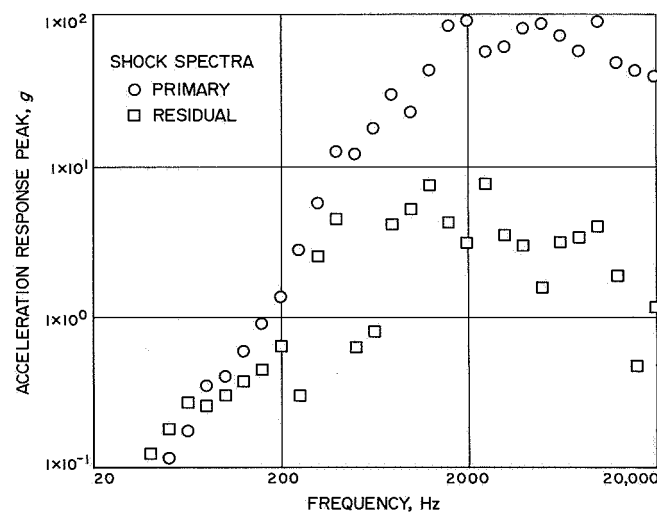
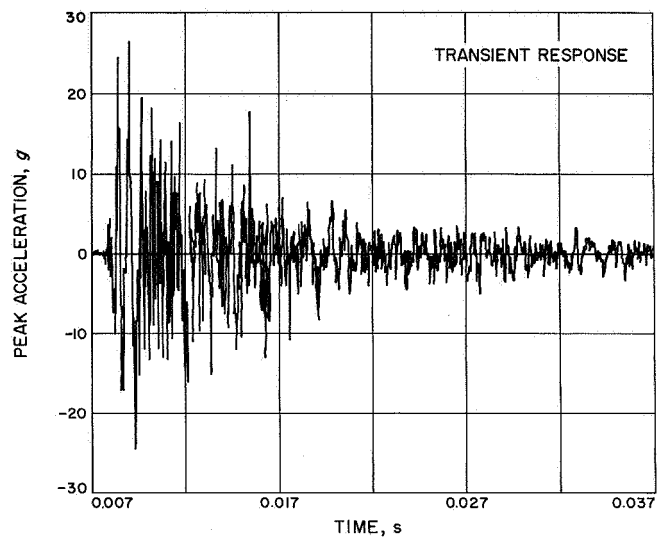


**Fig. A-2. Transient response and shock spectra at accelerometer F4 (flight transducer, umbilical door slam event)**

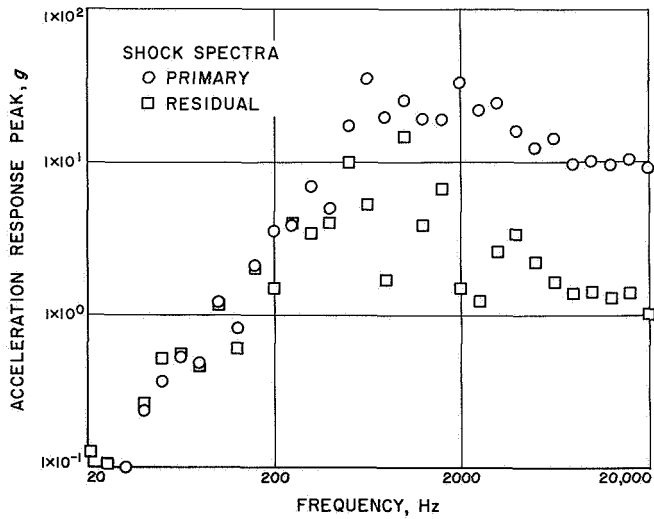
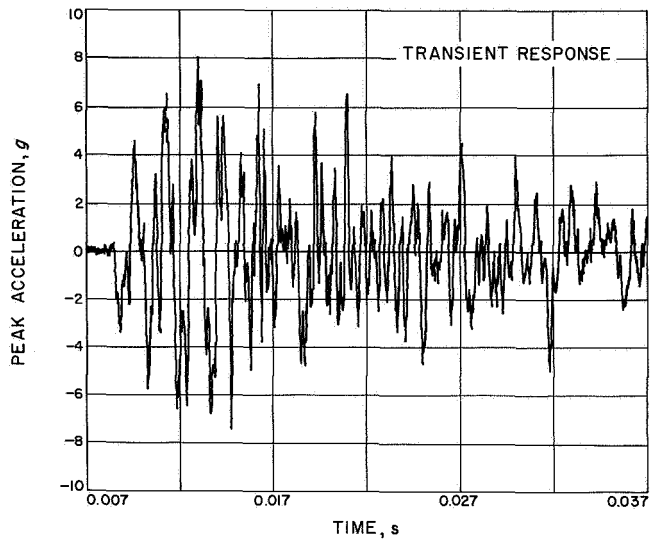


**Fig. A-3. Transient response and shock spectra at accelerometer F1 (umbilical door slam event)**

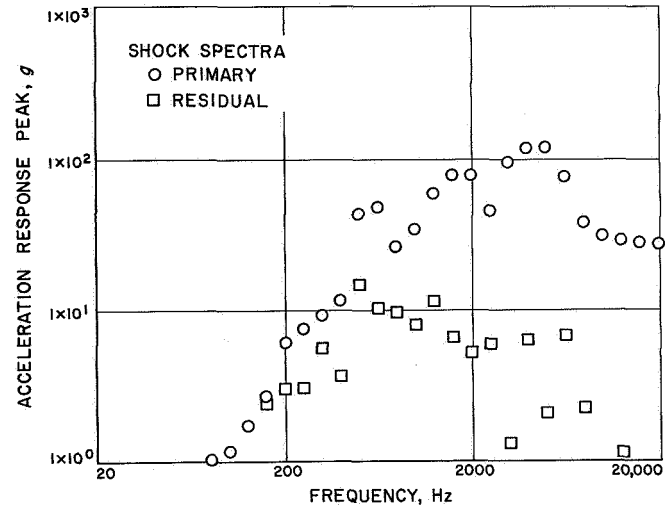
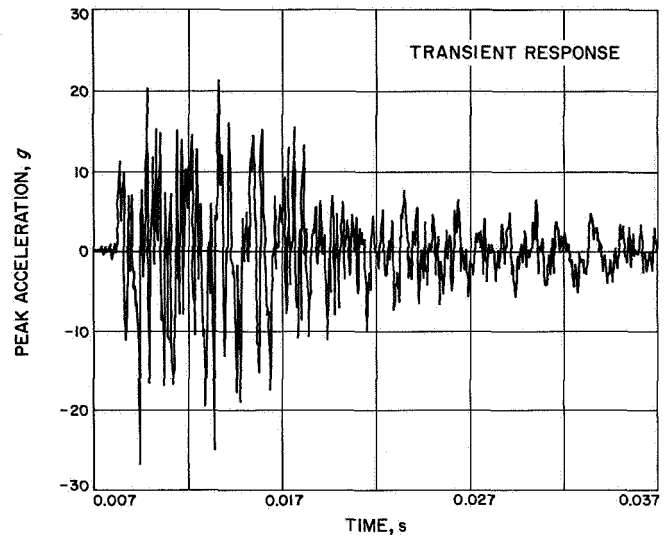


**Fig. A-4. Transient response and shock spectra at accelerometer F3 (umbilical door slam event)**



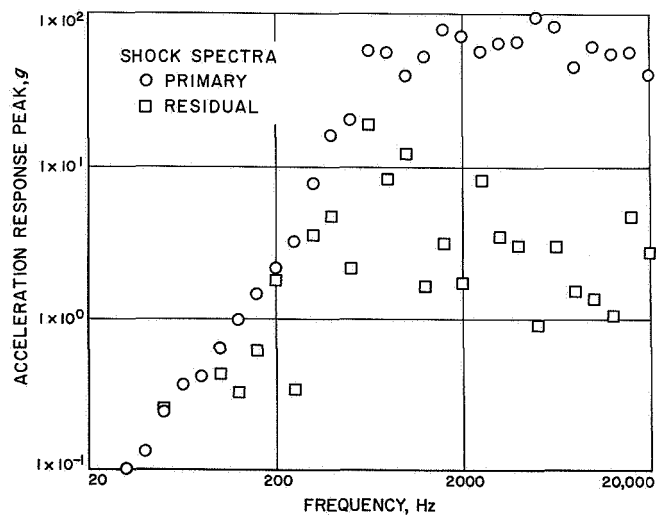
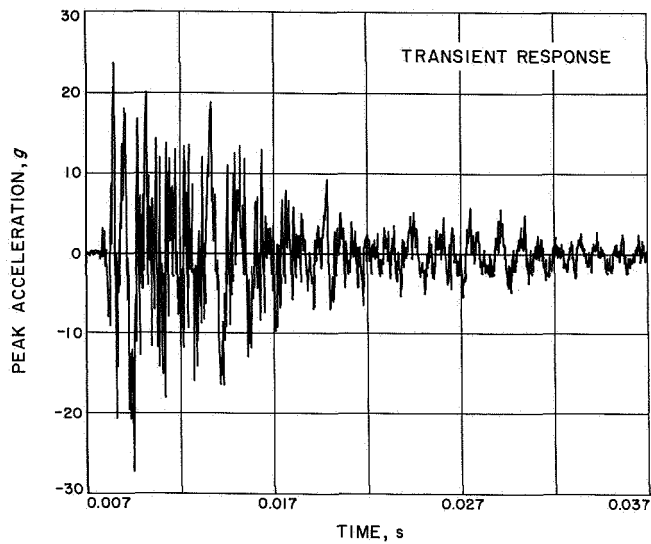


**Fig. A-5. Transient response and shock spectra at accelerometer F4A (umbilical door slam event)**

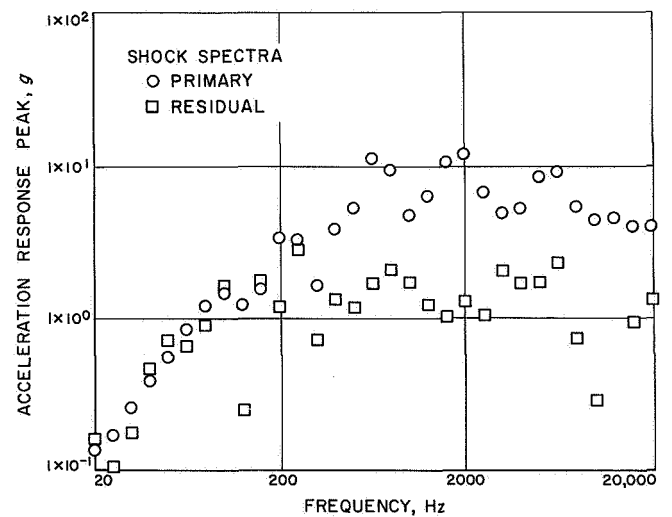
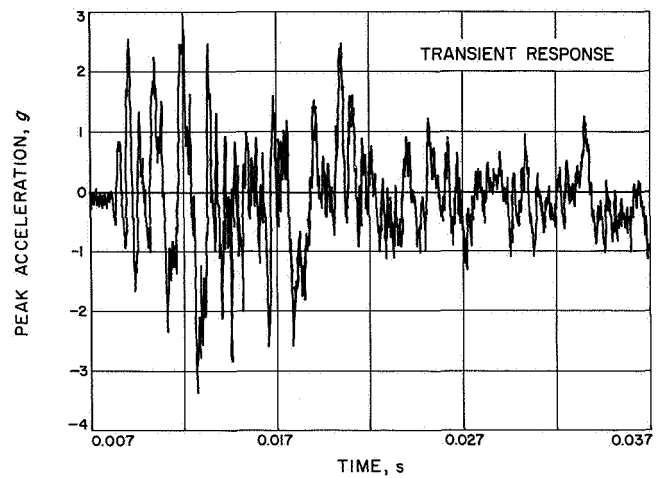


**Fig. A-6. Transient response and shock spectra at accelerometer B1A (umbilical door slam event)**

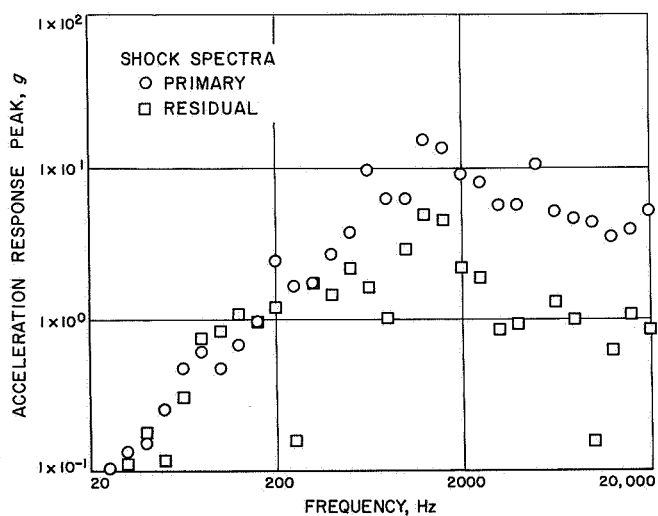
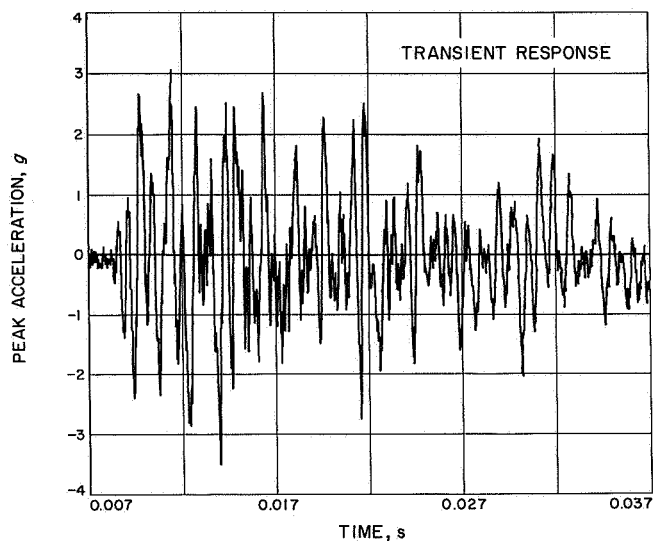


**Fig. A-7. Transient response and shock spectra at accelerometer B2A (umbilical door slam event)**

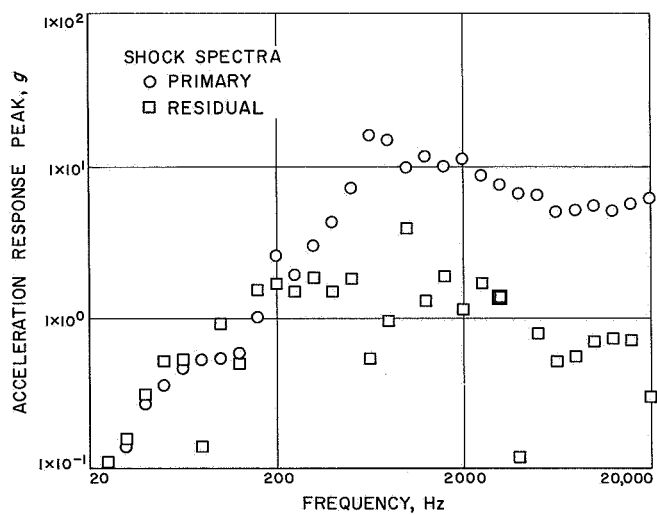
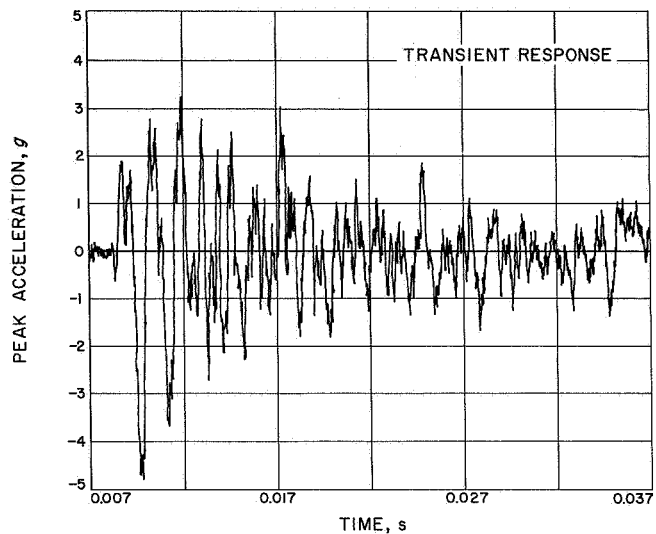


**Fig. A-8. Transient response and shock spectra at accelerometer B3A (umbilical door slam event)**

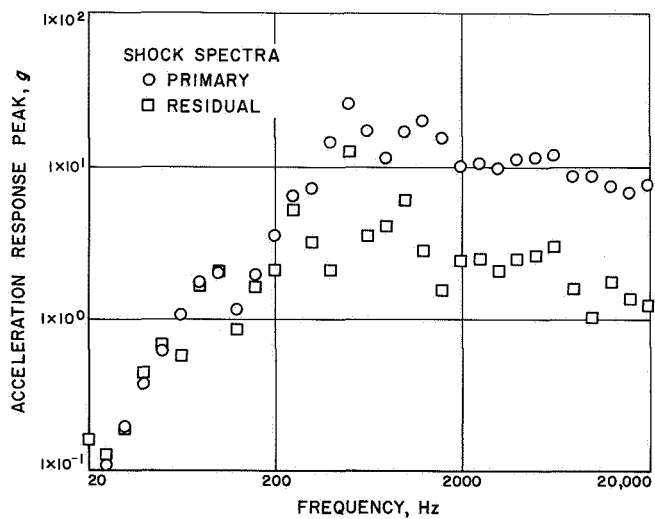
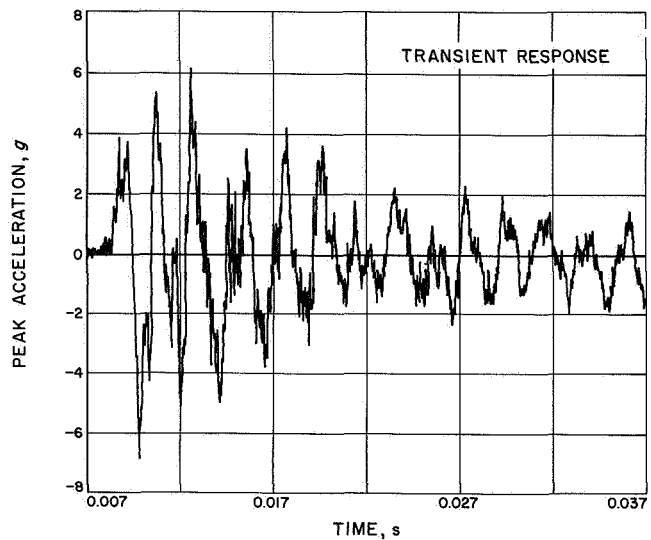


**Fig. A-9. Transient response and shock spectra at accelerometer BB1 (umbilical door slam event)**

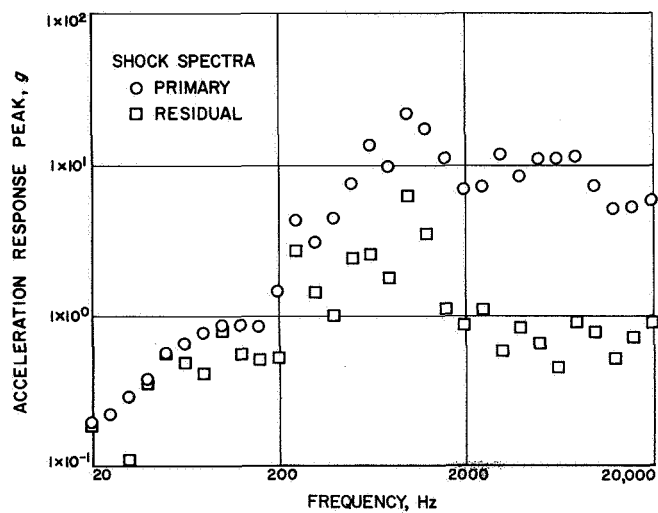
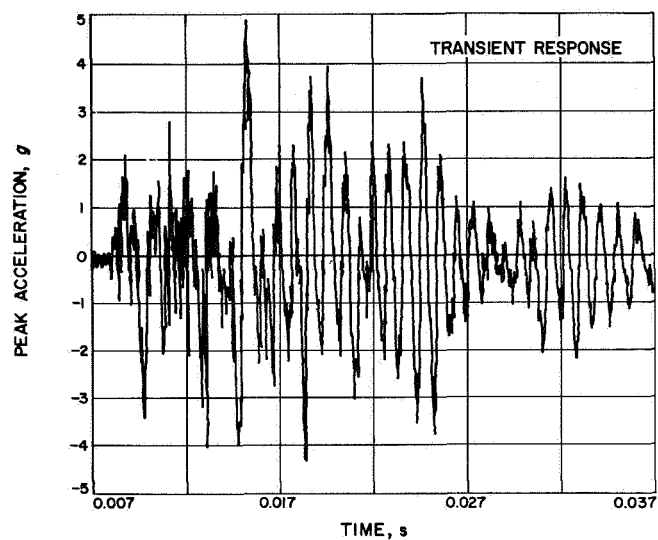


**Fig. A-10. Transient response and shock spectra at accelerometer BB2 (umbilical door slam event)**

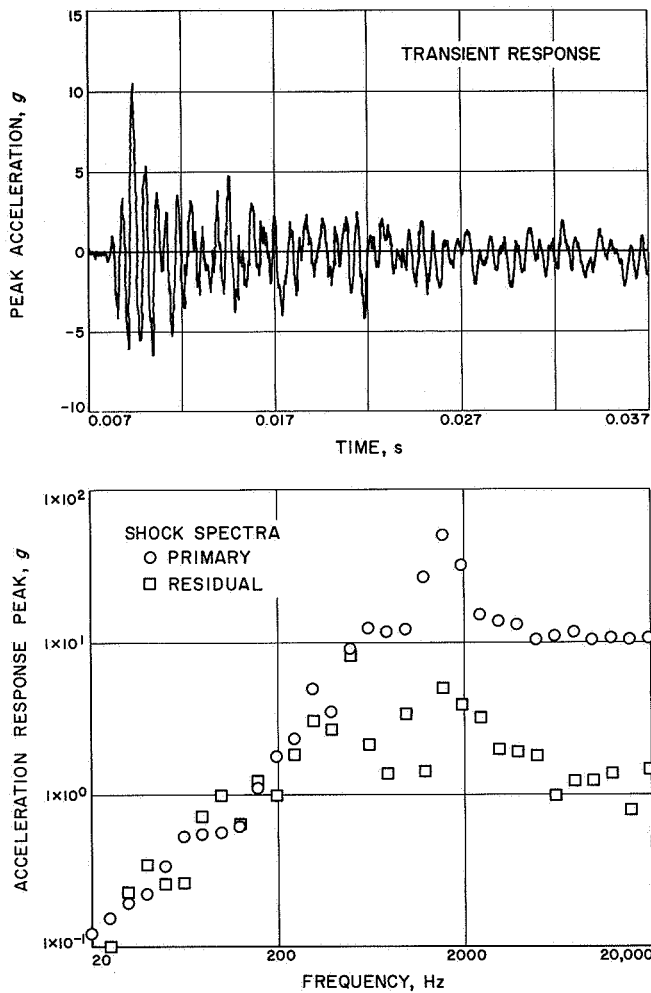


**Fig. A-11. Transient response and shock spectra at accelerometer BB3 (umbilical door slam event)**

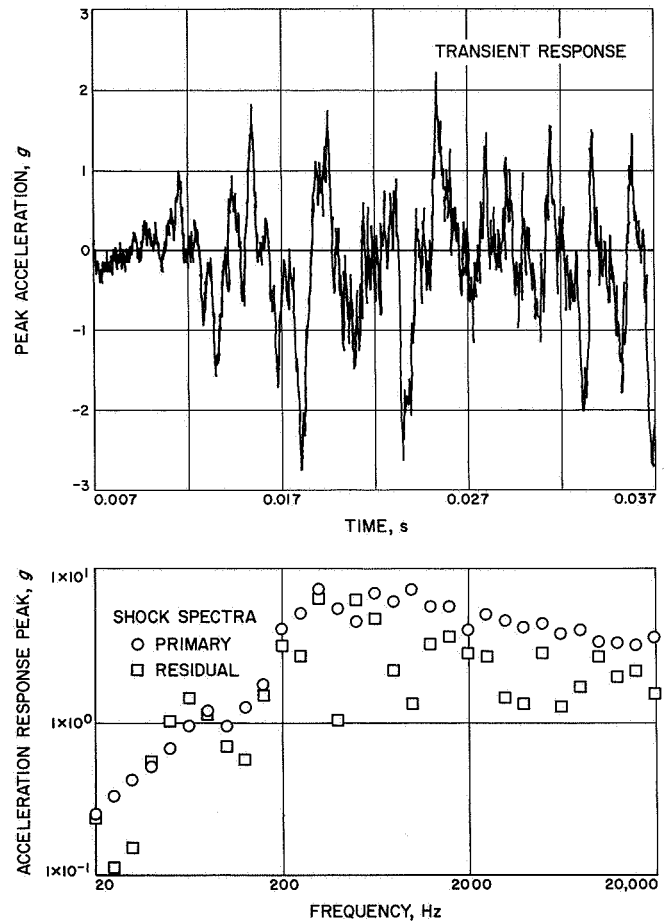


**Fig. A-12. Transient response and shock spectra at accelerometer AS2 (umbilical door slam event)**

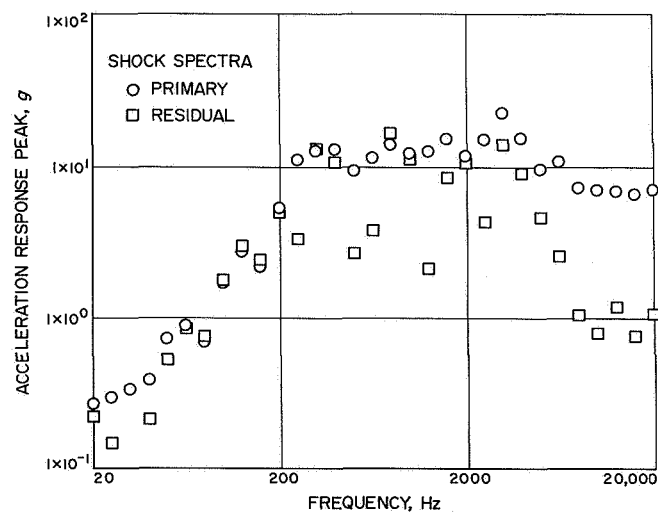
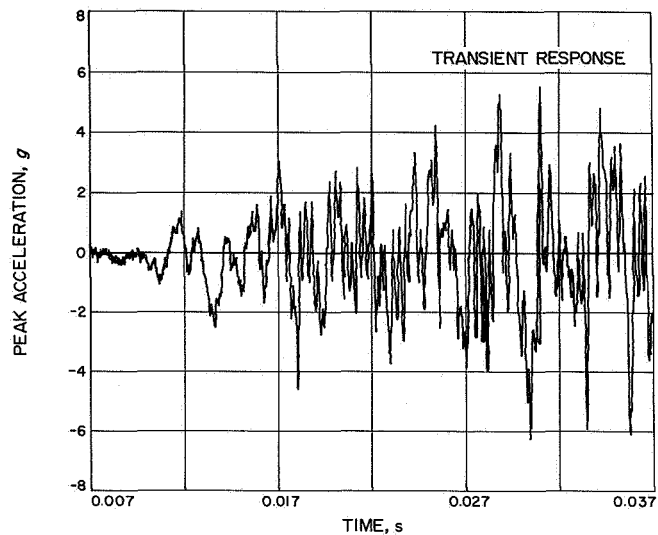


**Fig. A-13. Transient response and shock spectra at accelerometer 1C4 (umbilical door slam event)**

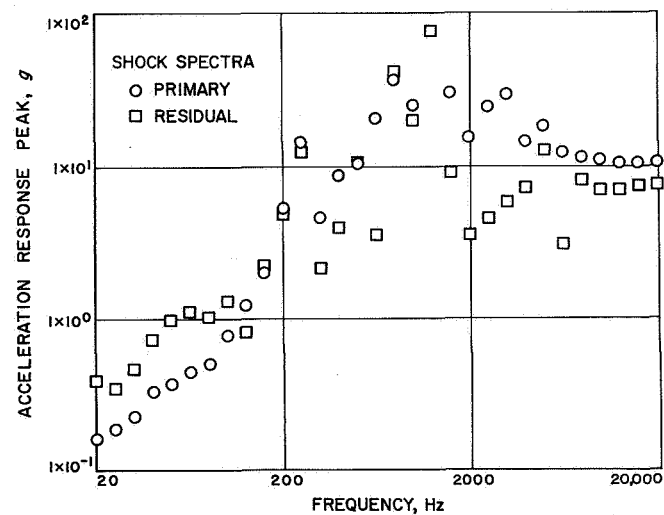
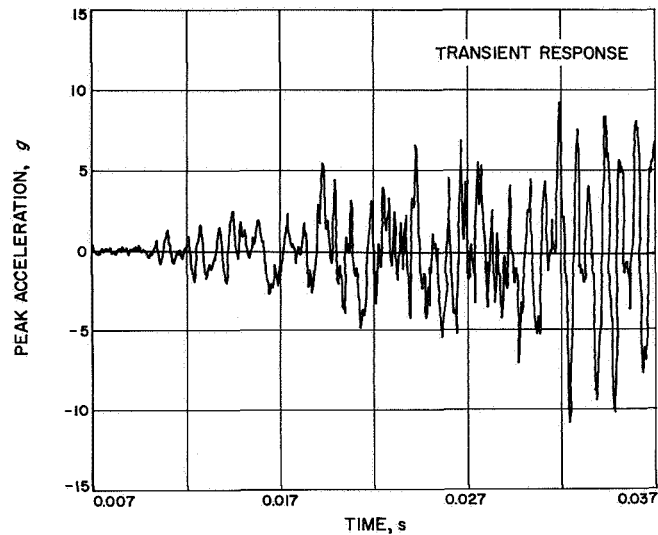


**Fig. A-14. Transient response and shock spectra at accelerometer 3T3 (umbilical door slam event)**

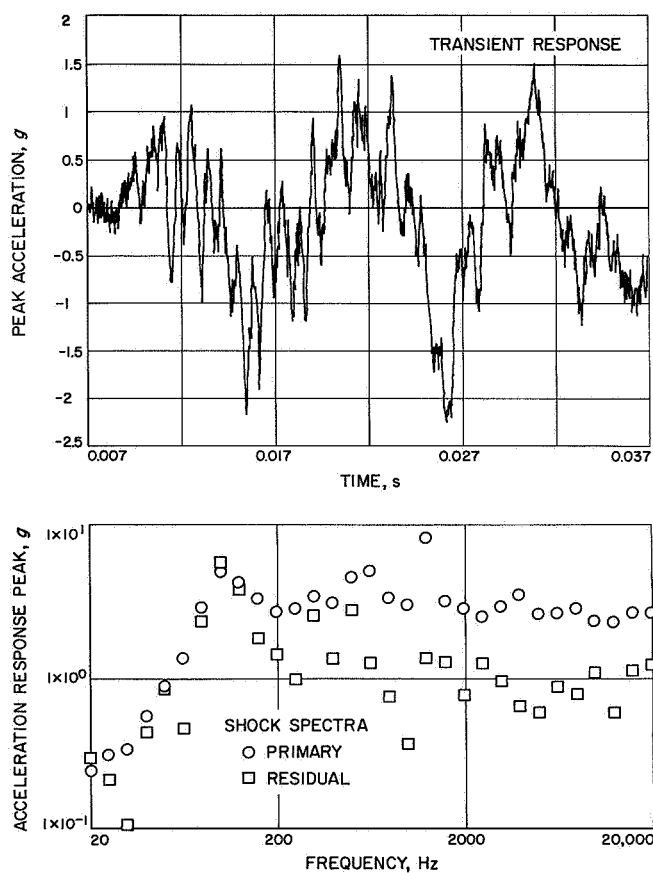


**Fig. A-15. Transient response and shock spectra at accelerometer MCV1 (umbilical door slam event)**

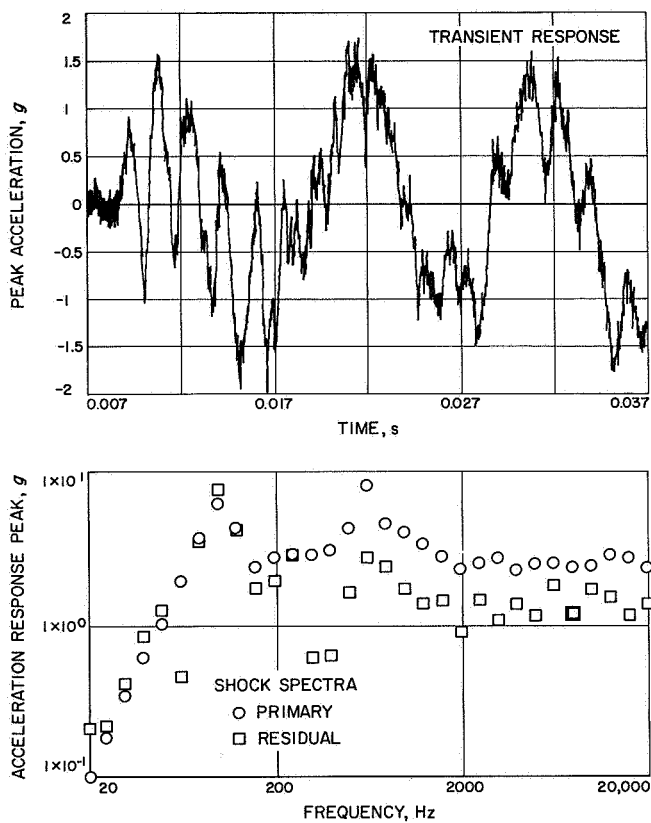


**Fig. A-16. Transient response and shock spectra at accelerometer MCV4 (umbilical door slam event)**

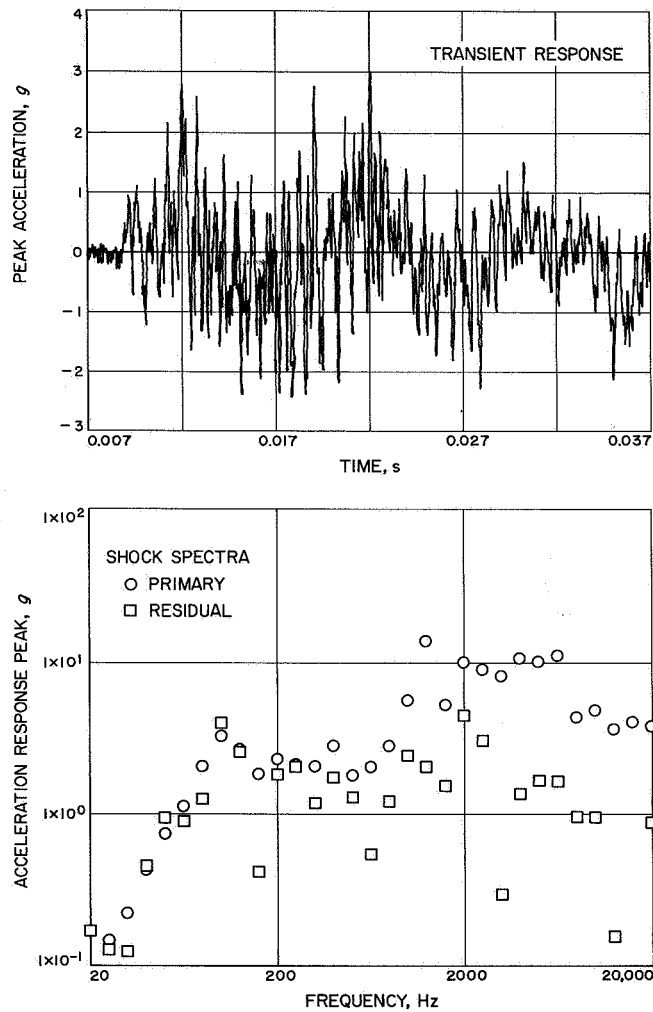


**Fig. A-17. Transient response and shock spectra at accelerometer MC4 (umbilical door slam event)**